The Pennsylvania State University

The Graduate School

Department of Electrical Engineering

MEASUREMENT AND ANALYSIS OF OPTICAL EXTINCTION PROPERTIES

A Thesis in

Electrical Engineering

by

Sameer Unni

Submitted in Partial Fulfillment
of the Requirements
for the Degree of

Master of Science

December 2003

I grant The Pennsylvania State University the nonexclusive right to use this work for the University's own purposes and to make single copies of the work available to the public on a not-for-profit basis if copies are not otherwise available.

_____

Sameer Unni

We approve the thesis of Sameer Unni.

Date of Signature

_____ _____

C. Russell Philbrick
Professor of Electrical Engineering
Thesis Advisor

_____ _____

Sven G. Bilén
Assistant Professor of Electrical Engineering

_____ _____

Kenneth Jenkins
Professor of Electrical Engineering
Head of the Department of Electrical Engineering

ABSTRACT

Remote sensing techniques can be used to characterize airborne particulate matter and results have been compared with atmospheric extinction, aerosol optical depth, and particle size distribution measurements from other sensors. Lidar was used to measure atmospheric constituents and provide a continuous monitor of the optical properties in the lower atmosphere during the NEOPS-DEP campaign of 2002. These studies were conducted in the Philadelphia urban environment where a combination of pollution sources exists. The PSU Lidar Atmospheric Profile Sensor (LAPS) measured ozone, water vapor, temperature, and optical extinction. LAPS was also used to measure vertical profiles of the Angstrom exponent using scattering and extinction data. The Met (Meteorological) tower included a radiometer that measured solar irradiance, from which transmittance values were derived. The Millersville University nephelometer and the Clarkson University optical scatter instruments were used to measure the single scattering albedo and Angstrom exponent. Optical extinction plots from LAPS, at both visible and ultraviolet wavelengths, are integrated and smoothed to obtain vertical profiles. Transmittances obtained from these vertical profiles are found to generally agree with solar transmission from radiometric data. The aerosol optical depths from extinction profiles measured using LAPS and the Met tower data are found to be consistent with the Millersville University nephelometer scattering coefficients. Finally, the single scattering albedo is calculated from the Millersville University nephelometer and the Angstrom exponent is calculated for LAPS and the Millersville University nephelometer. These parameters are compared with the extinction and scattering from LAPS, as well as the scattering form the Millersville University nephelometer and the carbon and PM profiles

from the Clarkson University surface sensors. Analysis of the single scattering albedo and the Angstrom exponent for various episodes provides a better understanding of the relationship between atmospheric pollution episodes and particle size distribution.

LIST OF FIGURES

LIST OF TABLES

ACKNOWLEDGEMENTS

I would like to thank my advisor, Professor C. Russell Philbrick, for his support and guidance through my research. I would also like to thank Dr. Sven Bilén for his support and recommendations.

I would like to thank Guangkun (Homer) Li, Karoline Mulik, Corey Slick, Sachin Verghese, Adam Willitsford, and Jason Collier for their assistance. The efforts of Dr. Richard Clark of Millersville University, Phil Hopke of Clarkson University, and William Ryan of University of Maryland have contributed significantly to the success of this thesis.

I acknowledge the support of my graduate research by the United States Environmental Protection Agency, grant # R826373, and by the Pennsylvania Department of Environmental Protection.

Finally, I would like to thank my family and friends for their constant love and support, which have been major sources of strength throughout my academic career.

CHAPTER 1

INTRODUCTION

1.1 Aerosol Measurements using Remote Sensing

The term “remote sensing”, as applied to aerosols, is viewed by most people as satellite images of clouds and Earth resources. However, in this thesis, the term is applied to the use of laser remote sensing to measure aerosol properties. An aerosol is a colloidal dispersion of solid or liquid particles in a gaseous medium, such as smoke or fog [Seinfeld and Pandis, 1998]. Lidar techniques extend our capability to characterize the spatial and temporal distribution of the aerosols.

Existing ground-based and airborne lidar systems yield measurements with high temporal and range (altitude) resolution. Ground-based lidars have been used to provide height- and time-resolved measurements of the atmospheric backscattering ratio, depolarization ratio, and a measure of multiple scattering. The aerosol backscatter data can be combined with ancillary measurements of the aerosol size distribution and composition to infer wavelength-dependent optical properties such as aerosol extinction and effective particle size. Raman lidars are also presently being used to measure water vapor, temperature, ozone and aerosol extinction profiles. Our goal is to combine these results with scattering measurements by other ground-based instruments to provide a better understanding of aerosol size distribution variations with atmospheric conditions [IGAP plan, 1991].

The purpose of this thesis is to present a comparative analysis of various atmospheric parameters measured by the Penn State Raman lidar with other ground-based instruments

to show the unique advantages of using Raman Lidar as an effective tool. The investigation should also provide a better understanding of the relationship between meteorological observations and atmospheric processes.

1.2 Background

Characterization of airborne particulate matter has been a major challenge to researchers. Recent studies have associated increases in airborne particulate matter with increased morbidity and mortality, particularly in the elderly and individuals with respiratory impairments. Knowledge of aerosol optical properties assumes significant importance in the wake of studies strongly correlating airborne particulate matter with adverse health effects. The small aerosol component, $PM_{2.5}$, representing particles with aerodynamic size less than 2.5 μm, is of most concern to human health because these particles can be easily inhaled deep into the lungs. Along with health issues, aerosol particle distributions have significant implications for natural environment aesthetics and climatic changes [Li et al., 2000]. The changes in optical transmission of the atmosphere due to suspended airborne particulate matter alters the radiative energy balance of the Earth's environment. Increases in aerosol loading in the atmosphere can lead either to an increase or decrease in the mean global temperature of the Earth, because their optical properties in the visible and infrared portion of the spectrum depend on the size distributions of aerosols. Additionally, airborne particulate distributions significantly influence visibility, which affects many activities, for example, scheduled air traffic. The typically observed visual range, compared to a clean molecular atmosphere, is approximately 50-67% in the western United States and 20% in the eastern United States

[Albritton, 1998]. This increase in optical scattering in the eastern states is due to the generally eastward transport of airborne particulate matter (PM), which accumulates on long paths over the continent, and due to increased size of the hygroscopic aerosols caused by the higher east coast humidity.

Along with an improved knowledge of airborne particulate optical properties, a better understanding of the vertical distribution and airborne lifetime of PM is important. Source inventories for PM_{10} and $PM_{2.5}$ in the western states show that geologic dust contributes the major portion of the $PM_{2.5}$ [Li, 2003]. The measurements of the distribution and properties of airborne dust particulate matter in the surface layer will be helpful for better understanding the physical processes and for developing models of airborne particulate matter.

Lidar techniques have been used to make remote sensing measurements of the aerosol optical extinction and other optical properties from optical scattering profiles in the atmosphere. The Penn State University Raman Lidar was used to measure the optical extinction and scattering properties as part of the NARSTO-NEOPS (North east Oxidant and Particle Study) during the summers of 1998 and 1999 [Li et al., 2000]. Airborne particulate matter was analyzed using the gradients in the molecular profiles to determine optical extinction profiles at several wavelengths. The extinction coefficient was calculated from the change in signal strength through aerosols or clouds using the Beer-Lambert law :

$$\alpha = \frac{-\ln(I/I_0)}{2x}$$

where α is the extinction coefficient and x is the range bin size in meters.

Extinction is a measure of the total attenuation of a laser beam due to scattering and absorption. However, at the visible wavelengths used, scattering by aerosols predominated. Extinction was calculated by first subtracting the background signal from the raw photon count signal, and the signal was then corrected for range. At the ultraviolet wavelengths, ozone absorption plays an important role and must be subtracted from the overall extinction to find the extinction due to scattering. A detailed explanation of the extinction measurement technique is provided in Chapter 3.

Other research groups have also used Raman lidar for aerosol measurements. One of these applications of Raman lidar to measure optical properties of aerosols was the AERONET project in 2001. Combined observations with an advanced aerosol water-vapor temperature Raman lidar and a Sun photometer were used for a detailed characterization of geometrical and optical properties of a continental-scale Saharan dust event observed over Leipzig (51.3°N, 12.4°E), Germany, from 13 to 15 October 2001 [Ansmann et al., 2003]. Automatic observations of aerosol optical depth and sky brightness were made with the Sun photometer in the framework of the worldwide operating Aerosol Robotic Network (AERONET). The dust plume reached a top height of 6000 m. Sun photometer and lidar observations showed a constant increase of columnar optical depth at 532 nm from 0.25 on 13 October 2001 to a maximum of ~0.63 on 14 October 2001. According to observations with lidar, up to 90% of the optical depth at the wavelength of 532 nm was contributed by the dust layer above 1000-m height. Angstrom exponents from Sun photometer observations between 380 and 1020 nm were ~0.45 at the beginning of the dust period, and dropped to minimum values of 0.14 during the peak of the dust outbreak. Vertically resolved Angstrom exponents derived from lidar

profiles of the extinction coefficients at 355 and 532 nm showed a strong variability with values as low as 0.2 in the center of the dust plume. Below 1000-m height column-averaged Angstrom exponents strongly varied between 1.0 in the beginning of the dust period and 0.39 on 14 October 2001 when the dust penetrated into the boundary layer. Comparison of column-averaged optical depth and Angstrom exponents derived from lidar and Sun photometer observations showed good agreement.

As part of the Indian Ocean Experiment (INDOEX) anthropogenic aerosols advected from the Indian subcontinent over the Indian Ocean were observed with a unique six-wavelength aerosol lidar at Maldives International Airport in the spring of 1999 [Ansmann et al., 2000]. The eleven-channel aerosol lidar allowed the detection of signals elastically backscattered by air molecules and particles at multiple wavelengths and inelastically (Raman) scattered by nitrogen and water vapor. Profiles were determined from the lidar data for the particle backscatter coefficient at the six wavelengths between 355 and 1064 nm, the volume extinction coefficient of the particles at 355 and 532 nm, as well as the vertical distribution of the water vapor mixing ratio. The set of observational data was used to estimate the aerosol impact on climate.

The Raman lidar at the Atmospheric Radiation Measurement (ARM) program's site in north-central Oklahoma has been used to derive water vapor mixing ratio, relative humidity, aerosol extinction and backscatter coefficient, linear depolarization profiles and aerosol optical thickness [Turner et al., 2002]. The extinction-to-backscatter ratio at 1 km is used with the aerosol backscatter coefficient profile to compute aerosol extinction from 60 m upwards. The aerosol extinction profile retrieved from this system was found to

agree within 10% with that from the National Aeronautics and Space Administration (NASA) Goddard Space Flight Center's scanning Raman lidar during a test at the site.

A group from Japan also used Raman lidar for aerosol measurements. The vertical distributions of tropospheric aerosol properties were measured during the Asian dust event over central Japan (35°–36°N, 136°–137°E), using a ground-based Raman lidar and aircraft-based instruments on 23 April 1996 [Sakai et al., 2003]. The lidar showed enhancements of aerosol backscattering in two regions, below an altitude of 4 km and between 5 and 8 km, where the total aerosol linear depolarization ratio showed peaks of 12–15% and the relative humidities were ~30%. The aircraft measurements showed that the aerosol particles consisted primarily of irregularly shaped mineral dusts and sea salts with a mode radius of ~1 μm and sulfates with a mode radius ~ 0.1 μm over the measured height range of 0.6–5.5 km.

Another example of Raman lidar measurements of aerosol optical properties is the three-year series of routine lidar measurements between December 1, 1997 and November 30, 2000 at Kuhlsungborn, Germany (54˚07'N, 11˚46'E) [Schneider et al., 2002]. Using a Raman lidar, aerosol backscatter coefficients were measured at three wavelengths in and above the planetary boundary layer. The aerosol extinction coefficient was measured at 532 nm, but only nighttime measurements were available since the 532 nm channel remained closed during the day. For climatological analysis, cloud-free days were selected out of a fixed measurement schedule. The backscatter coefficients in the planetary boundary layer were found to be about 10 times higher than that above the boundary layer. The mean aerosol optical depth above the boundary layer and below 5 km was 0.26 (±1.0) $\times 10^{-2}$ in summer, and 1.5 (± 0.95) $\times 10^{-2}$ in winter. A

cluster analysis of the backward trajectories yielded two major directions of air mass origin above the planetary boundary layer and four major directions inside the boundary layer. Comparing the measured backscatter coefficients with data from the Global Aerosol Data Set, a general agreement was found, but only a few conclusions with respect to the aerosol type could be drawn due to the high variability of the measured backscatter coefficients.

One of the recent experiments conducted in the field of Raman lidar measurements of aerosol optical properties includes the measurement of aerosol extinction profiles for a period of four months at nine EARLINET stations in Europe in 2002 [Matthias et al., 2003]. The measurements were made between May and September 2002 at Aberystwyth, Hamburg, Kuhlsungborn, Leipzig, Napoli, Potenza, Lecce, Thessaloniki, and Athens. The extinction profiles were determined using the Raman lidar technique at either 351 nm or 355 nm. The seasonal coverage of aerosol extinction measurements was quite different at the individual stations and the number of profiles also differed significantly depending on the weather conditions and technical details of the systems, such as the lowest measurement height. Aerosol optical depth was derived by integrating the aerosol extinction profiles with height. Due to the optical setup of some of the systems, aerosol extinction data could not be provided in the lowest 1000 m of the atmosphere. This led to problems in the comparability of the statistics from different sites, because the aerosol containing planetary boundary layer was not covered in a few cases.

New techniques and instrumentation have been developed and applied for remote atmospheric measurements by the NASA Goddard Space Flight Center (GSFC). Current research includes cloud and aerosol observations by an orbiting lidar launched in 2003

called the Cloud Physics Lidar (CPL). It provided information on aerosol optical properties (the amount of light they reflect and scatter), as part of the CRYSTAL experiment [CRYSTAL, 2003]. Other research includes instrumentation operated from a high-altitude NASA U-2 research aircraft, a network of ground-based lidar, and a shuttle hitchhiker experiment for specialized infrared (IR) cloud imaging. Active lidar sensing is employed in conjunction with advanced visible and IR sensors, and other atmospheric radiation measurements in large-scale atmospheric field programs. Development and application of new lidar technology is emphasized. This technology includes advanced ground-based and airborne Raman lidar for water vapor measurements, and development of holographic optical technology for remote sensing.

The measurements presented in this thesis were made during the summer 2002 North-East Oxidant and Particle Study (NE-OPS) in Philadelphia, PA, using the Pennsylvania State University LAPS (Lidar Atmospheric Profile Sensor). Details of the LAPS instrument and the process of Raman scattering are described in Chapter 3.

1.3 Research Outline and Hypothesis Statement

This section outlines the work that has been undertaken and the hypothesis of this thesis. The main research objectives are listed below:

1. Review and update the analysis techniques used to calculate the optical extinction from the Raman lidar (LAPS) at both visible and ultraviolet wavelengths.
2. Analyze measurements by carrying out integration and smoothing of data to obtain vertical profiles of extinction at two wavelengths and calculate transmittance and optical density.

3. Compare the lidar-derived transmittance values with MET tower visible radiometer.
4. Calculate and compare the aerosol optical depth (AOD) from LAPS extinction profiles with AOD from the visible radiometer of the meteorological (MET) tower.
5. Examine the variations in particle size distribution by calculating values of the single scattering albedo and Angstrom coefficients using data from LAPS, the Millersville University nephelometer, and the Clarkson University aethalometer.

The hypotheses, which I intend to investigate, are:

1. The integrated parameters obtained from LAPS extinction profiles provide results that are consistent and in general agreement with measurements from surface sensors.
2. The results of integrated values determined from vertical profiles of LAPS are consistent with the radiometric data.
3. The aerosol optical depths from extinction profiles measured using LAPS and the Met tower data are consistent with the Millersville University nephelometer scattering coefficients.
4. The Angstrom coefficient results obtained from multiple wavelength extinction profiles using LAPS are consistent with the scattering coefficients and single scattering albedo obtained from the Millersville University nephelometer and the Clarkson University aethalometer.

CHAPTER 2

ATMOSPHERIC AEROSOL

2.1 Importance of Aerosols

Studies of aerosols have generally been focused on two areas: effects on climate and effects on electro-optic systems. Scattering and absorption by particles, those in aerosols and clouds, together with the contributions from molecular scattering and absorption by gases, play a major role in determining what fraction of the solar radiation incident at the top of the atmosphere reaches the Earth's surface. In certain parts of the spectrum, the absorption by water vapor, ozone and other molecules play a dominant role in determining the transmittance. Aerosols are a major factor in determining the Earth's climate because of their effect on the radiation budget.

2.2 Aerosol Description

An aerosol is a colloidal dispersion of solid or liquid particles in a gaseous medium, such as smoke or fog [Seinfeld and Pandis, 1998]. Aerosols vary greatly in concentration and chemical composition, making them difficult to model. Aerosol types are classified three different ways: by size, by geographical region of formation, and by production mechanism. Junge [1955] classified aerosols by their geographical source region: maritime, continental, and background. He also classified them by size according to their radius, as shown in Table 2.1. Whitby [1973] categorized aerosols into groups according to their production mechanism, some of which are shown in Table 2.1. The various production mechanisms include (i) gas-to-particle conversion, (ii) growth and

coagulation, (iii) particle injection from breaking waves on the ocean, (iv) wind-blown effects, (v) direct emissions, and (vi) meteoric dust.

Table 2.1. Particle types classified according to radius and formation mechanism [Watson and Chow, 2000].

			Formation Mechanism	**Size**
Type I	Aitken	nucleation mode	gas-to-particle conversion	0.001-0.1μm
Type II	large	accumulation mode	coagulation/heterogeneous	0.1-2.5 μm
Type III	giant	coarse particle mode	mechanical process	>2.5 μm

The smallest or "ultrafine" particles are produced by the gas-to-particle conversion processes. If the vapor concentrations are sufficiently high, particles may be formed in free air by 'homogeneous nucleation', which means the vapors condense on the particles when sufficient numbers of particles are present. This process usually occurs when the particle size is between 0.001–0.1 μm. Nucleation processes require photochemistry and new particle formation occurs best during mid-day hours under sunny and dry conditions [Birmili et al., 2003]. The number of newly formed particles has been found to correlate with solar irradiance and ambient concentrations of H_2SO_4. Combustion processes from automobiles and heavy industry also contribute to the formation of these particles.

There are various sources for the intermediate size particles between 0.1 and 2.5 μm. These include combustion and chemical transformation of gases to produce secondary products including sulfates, nitrates, and organics. Particle sizes larger than 2.5 μm are contributed primarily by wind-blown effects. The processes that contribute to generation and removal of particles are shown in Figure 2.1.

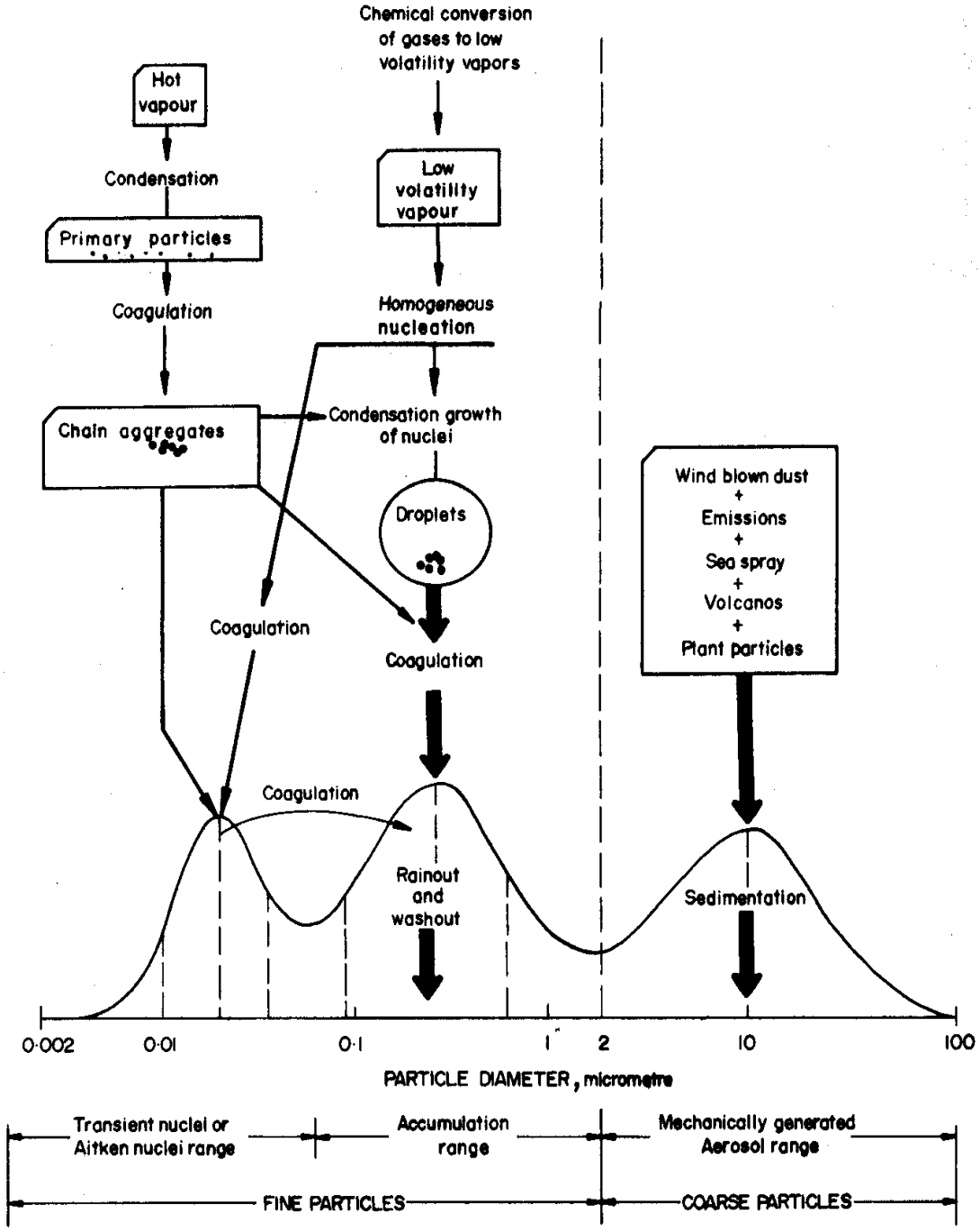

Figure 2.1. Atmospheric aerosol surface-area distribution [Whitby, 1980]

As seen in Figure 2.1, vapors with low volatility condense on particles by homogeneous nucleation to produce the ultrafine particles (0.001-0.1 μm). The hygroscopic particles, such as ammonium sulfate and ammonium nitrate, absorb moisture and coagulate to produce the fine particles (0.1-2.5 μm). Wind-blown dust, sea-spray and volcanic activity produce the coarse particles (>2.5 μm).

2.3 Aerosol Size Distributions

As indicated by Figure 2.2, tropospheric particles span a wide size range from molecular clusters smaller than 1 nm to "giants" of 100 μm or more in diameter [Part. Mat. Sc., 2003]. Particle number concentrations (upper panel of Figure 2.2) are dominated by the "ultrafine particles", which are nominally smaller than 0.1 μm in diameter. The ultrafines originate from combustion and nucleation. Although the ultrafine mode generally contains the most particles, it frequently contains nearly negligible mass (volume) and very little surface area and so it takes many particles in this mode to affect the optical scattering intensity. Aerosol mass distributions (lower panel of Figure 2.2) are dominated by particles larger than 0.1 μm, which include "fine particles" up to 2.5 μm diameter and "coarse particles" larger than 2.5 μm. $PM_{2.5}$ designates the mass concentration of particles with aerodynamic size smaller than 2.5 μm (the fine particle mass), and PM_{10} designates the total mass concentration of coarse particles with aerodynamic size less than 10 μm.

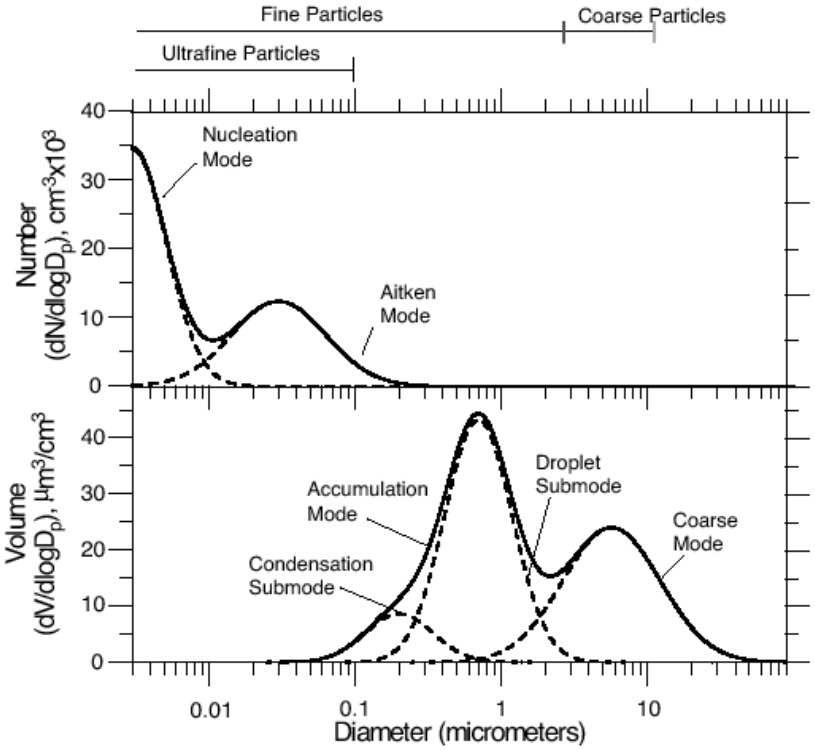

Figure 2.2. Typical number and volume distributions of atmospheric particles [Part. Mat. Sc., 2003]

The fine particles derive principally from combustion and chemical transformations of gases to produce secondary products including sulfates, nitrates, and organics. The most important precursor gases for secondary aerosols are sulfur dioxide (SO_2), nitrogen oxides (NO_x), and certain volatile organic compounds (VOC). Ammonia (NH_3) reacts with sulfates and nitrates to form particulate salts, such as ammonium sulfate ($(NH_4)_2SO_4$) and ammonium nitrate (NH_4NO_3). These particles are hygroscopic and act as growth centers for the formation of larger particles that can dominate the optical environment [Part. Mat. Sc., 2003].

The coarse mode originates mainly from mechanical processes, such as erosion, mining, soil tilling, and resuspension through impact. Although the least plentiful in number, the coarse mode is responsible for the majority of mass (volume) of aerosol in

the atmosphere, and significantly contributes to the degradation of visibility. However, due to their larger size, coarse mode particles generally fall out rapidly from the atmosphere [Seinfeld and Pandis, 1998, Watson and Chow, 2000].

2.4 Significance of Aerosol particle size and composition

Aerosol particle size and composition are strong determinants of numerous physical phenomena and physiological impacts, as well as useful indicators of a pollutant's origin and atmospheric history [Part. Mat. Sc., 2003]. An increase in particle size, if sufficient numbers are available, indicates a transition from a relatively clear atmosphere to one with high extinction. This information, regarding change in particle size, when combined with back trajectories, serves as a useful indicator of pollutant origin and transport. Two of the most important physiological impacts of aerosol size distribution and composition are respiratory-tract deposition and visibility reduction [Part. Mat. Sc., 2003].

Particle composition plays a role in direct radiation impacts as well. For example, sulfate and organic carbon (OC) particles largely scatter light, leading to atmospheric cooling, whereas black carbon (BC) particles absorb light, with a corresponding warming tendency [Part. Mat. Sc., 2003]. So-called "indirect effects" depend on both particle size and composition.

Figure 2.3 shows the typical relationships between pollutants and their resulting influence on meteorological episodes. As seen in Figure 2.3, the relative mass fractions of secondary PM can change with changing precursors, owing to the complex chemistry of secondary PM formation. As sulfur dioxide emissions decline, so will particulate sulfate PM concentrations and acid rain. The presence of ammonia allows the formation of

ammonium nitrate and ammonium sulfate. As sulfate is removed, more ammonium nitrate can be formed, provided sufficient ammonia and nitric acid are present. The black carbon fraction will decrease in direct response to reductions in source emissions from, for example, diesel combustion. The organic carbon fraction stems from both direct emissions of organic PM and the oxidation of VOC emissions. Thus, as the particle-forming VOCs, acids, and oxidants decrease, so would the secondary organic carbon fraction. The information in Figure 2.3 is useful for investigators to predict how particle mass and composition would change in response to changing natural and anthropogenic conditions.

Reduction in pollutant emissions	Change in associated pollutant or atmospheric issue					
		PM Composition				
	Ozone	Sulfate	Nitrate	Organic compounds	$PM_{2.5}$	Acid Deposition
SO_2		↓	↑ [f]		↓	↓
NO_x	↓↑ [b]	↑↓ [d]	↓ [g]	↓↑ [i]	↓↑	↓↑
VOC	↓	↑↓	↓↑ [h]	↓ [j]	↓↑	↓↑
NH_3		↓ [e]	↓		↓	↑ [l]
Black Carbon	↑ [c]			↓ [k]	↓	
Primary Organic Compounds	↑ [c]			↓	↓	
Other primary PM (crustal, metals, etc.)	↑ [c]				↓	↑ [l]

[a] Arrow direction denotes increase (↑) or decrease (↓); arrow color denotes undesirable (red) or desirable (blue) response; arrow size signifies magnitude of change. Small arrows signify possible small increase or decrease. Blank entry indicates negligible response.
[b] In and downwind of some urban areas that are VOC limited.
[c] Effect on daytime O_3 due to increase in solar flux and decrease in radical scavenging; effect on nighttime O_3 unknown.
[d] Due to effect of NO_x on oxidant levels (OH, H_2O_2 and O_3); e.g., see SAMI modeling results.
[e] Due to effect of NH_3 on cloud/fog pH.
[f] Decrease in sulfate may make more NH_3 available for reaction with HNO_3 to form NH_4NO_3, more important when NH_4NO_3 is NH_3 limited.
[g] Decrease except special cases (e.g., SJV); decrease in NO_x may lead to increase in O_3 with associated increase in HNO_3 formation.
[h] Increase due to less organic nitrate formation and more OH available for reaction with NO_2; decrease due to decrease in oxidant levels.
[i] Related to effect of NO_x on oxidant levels (OH, O_3 and NO_3).
[j] Decrease of secondary component; magnitude depends on OC fraction that is secondary anthropogenic.
[k] Reduction of OC adsorbed or emitted with black carbon.
[l] Refers to net acidity atmospheric deposition, not to acidification potential to ecosystem.

Figure 2.3. Typical pollutant/atmospheric issue relationships [Part. Mat. Sc., 2003]

The following chapters will provide examples that illustrate these pollutant-atmospheric issue relationships. In Chapter 4, we observe how transmittance of the atmosphere changes in response to the percentage of pollutants present in the region of concern. On a relatively clear day, the mid-visible transmittance vertically through the atmosphere is in the range of 0.7-0.8, whereas in the presence of haze, the average transmittance is found to fall by approximately 20%. In Chapter 5, we examine the relationship between aerosol optical depth and extinction. Finally, in Chapter 6, we observe three different episodes where particle size varies according to the concentration of pollutants being transported into the region. These examples and their analyses will serve to better understand the relationship between PM, its components and other air pollution problems.

CHAPTER 3

LIDAR TECHNIQUES FOR AEROSOL MEASUREMENTS

Optical remote sensing using molecular Raman scattering provides a useful method for studying the atmosphere and its constituents. The remote sensing instrument that is utilized for these studies is lidar, which is the acronym for LIght Detection And Ranging, commonly referred to as laser radar. A lidar system transmits a pulsed laser beam at a certain wavelength into the atmosphere, and a telescope collects the return signals, which are separated by a detector system into components such as direct backscatter, vibrational Raman and rotational Raman signals, at different wavelengths. The measured signals are then analyzed to obtain measurements of atmospheric constituents and properties.

3.1 Raman Scattering

Raman lidar utilizes the signals from inelastic scattering by atmospheric molecules, where the vibrational and rotational energy levels of the molecules are involved. Consider the process when electromagnetic energy is scattered by a molecule. The process is said to be elastic (Rayleigh scattering) if the scattered frequency is nearly the same as the incident frequency (only different by the Doppler velocity shifts for wind and temperature), and inelastic (Raman scattering) if the scattered frequency and the incident frequency are different. A Raman shift occurs when a beam of light is scattered by molecules at wavelengths that correspond to energy differences associated with the vibrational and rotational energy states of the molecules [Measures, 1984]. This shift in

frequency of the scattered photon is due to the energy difference that is characteristic of the vibrational and rotational energy states of each molecule. If the resulting radiation has a longer wavelength, or lower frequency, the molecule has gained energy, and the red-shifted scattered radiation is referred to as the Stokes component. If the molecule loses energy, the scattered radiation (blue shifted) is referred to as the anti-Stokes component [Measures, 1984]. The energy shift of the Stokes and anti-Stokes components are shown in Figure 3.1. As seen in the figure, one molecule loses energy (E = h**n**-**D**E), resulting in the Stokes component, whereas the other molecule gains energy (E = h**n**+**D**E), resulting in the anti-Stokes component.

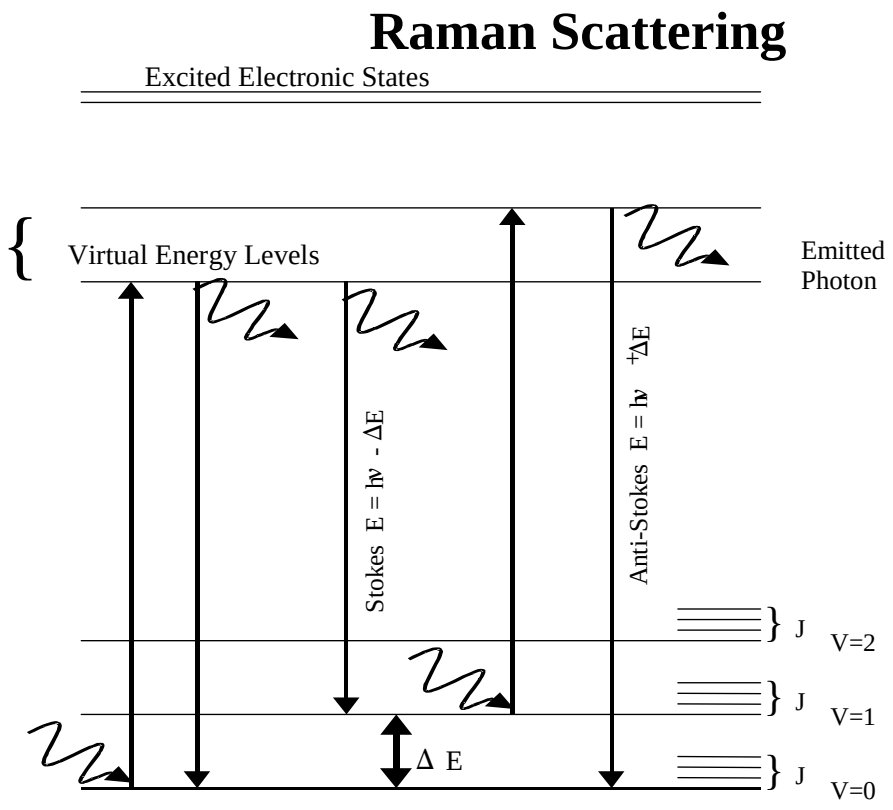

Figure 3.1. Stokes and anti-Stokes energy shifts are shown that schematically represent Raman scattering theory [Adapted from Measures, 1984].

The Raman spectrum consists of scattered radiation at wavelengths corresponding to the energies of the molecule's vibrational states and rotational states. Typically, Raman lidar measurements of an atmospheric species are made as a ratio of signals of specific molecules to a signal that represents the total density, such as N_2 or O_2. This ratio provides a direct measurement of the relative concentration of the species and removes much uncertainty by canceling the effects of many system parameters. The vibrational and rotational Raman signals expected from the doubled output of a Nd:YAG laser at 532 nm are shown in Figure 3.2.

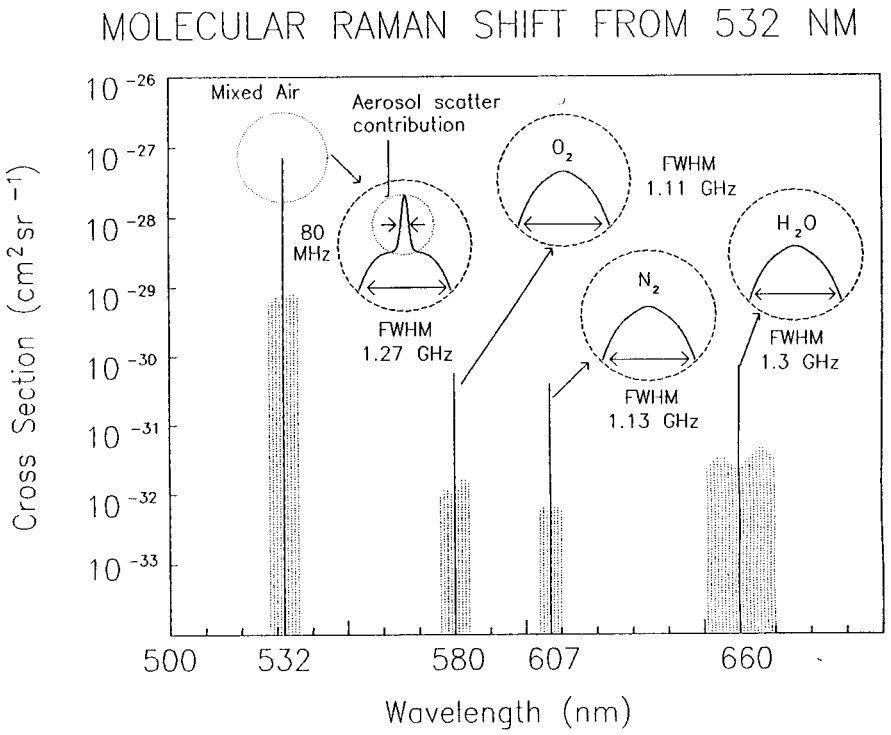

Figure 3.2. Relative sensitivity is indicated by the cross-section of vibrational and rotational Raman shifts for O_2, N_2, H_2O, and aerosol scatter for a 532-nm laser transmitter [Philbrick, 1994].

The intensity of a Raman signal is directly proportional to the density of the scattering molecules [Measures, 1984]. The wavelength shift and narrow spectral width of the Raman return signal allows unique identification of atmospheric constituents, such as water vapor and ozone. The LAPS instrument uses the vibrational Raman scattered signals to measure water vapor, ozone and optical extinction, and uses the rotational Raman scatter signals to measure temperature. It collects the rotational Raman backscatter signals at 528 nm and 530 nm and the vibrational Raman backscatter signals at 607 nm, 660 nm, 277 nm, 284 nm and 295 nm. The 607- and 660-nm signals are the 1st Stokes vibrational Raman shifts from the N_2 and H_2O molecules in the atmosphere excited by the second harmonic (532 nm) of the Nd:YAG laser. The 277-, 284- and 295-nm signals correspond to the 1st Stokes vibrational Raman shifts from the O_2, N_2, and H_2O molecules in the atmosphere excited by the fourth harmonic (266 nm) of the Nd:YAG laser. The ratio of rotational Raman signals at 528 and 530 nm provides the measurement of atmospheric temperature [Haris, 1995]. Since the rotational states of all the molecules in the lower atmosphere are distributed according to the local temperature, the temperature can be directly measured by taking the ratio of the backscatter signals at two wavelengths in this distribution. Optical extinction is measured using the gradient of the measured molecular profile compared with that expected for the density gradient [O'Brien et al., 1996]. The technique to measure extinction will be discussed in Section 3.4.

3.2 Lidar Atmospheric Profile Sensor Instrument

Measurements presented in this thesis were made during the 2002 North-East Oxidant and Particle Study (NE-OPS) pilot study in Philadelphia, PA, using the Penn State University lidar, referred to as LAPS (Lidar Atmospheric Profile Sensor) [Philbrick, 1998]. LAPS was originally designed as a rugged prototype instrument for the U.S. Navy to obtain RF refractivity measurements in severe environments, and it has several useful features such as environmental control and real time data display for profiles of atmospheric properties [Esposito, 1998; Philbrick, 1994; Philbrick, 1998]. The LAPS instrument is a multi-wavelength Raman lidar that can take measurements during the daytime and nighttime under a wide range of weather conditions and is capable of operating autonomously.

The LAPS instrument consists of a console and a deck unit, which are connected by fiber optic cables. The main components of the deck unit are a Nd:YAG laser, beam expander telescope, collecting telescope, and control/data system. The Nd:YAG laser is pulsed at 30 Hz with an output power of 1.6 joules per pulse at the fundamental wavelength, 1064 nm. The 1064-nm laser beam is sent through two frequency-doubling crystals to transmit at wavelengths of 532 nm (2^{nd} harmonic) and 266 nm (4^{th} harmonic), and the radiation scattered from these two incident wavelengths is measured by the instrument. The output energy of the laser is not eye-safe and several safety precautions are taken during operation. A radar with a six-degree cone angle around the vertical laser beam is used to detect aircraft and send a signal to shut off the beam if detection occurs. The laser transmitter system of LAPS is shown in Figure 3.3. The transmission system characteristics of LAPS are given in Table 3.1 [Durbin, 1997; Philbrick, 1998].

Figure 3.3. LAPS Transmitter optics [photo credit, C.R. Philbrick].

Table 3.1. LAPS Transmitter Characteristics [Philbrick, 1998].

Laser	Continuum Model 9030 with 5X Beam Expander
Pulse Frequency	30 Hz
Pulse Duration	8 ns
Fundamental Power	1.6 J/Pulse
Power Output at 1064 nm	Dumped into heat sink
Power Output at 532 nm	600 mJ
Power Output at 266 nm	130 mJ

The return signal is collected in an upward pointing prime focus paraboloid telescope and focused into a 1-mm fiber. The LAPS transmitter and receiver system configuration is shown in Figure 3.4 [Durbin, 1997; Jenness, 1997].

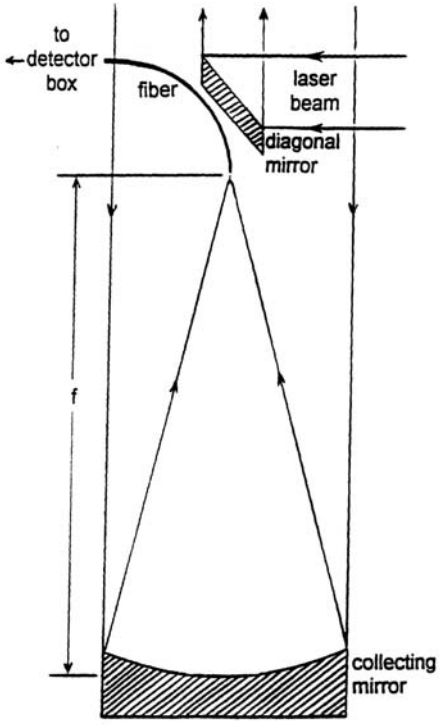

Figure 3.4. LAPS receiver system components [Jenness, 1997].

A fiber optic cable then transfers the return signal to an eight-channel detector box in the console unit, which contains optical filters, steering optics, lenses, and photomultiplier tubes (PMT's). Seven of the filters isolate several vibrational and rotational Raman-shifted wavelengths from the transmitted laser beams at 532 nm and 266 nm. The eighth filter is set at 532 nm to measure the direct backscatter. The signals from the fiber optic cable are split into optical paths in the detector and filtered at each of the selected Raman scatter wavelengths for different atmospheric constituents. The optical signals are then transferred to the corresponding PMT's, where photon-counting techniques are used to measure the signals. Due to the low Raman scatter cross-sections, the scattered photons

require high-sensitivity photomultipliers and photon-counting techniques for detection. For optimal detection performance, the PMT's are selected for low noise and high photocathode quantum efficiency in the spectral region of interest. The detector box with the steering optics for each PMT channel is shown in Figure 3.5.

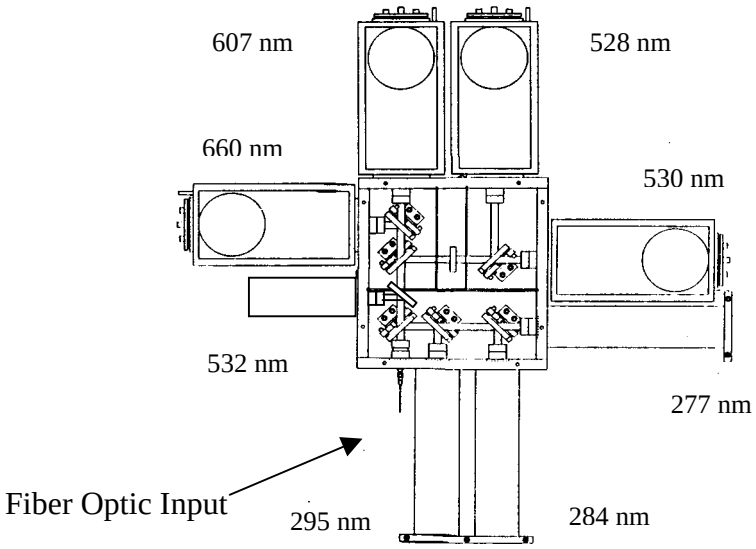

Figure 3.5. LAPS detector box with the steering optics and the layout of each PMT [Mulik, 2000].

The console provides a terminal for the operation of the instrument and includes a computer for data collection and display. Data analysis programs also provide output files of the photon counts with a vertical resolution of 75 meters for seven Raman channels and a vertical resolution of 3 meters for the Rayleigh backscattered signal. Table 3.2 summarizes the features of LAPS.

Table 3.2. Summary of LAPS Features [Mulik, 2000].

Transmitter	Continuum 9030–30 Hz 5X Beam Expander	600 mJ @ 532 nm 130 mJ @ 266 nm
Receiver	61-cm Diameter Telescope Focal length – 1.5 m	Fiber optic transfer
Detector	Eight PMT channels Photon Counting	660 and 607 nm – Water Vapor 528 and 530 nm – Temperature 295 and 284 nm – Daytime Water Vapor 277 and 284 nm – Raman/DIAL Ozone 607, 530, and 284 nm – Extinction 532 nm – Backscatter
Data System	DSP 100 MHz	75-meter range bins
Safety Radar	Marine R-70 X-Band	Protects 6° cone angle around beam

3.3 Measurement Techniques

The LAPS system uses Raman scattering techniques to measure vertical profiles of aerosol extinction, water vapor, temperature, and ozone. Rotational Raman scatter is used to measure temperature, and vibrational Raman scattering is used to measure profiles of water vapor, ozone, and optical extinction. The vibrational and rotational Raman signals are measured for the 532-nm transmitted wavelength (refer to Figure 3.2 and Table 3.2) and for the 266-nm transmitted wavelength. The raw data obtained in photon counts provides information about the concentrations of N_2, O_2, and H_2O at different altitudes. These measurements can be interpreted using the basic lidar scattering equation. The lidar scattering equation can be described by the power of the signal received by a monostatic lidar denoted by $P(\lambda_R,z)$, given by [Esposito, 1999; Measures, 1984]:

$$P(\lambda_R, z) = E_T(\lambda_T)\xi_T(\lambda_T)\xi_R(\lambda_R)\frac{c\tau}{2}\frac{A}{z^2}\beta(\lambda_T, \lambda_R)\exp\left[-\int_0^z [\alpha(\lambda_T, z') + \alpha(\lambda_R, z')]dz'\right] \quad , \qquad [3.1]$$

where,

z	is the altitude of the volume element where the return signal is scattered,
λ_T	is the wavelength of the laser light transmitted,
λ_R	is the wavelength of the laser light received,
$E_T(\lambda_T)$	is the light energy per laser pulse transmitted at wavelength λ_T,
$\xi_T(\lambda_T)$	is the net optical efficiency at wavelength λ_T of all transmitting devices,
$\xi_R(\lambda_R)$	is the net optical efficiency at wavelength λ_R of all receiving devices,
c	is the speed of light,
τ	is the time duration of the laser pulse,
A	is the area of the receiving telescope,
$\beta(\lambda_T,\lambda_R)$	is the back scattering cross section of the volume scattering element for the laser wavelength λ_T at Raman shifted wavelength λ_R,
$\alpha(\lambda,z')$	is the extinction coefficient at wavelength λ at range z'.

Using this relation, the number of photon counts expected from the received signal can be determined and the vertical profiles of the atmospheric properties can be obtained. It should be noted that return signals for the LAPS system using Equation 2.1, $P_T(\lambda_T)$ are the time-averaged values for transmitted energy, E_T, at wavelength, λ_T. It becomes apparent that the Raman scattering techniques use ratios of the lidar equation, which greatly simplifies the measurement of the various parameters. In the above equation, $\xi_R(\lambda_R)$ is the net optical efficiency at wavelength λ_R of all receiving devices, and includes the geometrical form factor that is critically dependent upon the details of the receiver optics. Most of these factors cancel in the ratio or result of known quantitative values. The analysis of the near field data (<800 m) is also important, because overfilling of the detector causes the effective profile of the received signal to be distorted by vignetting [Mulik et al., 2000]. This signal distortion can be measured and corrected by normalizing the detected signal.

3.4 Extinction Measurement Technique

Extinction (units of km^{-1}), is the total attenuation of a laser beam through the atmosphere due to scattering and absorption by both aerosols and molecules. The LAPS instrument measures extinction at three different wavelengths using the vertical gradients in the profiles of the principal molecular species [O'Brien et al., 1998; Li et al., 2000]. Extinction is measured using the Raman scatter signal profiles of molecular nitrogen at 607 nm and at 284 nm, resulting from the 532-nm and 266-nm transmitted wavelengths, respectively. Another extinction measurement is made by using the rotational Raman signals from the mixture of nitrogen and oxygen molecules at 530 nm, resulting from the 532-nm transmitted wavelength. The Beer-Lambert Law is used to calculate the extinction coefficient, α, by comparing the gradient of the measured signals with the gradient expected from molecular scattering in a pure molecular atmosphere. The extinction coefficient from Beer's Law includes the path up and back down through the path element, x, and is written as [Stevens, 1996]:

$$\alpha = \frac{-\ln(I/I_0)}{2x} \qquad [3.2]$$

where I is the measured return signal and I_0 is the return signal expected from molecular scattering in a pure molecular atmosphere.

The total extinction in the atmosphere is given by the absorption and scattering of both molecules and aerosols as:

$$\alpha_{\text{tot}} = \alpha_{\text{mol,abs}} + \alpha_{\text{aer,abs}} + \alpha_{\text{mol,sca}} + \alpha_{\text{aer,sca}} \qquad [3.3]$$

where,

$\alpha_{\text{mol,abs}}$ is the extinction due to molecular absorption,
$\alpha_{\text{aer,abs}}$ is the extinction due to aerosol absorption,

$\alpha_{mol,sca}$ is the extinction due to molecular scattering,
$\alpha_{aer,sca}$ is the extinction due to aerosol scattering.

Extinction due to molecular scattering can be calculated from the estimated number density of the molecules. The number density is calculated using the hydrostatic equation with input of the temperature profile and a measurement of surface pressure. The extinction profile due to molecular scattering can be then subtracted from the total extinction to find the extinction profiles that are attributed to aerosol scattering and absorption. Optical extinction profiles due to aerosol scattering at the visible wavelengths of 530 nm and 607 nm are very similar to each other, as shown in the example in Figure 3.5. These values are significantly less than the extinction measurements at 284 nm because of the larger scattering cross-section of the particles at the ultraviolet wavelengths. The extinction measurement at the ultraviolet wavelength, 284 nm, includes both scattering and ozone absorption, which can be corrected using the known absorption coefficients for the Hartley band of ozone. Figure 3.6 shows a plot of the extinction due to aerosol scattering at each wavelength measured during the NE-OPS pilot study at a time when the atmosphere was relatively clean. Error bars, which are included to indicate the accuracy, will be discussed in detail in Section 3.5.

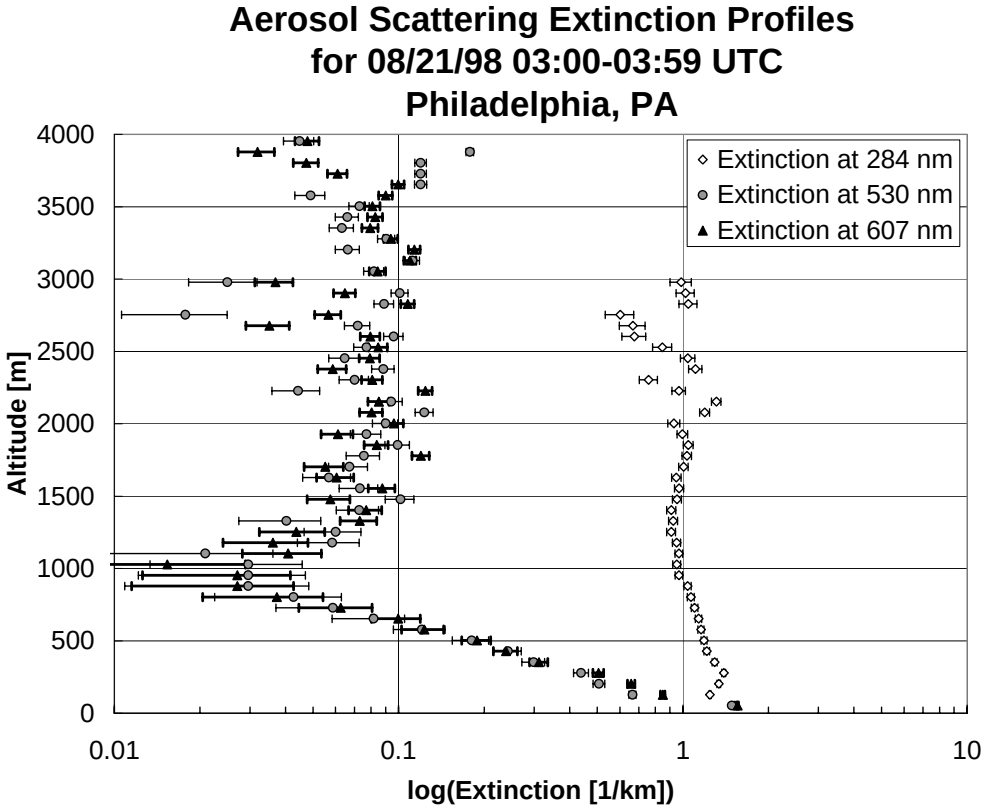

Figure 3.6. Vertical extinction profiles measured by LAPS at 284 nm, 530 nm, and 607 nm on 08/21/98 from 03:00–03:29 UTC show the error bars associated with the measurement at each altitude [Mulik, 2000].

3.5 Error Analysis

Error analysis involves determining the uncertainty of results and how errors propagate through calculations used to obtain the results. The uncertainty due to lack of precision in instruments can be expressed as the difference between the true or actual value and the measured value. Since the scattering cross-sections and other parameters are known to an accuracy of about 1-2 %, the major errors in the measurement are due to the photon counting statistics. Note, however, that most instrument errors for LAPS are cancelled in calculating the ratio of signals at two different wavelengths to obtain the

different parameters. If the uncertainty in the measurement is due to statistical fluctuations and not lack of precision, the uncertainties can be represented by the standard deviation, sd, of the measured quantity and are assumed to have a Poisson distribution [Bevington, 1969]. The Poisson distribution is applicable for measuring a small number of signals within a time interval when the number of scattered photons returned is much smaller than the actual number scattered, so it provides a good description for the lidar return of photon counts. Relative uncertainty is the ratio of the standard deviation to the mean and can be expressed as a Poisson distribution as [Bevington, 1969]

$$\frac{\mathrm{sd}}{\mathrm{x}} = \frac{\sqrt{\mu}}{\mathrm{x}} = \frac{1}{\sqrt{\mu}}, \qquad [3.4]$$

where,

sd is the standard deviation,
μ is the mean,
x is the number of events.

It is common in data analysis to use independent measurements as parameters for calculating dependent variables. The uncertainty in these independent variables must be carried through the calculations in order to define the uncertainty in the dependent variable, and this procedure is referred to as propagation of errors [Bevington, 1969]. The propagation of errors procedure can be applied to the lidar data when the ratio of signals is taken to calculate an atmospheric parameter, such as water vapor. The propagation of error of a ratio z = x/y is given by [Bevington, 1969; Esposito, 1999]:

$$\frac{\mathrm{sd_z}}{\mathrm{z}} = \sqrt{\left(\frac{\mathrm{sd_x^2}}{\mathrm{x^2}} + \frac{\mathrm{sd_y^2}}{\mathrm{y^2}} - 2\frac{\mathrm{r_{xy}\,sd_x\,sd_y}}{\mathrm{xy}} \right)}, \qquad [3.5]$$

where,

sd_z is the standard deviation of z,
sd_x is the standard deviation of x,
sd_y is the standard deviation of y,
r_{xy} is the correlation between x and y.

The correlation, r_{xy}, is neglected, since it is very small in comparison with the standard deviations. These statistical techniques are used to apply error bars to the measured signals, as shown in the extinction measurements in Figure 3.6. An important point to be noted here is that the propagation of errors can also be calculated for the case where the measurement is not a simple ratio, such as the calculation of optical extinction.

Raman lidar techniques for measuring vertical profiles of the atmosphere have proven to be very useful in describing the dynamics of the atmosphere, as well as in determining the distributions of chemical species and airborne particulates. Lidar profiles are also useful for atmospheric model evaluation, since vertical profiles provide information about the concentrations of PM and ozone in different layers of the atmosphere.

3.6 Summary

LAPS serves as an effective tool for providing continuous measurements of water vapor, ozone, extinction, and temperature. Water vapor is the most effective marker of the thickness of the planetary boundary layer, which describes the dilution volume of the chemical species. Ozone is an important tracer of pollutant transport, and is of high importance because of its direct effects on the respiratory system. Extinction provides knowledge of the vertical distribution of aerosol optical properties, which are important

because of the correlation of aerosol concentration with adverse health effects, mean global temperature of the Earth, and visibility.

In the following chapters, we analyze optical extinction measured by LAPS, in comparison with other instruments, and gain an insight into particle size distribution with the help of parameters such as single scattering albedo and Angstrom exponent. Comparative analysis of the aerosol extinction profiles with ozone points to the common photochemical production processes, regional meteorology accumulation processes, and transport from industrial and power generation sources. In addition, studies using the ultraviolet lidar wavelengths provide a better understanding of the relative contribution to extinction from ozone absorption and from aerosol scattering.

CHAPTER 4

A COMPARATIVE ANALYSIS OF LAPS AND SOLAR RADIOMETER

4.1 Introduction

Total Solar Irradiance (TSI) is the radiant energy received by the Earth from the Sun, over all wavelengths, above the top of the atmosphere. TSI is very nearly constant and the small changes of intensity caused by the eccentricity of the Earth's orbit and the changes due to the tilt of the Earth's axis cause interaction with the Earth's atmosphere, oceans and landmasses are the biggest factors determining our climate. To put it into perspective, decreases in TSI of 0.2% occur during the weeklong passage of large sunspot groups across our side of the Sun [Online, Available: http://www.scienceblog.com/community/article1272.html]. These changes are relatively insignificant compared to the total output energy of the Sun, yet equivalent to all the energy that mankind uses in a year. Evidence from TSI monitoring and correlative climate data indicates that solar variability has been a significant factor in climate forcing in the past. The periodic character of this record indicates that it will be again in the future and is, in fact, a continuously varying contributor to climate change.Monitoring TSI variability is clearly an important component of climate change research, particularly in the context of understanding the relative contributions of natural and anthropogenic processes.

Variations in solar activity drive the Earth's climate. Changes in UV radiation heat the upper atmosphere, which, in turn, affects the weather at ground level. The lowered boundary also changes the circulation of air from the stratosphere downward into

regions of low pressure, which, in turn, affects the flow patterns that steer weather systems.

The influence of external factors on climate can be broadly compared using the concept of radiative forcing. A positive radiative forcing, such as that produced by increased concentrations of greenhouse gases, tends to warm the surface. A negative radiative forcing, which can arise from an increase in some types of aerosols, tends to cool the surface. Natural factors, such as changes in solar output or explosive volcanic activity, can also cause radiative forcing.

Characterization of these climate forcing agents and their changes over time is required to understand past climate changes in the context of natural variations and to project what climate changes could lie ahead. Keeping this in mind, this chapter compares the transmittance (obtained from the solar irradiance) of the MET Solar Radiation Sensor with that obtained from LAPS. Comparison of the transmittance values from these two instruments provides a better understanding of how air pollution episodes affect the amount of solar irradiation reaching the Earth's surface.

4.2 Solar Radiation Sensor

The P/N 100553 Solar Radiation Sensor is a Silicon Cell Pyranometer used for total sun and sky radiation measurement. The sensor operates over a spectral wavelength range of 0.35 to 1.15 microns with a nominal sensitivity of 50 mV/cal/cm^2/min. The sensor consists of a photovoltaic cell mounted under a transparent, glass dome [Online, Available: http://www.climatronics.comT]. The base of the sensor mounts to Radiation Sensor Mount P/N 101096 [Specifications in Table 4.1].

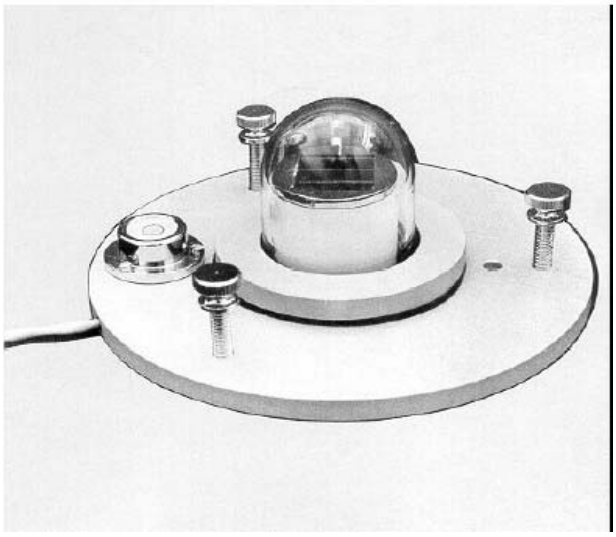

Table 4.1: Solar Radiation Sensor Specifications

Spectral Wavelength Range	0.35 to 1.15 microns
Output	1400 W/m^2 or 50 $mV/cal/cm^2/min$
Response Time	Less than 1 millisecond
Impedance	1.0 ohm
Temperature Compensation	40° to 140° F (4.5° to 60° C)
Weight	1 lb (0.45 kg)

4.3 LAPS – Solar Radiation Sensor Transmittance Comparison

To develop a continuous picture of the atmospheric extinction during the NEOPS-DEP 2002 summer campaign in Philadelphia, transmittance obtained from LAPS and the MET Tower Solar Radiation Sensor have been compared on a number of days in July, 2002.

Method:

Ground-based solar irradiance values, available from the radiation sensor, are used to calculate the vertical component of these irradiances at an altitude of 2 km, which is selected as a reference altitude, as shown in Figure 4.1.

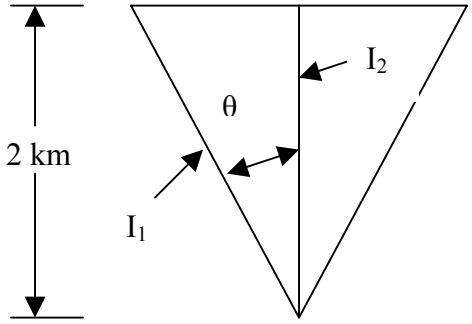

Figure 4.1: Met transmittance calculation using solar zenith angle

As seen in Figure 4.1, I_1 is the ground-based solar irradiance value, available from the radiation sensor, for a certain time of the day when the solar zenith angle has a value θ (degrees). Our calculation provides the vertical component of I_1, which is I_2, at an altitude of 2km. This calculation is repeated for every minute of the day so that we obtain the solar irradiance vertically above the Earth's surface at a common altitude of 2 km. The altitude of 2 km is selected as the reference altitude for comparison because this altitude represents the approximate top of the boundary layer, which contains most of the scattering aerosols on cloud-free days. The transmittance between the surface and this altitude is a measure of the important factor that accounts for the photochemistry within the boundary layer. The transmittance calculation uses the solar zenith angle on a minute-by-minute basis (using the NOAA Solar Position Calculator) to account for the difference in the path lengths traversed by the solar irradiance at different times of the day and the angular component of the solar irradiance. The transmittance is obtained from the vertical

component of the solar irradiance for every minute of the day under consideration, divided by the solar constant, which is 1370 W/m^2.

Transmittance for LAPS is calculated by smoothing the integrated extinction profiles at both visible (530 nm) and ultraviolet (284 nm) wavelengths. The visible measurements are present only at night, while the UV measurements are available for the entire day. The calculated extinction includes aerosol and molecular scattering, as well as the ozone absorption of the ultraviolet wavelengths. The lidar transmittance is calculated between the surface and 2 km for comparison with meteorological tower radiometer measurements described in the preceding paragraph.

Observations:

Several examples will be shown to compare the transmittance values of the two instruments for a few days in July 2002. For LAPS, the extinction due to molecular scattering is first calculated and removed from the total extinction to find the extinction due to aerosol scattering, and a Hanning filter is used to smooth the extinction values. At 284 nm, ozone absorption must also be removed from the total extinction to obtain the extinction due to aerosol scattering. The ozone concentration per cubic meter is first calculated by taking the product of the ozone concentration (parts per billion) and the corresponding atmospheric number density (per cubic meter). The resulting ozone concentration (per cubic meter) is multiplied by the ozone absorption cross-section at 266 nm on the uplag, which is 0.9×10^{-17} cm^2, and by the ozone absorption cross-section at 284 nm on the downlag, which is 0.3×10^{-17} cm^2 (obtained from the Hartley absorption

band) to yield the ozone absorption value. The transmittance for each bin range (75 m) is calculated using the formula:

$$tr2 = tr1 \times \exp(-ext_{total} \times 0.075),$$

where $tr1$ is the transmittance at one bin range altitude and $tr2$ is the transmittance at the next bin range altitude. The transmittance is calculated starting from the ground upward. Note that in all the cases that follow, the extinction used to calculate ultraviolet LAPS transmittance has been corrected for ozone absorption and molecular scattering.

The first case we study is July 31, 2002. As seen in Figure 4.2, this is a relatively clear day with average ultraviolet extinction above 0.5 km in the range of 0.5-1 km^{-1}. However, at altitudes below 0.5 km, the average ultraviolet extinction is in the range of 2.5-3 km^{-1}, which corresponds to an ultraviolet (284 nm) transmittance of 0.3-0.4. The LAPS (530 nm) visible transmittance at night is approximately 0.7 on the average, and this is found to line up quite well with the meteorological tower radiometer transmittance during the day. The dips in the LAPS transmittance values are due to invalid data present at those times, and need not be taken into consideration. An important point to be noted here is that repeated dips in the Met transmittance values are observed every hour on the hour and is probably due to encoder errors at the beginning of each hour. However, the dips in the Met transmittance values around noon are due to clouds passing over the radiometer. It is interesting to note that these dips are accompanied by peaks at the edges, which are due to sunlight scattering from the cloud as it enters and leaves the region directly on the path of the Met radiometer.

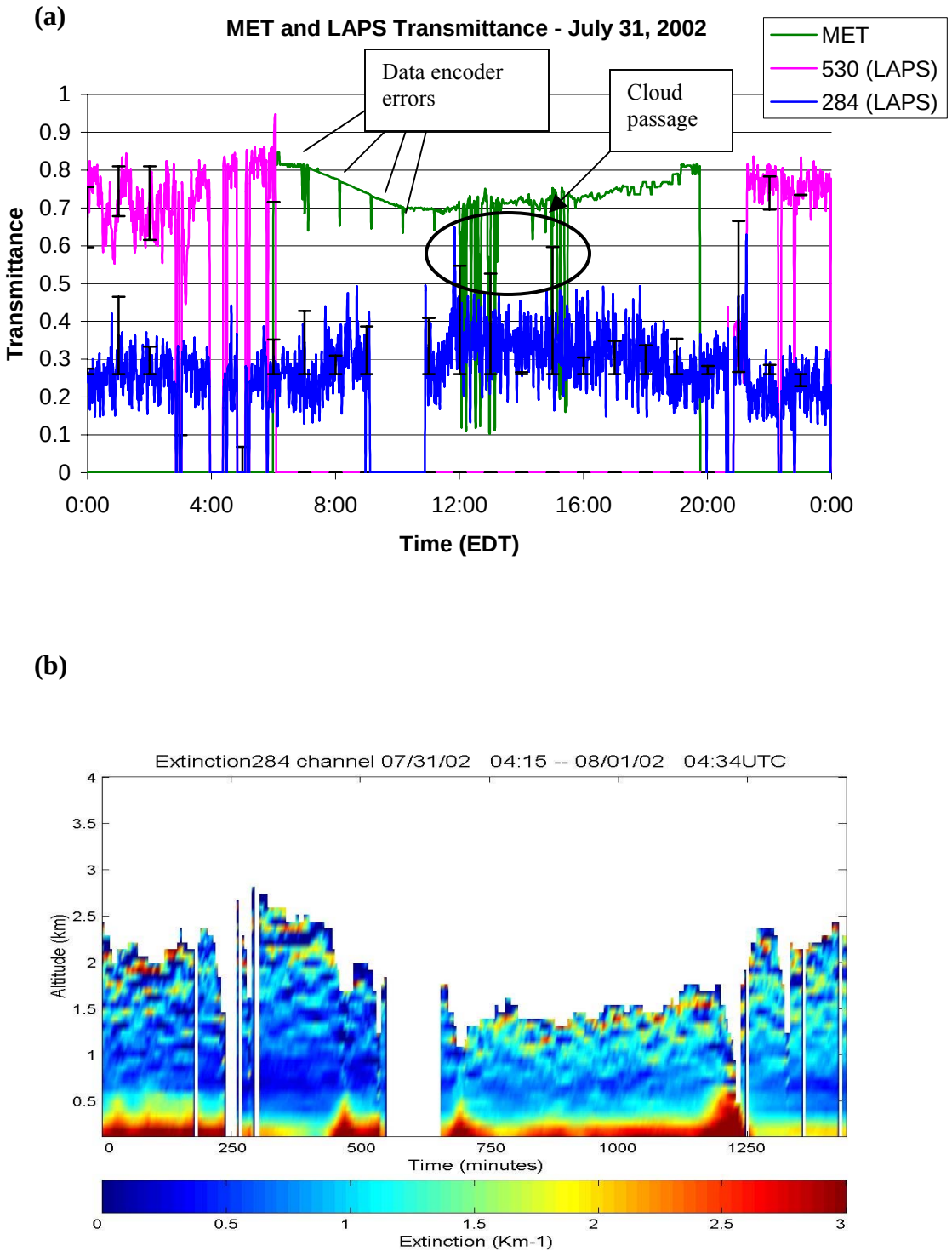

Figure 4.2: Data from July 31, 2002 (a) MET and LAPS visible transmittance are relatively high (~0.7) (b) the ultraviolet extinction contributes to UV transmittance of 0.3-0.4.

The next case is July 4, 2002, which was also a relatively clear day with average ultraviolet extinction approximately equal to 0.8 km^{-1}, corresponding to an average ultraviolet transmittance of approximately 0.2. Once again, we find that the visible LAPS (530 nm) transmittance at night lines up quite well with the daytime Met transmittance at sunrise and sunset, both showing an average value of about 0.7, as seen in Figure 4.3.

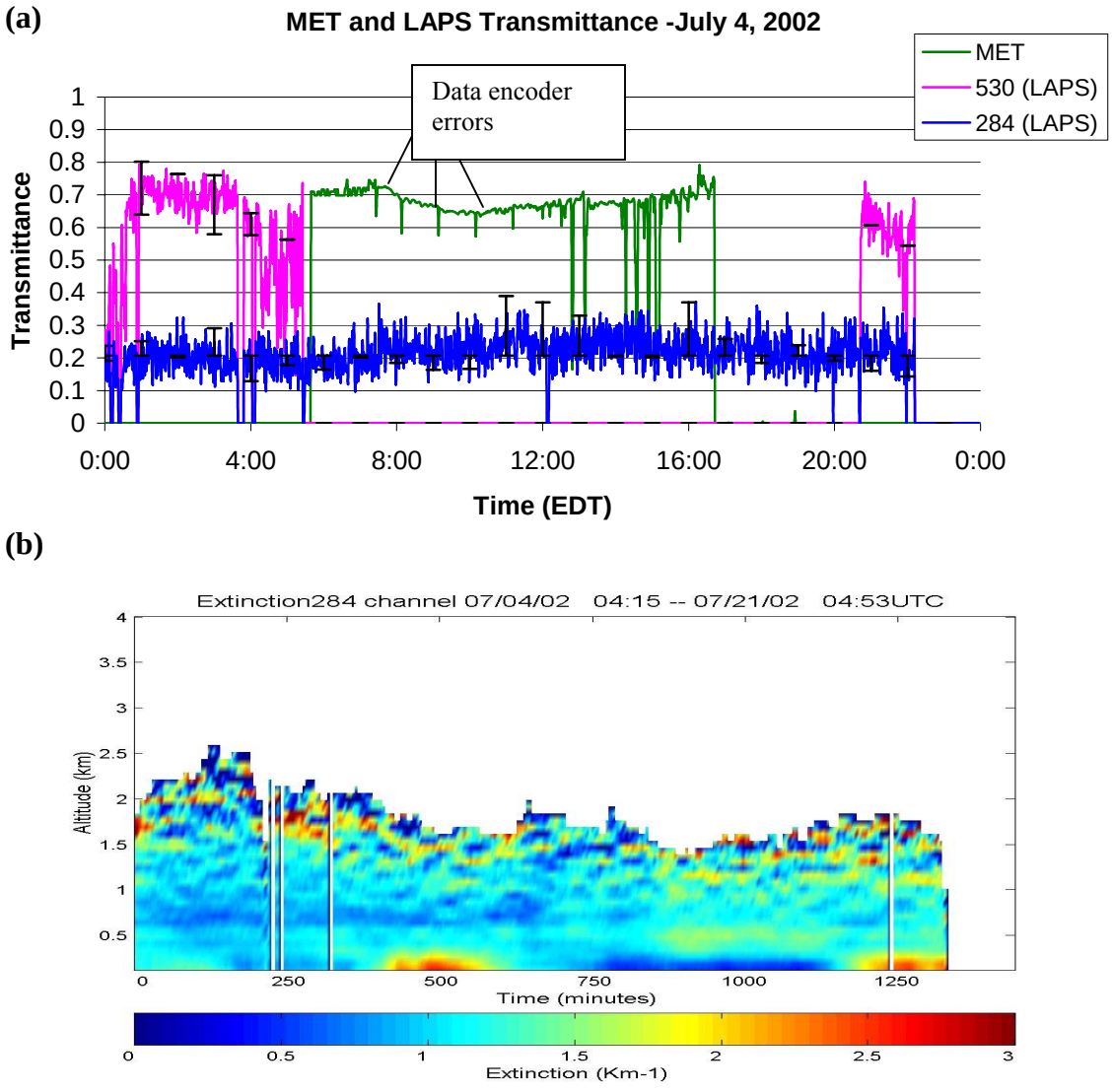

Figure 4.3: Data from July 4, 2002 (a) MET and LAPS visible transmittance are relatively high (~0.7) (b) the ultraviolet extinction contributes to UV transmittance of ~0.2.

Another case worth examining is July 23, 2002, as shown in Figure 4.4. This was a rather interesting day because moderate values of ultraviolet extinction, in the range of 0.5 to 1 km^{-1}, are observed from 0000-0800 hrs EDT, after which the extinction value rises to approximately 3 km^{-1} and remains high from 0800-2100 hrs EDT.

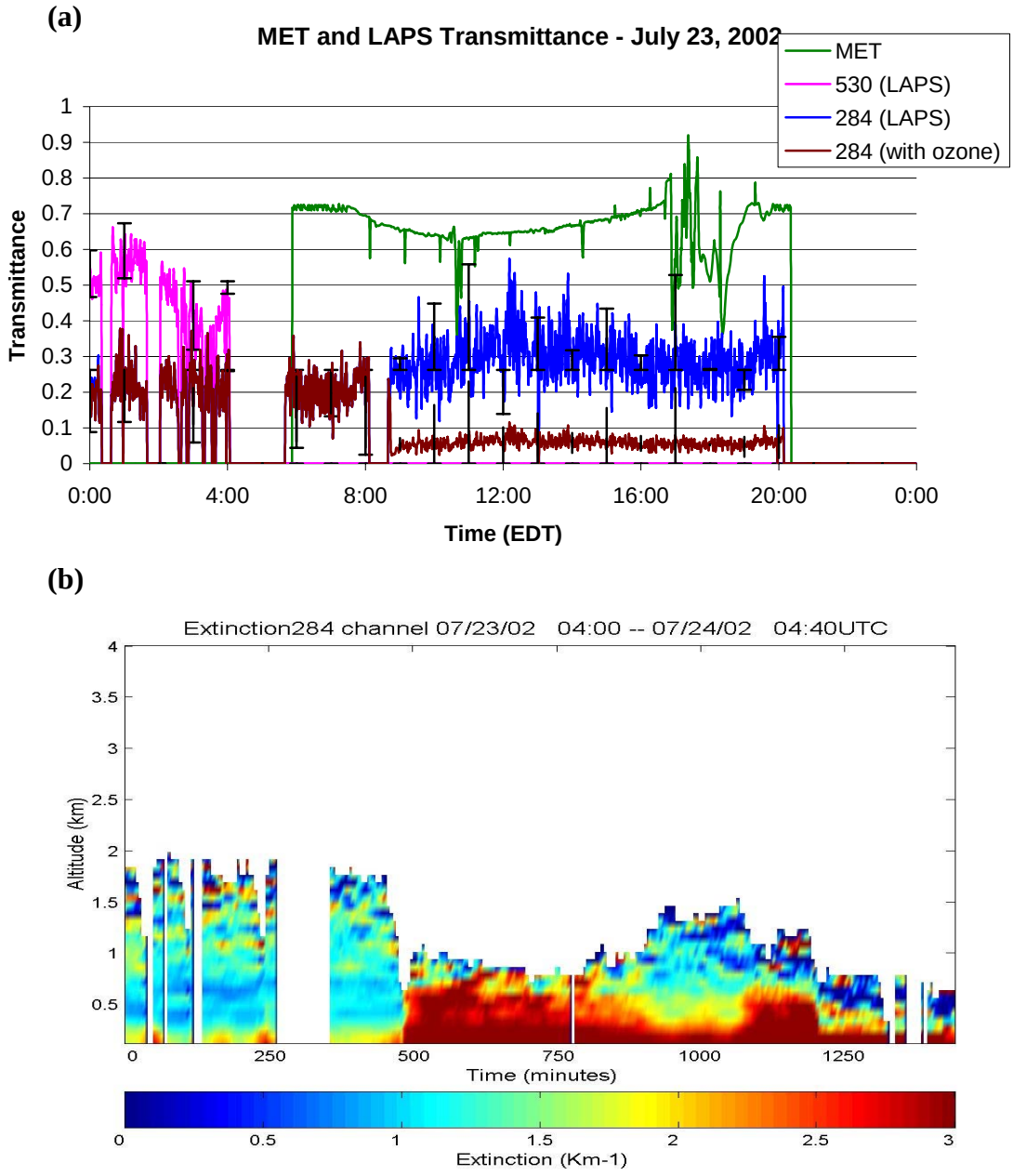

Figure 4.4: (a) MET and LAPS transmittance and (b) LAPS ultraviolet extinction on July 23, 2002.

An important point to note here is that the ozone absorption contributes to about 55% of the total extinction during the mid-day hours of July 23. Thus, the actual ultraviolet extinction due to scattering is only about 1.35 km^{-1} (after subtracting 55% of the observed extinction to account for ozone absorption). This corresponds to an ultraviolet transmittance of about 0.26, which is consistent with the calculated transmittance of approximately 0.28, as observed in Figure 4.4(a). Also seen in Figure 4.4(a) is a drop in the ultraviolet transmittance when ozone is not removed from the calculation. This is expected because ozone contributes to a major percentage of the observed ultraviolet extinction, and thus causes a corresponding decrease in the observed transmittance when not removed. In addition, the slight rise in the ultraviolet transmittance a little before noon is probably due to a decrease in the observed sulfate and nitrate concentrations at this time observed in the surface measurements [Clark, 2002], which causes the overall aerosol concentration to drop. As expected, the average Met transmittance during the day drops to about 0.65, which is consistent with increased values of extinction during the same time period. However, the visible LAPS (530 nm) transmittance during the early morning hours drops to about 0.4, which is probably due to fog formation at this time, based on the high relative humidity values of approximately 90%.

As a final case study, we analyze July 2, 2002, when a haze event developed in the region, resulting in increased integrated ultraviolet extinction, approximately equal to 2.5, and a corresponding decrease in the LAPS transmittance, as compared to the clearer days (July 4 and July 31) we observed earlier. As seen in Figure 4.5(a), the average transmittance at 530 nm is only about 0.5, as compared to average 530 nm transmittance values of approximately 0.7 on July 31 and July 4. In addition, the average 284 nm

transmittance drops from about 0.3-0.4 on July 31 and approximately 0.25 on July 4 to about 0.1-0.2 on July 2. An important point to note here is that the ozone concentration was very high starting at about 1100 hrs EDT on July 2, in the range of 100 ppb, which corresponds to an ozone absorption value of approximately 74%. Thus, the extinction purely due to scattering is only about 0.65 km^{-1} (after subtracting 74% of the observed extinction to account for ozone absorption). This corresponds to an ultraviolet transmittance of approximately 0.27, which is found to be consistent with the calculated ultraviolet transmittance during the same time period, as shown in Figure 4.5(a). As was the case on July 23, a drop in the ultraviolet transmittance is observed a little before noon when ozone is not removed from the calculation. This is expected because ozone contributes to 74% of the observed ultraviolet extinction during this time period, and thus causes a corresponding decrease in the observed transmittance when not removed. In addition, the slight rise in the ultraviolet transmittance a little before noon is, as was on July 23, due to a decrease in the observed sulfate and nitrate concentrations at this time, which causes the overall aerosol concentration to drop. Figure 4.5(a) does not show MET transmittance because the MET tower was not operational on July 2. The high extinction and decreased transmittance values are further corroborated by the fact that increased $PM_{2.5}$ concentrations are observed in the region on July 2, rising from 40 $\mu g/m^3$ on July 1 to 80 $\mu g/m^3$ on July 2, as seen in Figure 4.6.

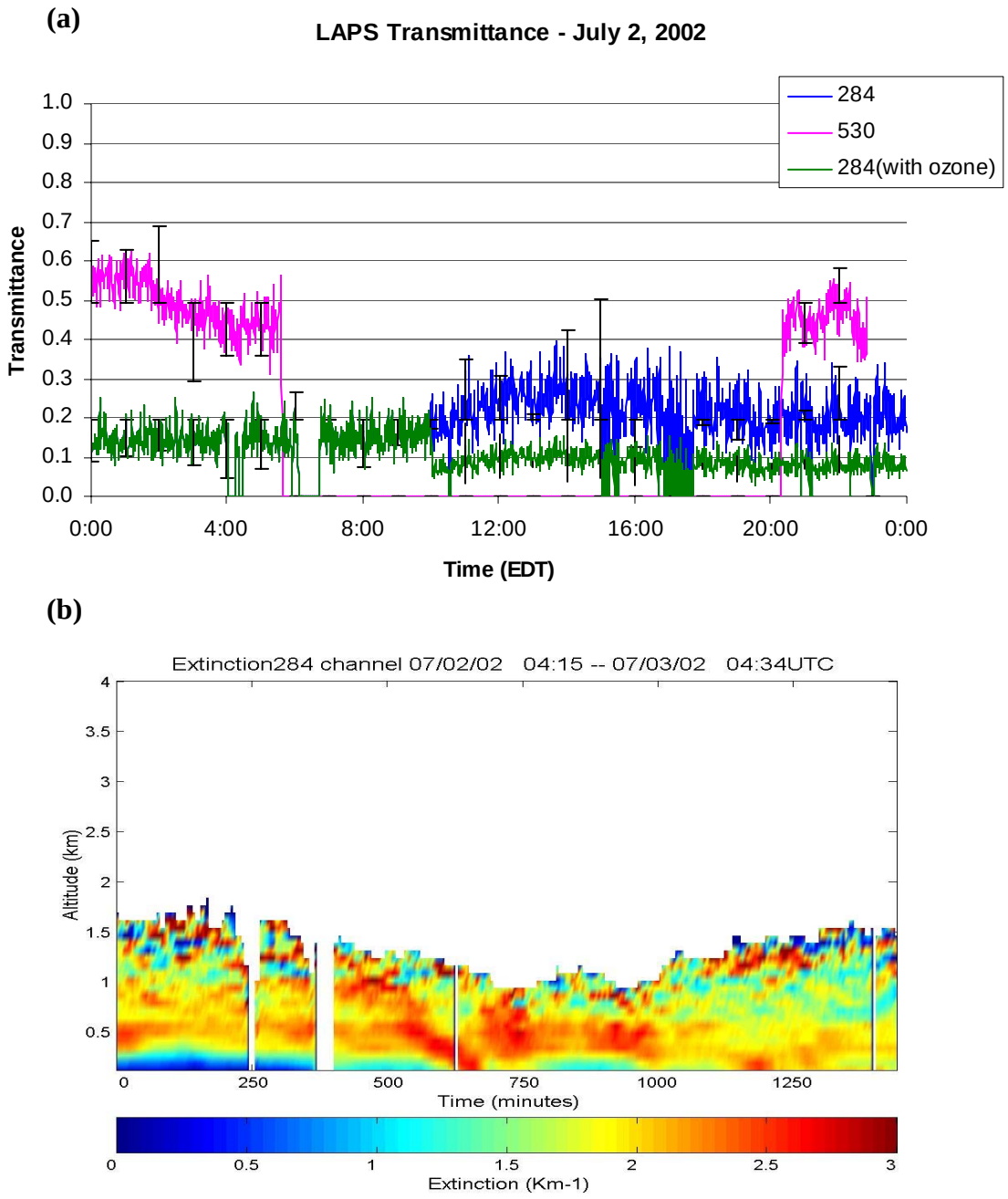

Figure 4.5: (a) Decreased LAPS transmittance and (b) corresponding high extinction on July 2, 2002.

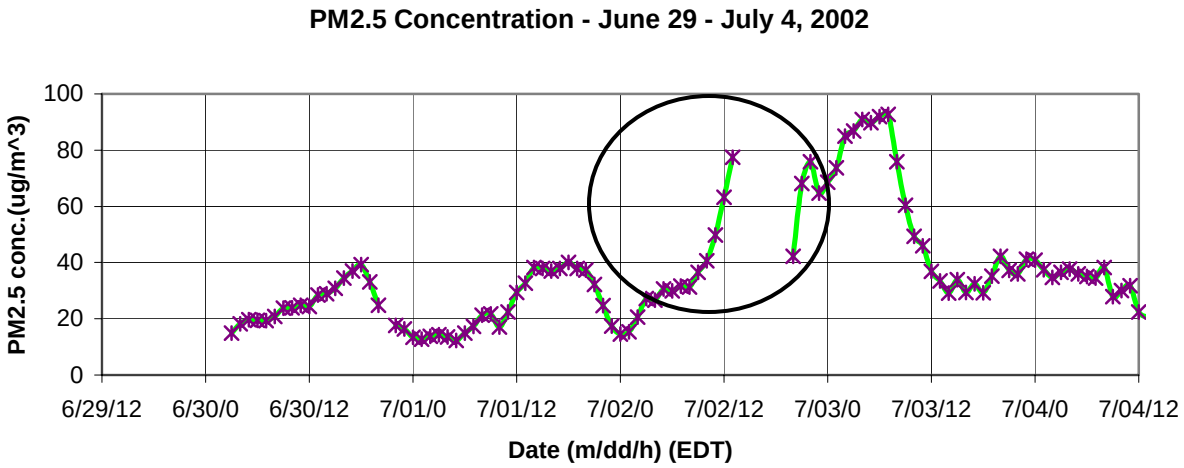

Figure 4.6: $PM_{2.5}$ concentration from June 29 to July 4, 2002 [Hopke, 2002]

Thus, as seen in the preceding examples, the visible LAPS transmittance is found to be relatively high (~0.7) on haze-free days such as July 4 and July 31, 2002. However, on July 2, when a haze event developed in the region, the visible transmittance dropped by almost 0.2 (from an average value of 0.7 to about 0.5), which is consistent with increased $PM_{2.5}$ and extinction values in the region. This is because a transmittance of 0.7 corresponds to an extinction of 0.18 km^{-1} (tr = 0.7, thus $\int_0^2 \alpha dx = 0.36$, which gives α = 0.18), whereas a transmittance of 0.5 corresponds to an extinction of 0.35 km^{-1} (tr = 0.5, thus $\int_0^2 \alpha dx = 0.69$, which gives α = 0.35), and this increase in the extinction is consistent with the increase in $PM_{2.5}$. Also, the ultraviolet extinction is found to be consistent with the ultraviolet transmittance values after accounting for the ozone absorption at 284 nm.

Finally, the general consistency between the LAPS transmittance at night and the Met tower radiation sensor transmittance during the day provides a more complete picture of the dynamics related to optical extinction.

CHAPTER 5

A COMPARATIVE ANALYSIS OF AEROSOL OPTICAL DEPTH USING LAPS, MET, AND NEPHELOMETER DATA

5.1 Introduction

The decrease in planetary absorption of short-wave radiation due to scattering by anthropogenic aerosols during clear-sky conditions, termed direct aerosol radiative forcing, is estimated to be roughly 1 Wm^{-2} on a global annual average [Charlson et al., 1992, Kiehl et al., 1993], and may be as high as 50 Wm^{-2} locally and instantaneously near source regions [Schwartz, 1996].

The key aerosol property governing direct shortwave radiative forcing is Aerosol Optical Depth (AOD). The AOD is a measure of how much light is prevented by airborne particles from passing through a column of atmosphere. Aerosols tend to absorb and scatter incoming sunlight, thus reducing visibility (transmittance) and increasing the optical depth. An aerosol optical depth of 0.1 indicates a relatively clear sky with high visibility (or transmittance), whereas a value of 4 (1.8% transmittance) indicates the presence of aerosols so dense that it would be hard to see the shape of the sun at mid-day. Aerosols are scientifically important because they represent an area of great uncertainty in efforts to understand and predict global climate change. For example, the climate model computations of Hansen et al. (1980) indicate that an increase in average aerosol optical depth of 0.1 would cool the earth's surface by about 1°C.

In this chapter, the AOD from extinction profiles measured using LAPS and the MET tower data are compared with the Millersville University TSI integrating

nephelometer scattering coefficients on three days in the month of July 2002. These measurements were made during the NEOPS-DEP summer campaign in Philadelphia, PA.

5.2 LAPS-MET Optical Depth Comparison

Method:

The AOD can be expressed in terms of the aerosol extinction coefficient, as

$$\text{AOD} = \int_0^\infty \alpha(\lambda, z)dz \,,$$

where $\alpha(\lambda, z)$ is the vertical profile of the aerosol extinction coefficient as a function of wavelength λ and z is the altitude over which the extinction is integrated. For LAPS, the smoothed extinction coefficient is integrated at a wavelength of 530 nm over an altitude of 2 km, which is taken to be the extent of the mixing layer, as observed in the water vapor time sequences.

Since the radiometer on the Met tower measures the intensity at the ground, the AOD is obtained from Beer's Law as

$$I = I_o \times \exp(-\text{AOD} \times \text{AMF}),$$

where I_o is the intensity at the top of the atmosphere and AMF is the airmass factor. The AMF describes the enhancement of the slant path over the vertical, approximated by

$$\text{AMF} = [\cos(\text{SZA})]^{-1},$$

where SZA (Solar Zenith Angle) [Kasten and Young, 1989].

This expression for the AMF holds as long as the sun is fairly high in the sky (SZA<70^o corresponding to AMF<3). Otherwise, a modified expression should be used which accounts for the sphericity of the Earth,

$$AMF = [\cos(SZA) + 0.50572(1.46468 - SZA)^{-1.6364}]^{-1}.$$

Observations/Analysis:

The following figures (5.1-5.8) show the comparative aerosol optical depths for the two instruments on July 3, July 22 and July 23, 2002. The LAPS AOD is calculated for the visible wavelength of 530 nm. The AOD's are compared for the duration of the three days. However, it is important to note that LAPS did not have readings at visible wavelengths during the day, since the visible channels remain closed. Also, the solar radiometer on the meteorological tower only obtained useful readings between about 1030 and 1600 hrs local, because the cosine of the solar zenith angle is zero atsunrise and at sunset.

As observed in Figure 5.1, on July 3, 2002, the LAPS AOD shows an increase, from 0.4 to approximately 0.7, at about 0330 hrs EDT, which is at the same time as an increase in the visible and UV extinction. The visible extinction rises to about 0.75 km^{-1}. This is consistent with an increase in the AOD from 0.4 to 0.7.

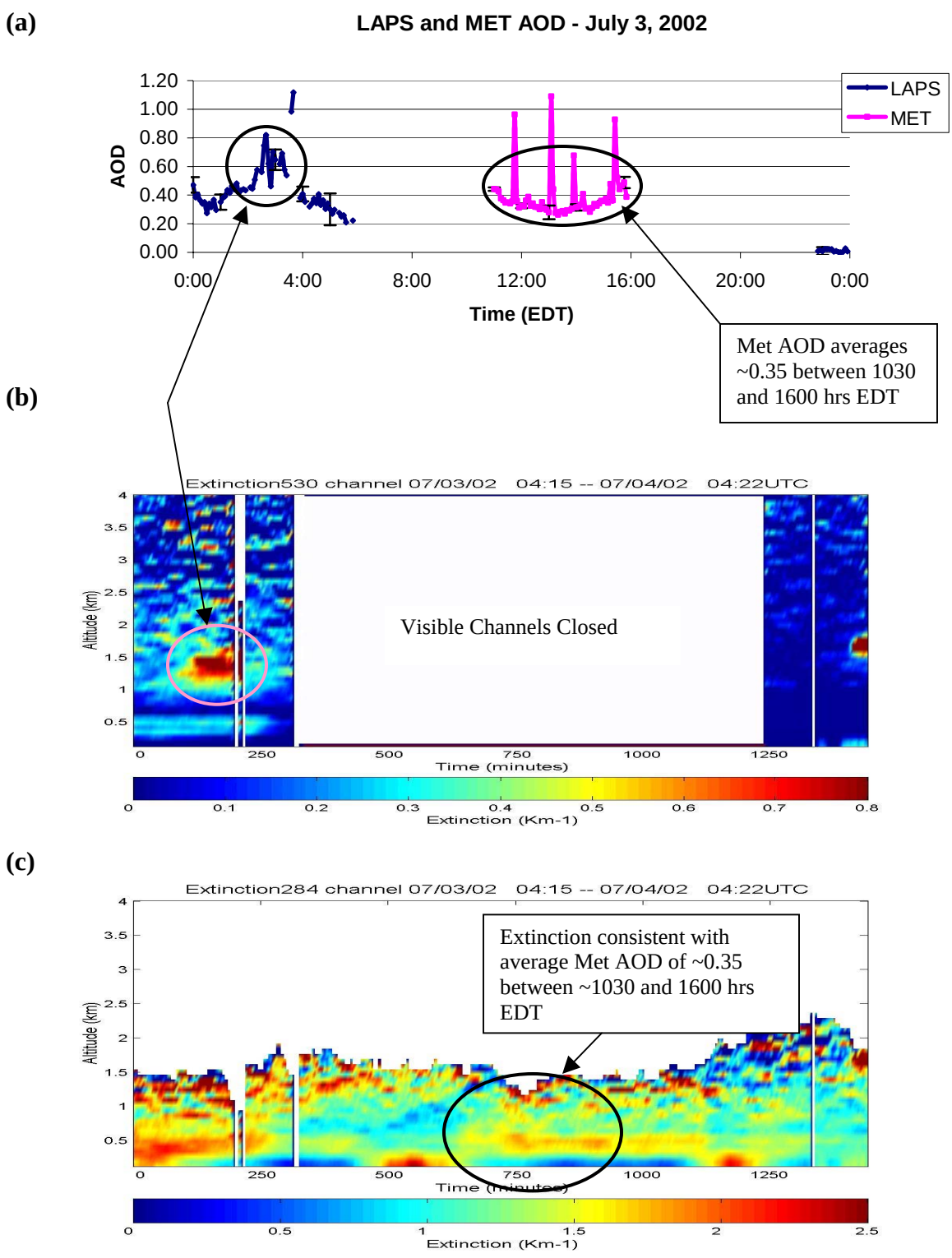

Figure 5.1: (a) Plots of aerosol optical depth (AOD), (b) visible extinction and (c) ultraviolet extinction on July 3, 2002.

The UV extinction is in the range of 1.5 to 2 km^{-1}. However, it is important to note that the ozone concentration around the same time is approximately 70 to 80 ppb, which gives an ozone absorption value of about 55%. Thus, 55% of the UV extinction is due to ozone absorption, which makes the extinction due to aerosols about 0.7 to 0.9 km^{-1} (45% of the observed extinction). Note that increased values of scattering are observed around the same time period as the rise in extinction and LAPS AOD, as shown in Figure 5.2.

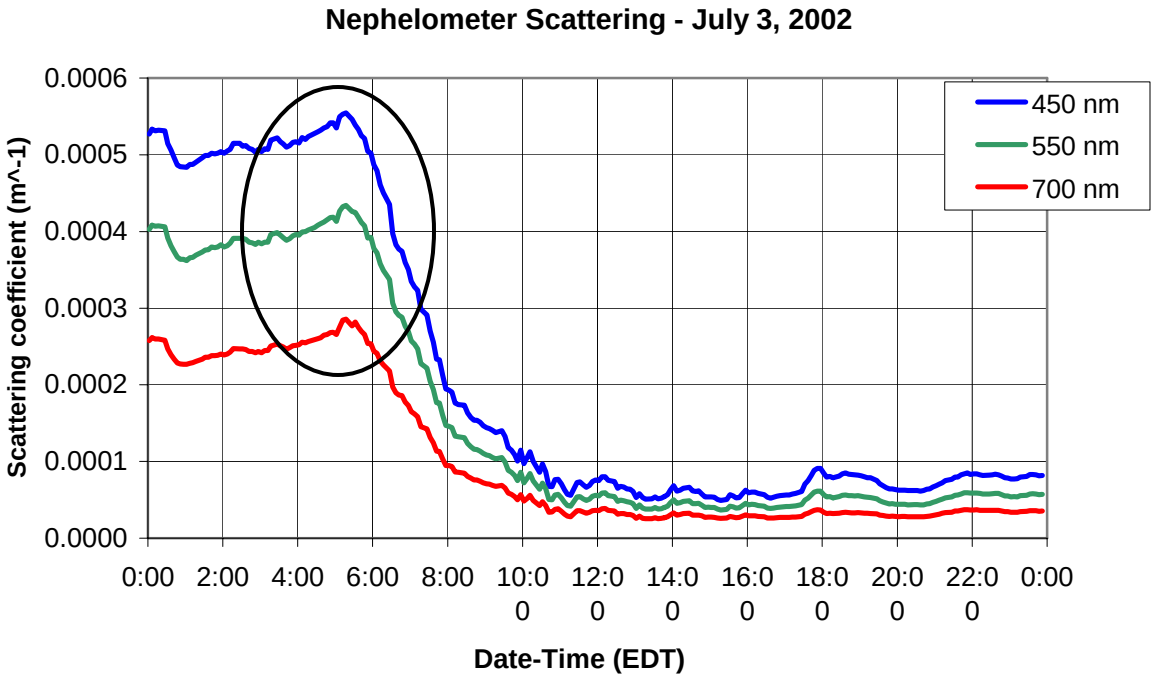

Figure 5.2: Nephelometer Total Scattering Coefficient on July 3, 2002 [Clark, Millersville University]

The Met AOD is found to have an average value of approximately 0.35 through the duration of its operation between 1030 to 1600 hrs EDT. The UV extinction between the surface and approximately 300m at the same time averages about 1 km^{-1}. At this time, the ozone concentration is only about 50 ppb, giving an absorption value of

approximately 35%. This indicates that 65% of the increased UV extinction observed (0.65 km^{-1}) is due to aerosols, which corresponds to an AOD of ~0.2 (0.65 $km^{-1} \times 0.3$ km). This is found to be relatively consistent with a Met AOD of 0.35. A point to be noted here is that the sudden spikes in the Met AOD are probably due to clouds passing through the field of view of the radiometer at those times.

The next case we study is that of July 22, 2002. As shown in Figure 5.3, values of LAPS AOD are in the range of 0.4 to 1.4, with a mean of about 0.64, from 0200 to 0400 hrs EDT. The visible extinction values are in the range of 0.9 to 1 km^{-1} between 1.2 and 1.8 km and ~0.5 km^{-1} between 1 and 1.2 km during the same time period, which corresponds to an AOD of approximately 0.7. This is found to be quite consistent with the mean LAPS AOD of 0.64. The Met AOD is found to range from 0.3-0.5, with an average value of approximately 0.4, through the duration of its operation, from around 1030-1600 hrs EDT. As shown in Figure 5.4, the UV extinction between the surface and approximately 700 m at the same time averages about 3 km^{-1}. The ozone concentration during this time period is approximately 70-80 ppb, which gives an ozone absorption value of about 55%. Thus, only a little less than half of the observed UV extinction is due to aerosols, which amounts to an extinction of about 1.35 km^{-1} (45% of the observed extinction). This corresponds to an AOD of ~0.9, which is much higher than the average Met AOD of 0.4. An interesting point to be noted here is that the moderately high values of UV extinction (1.35 km^{-1}) purely due to scattering are observed around the same time as a moderate increase in the nephelometer scattering values, as shown in Figure 5.5 (shown circled).

(a)

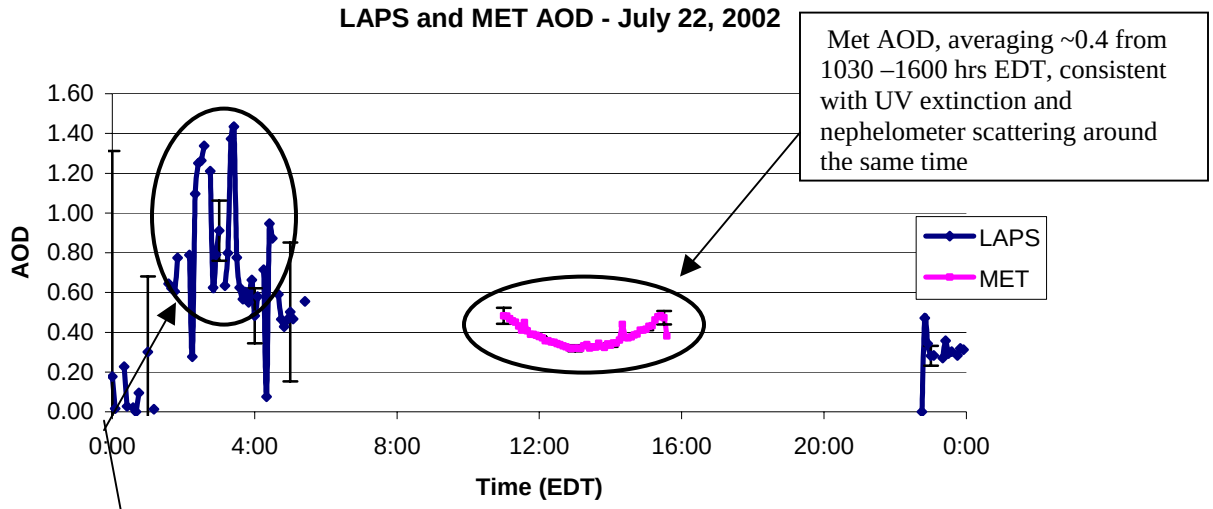

(b)

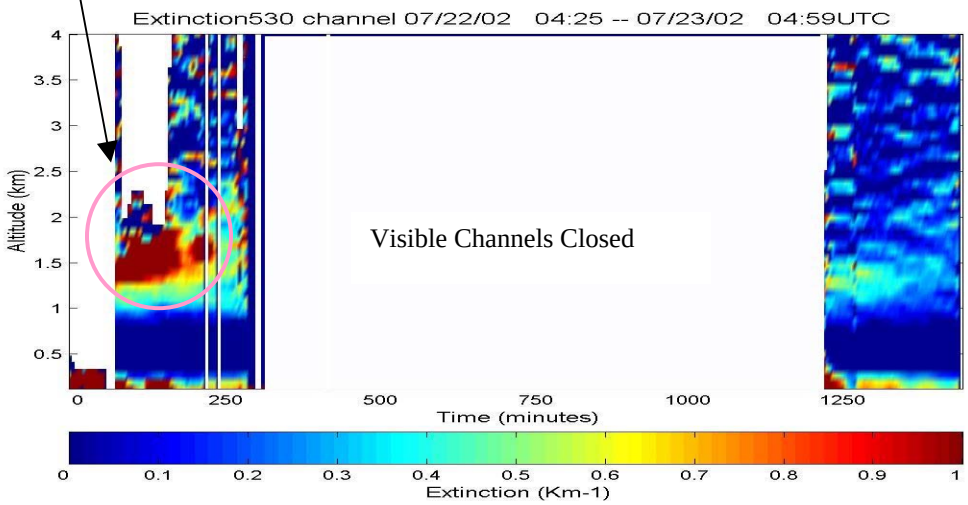

Figure 5.3: Plots of (a) AOD and (b) visible extinction on July 22, 2002.

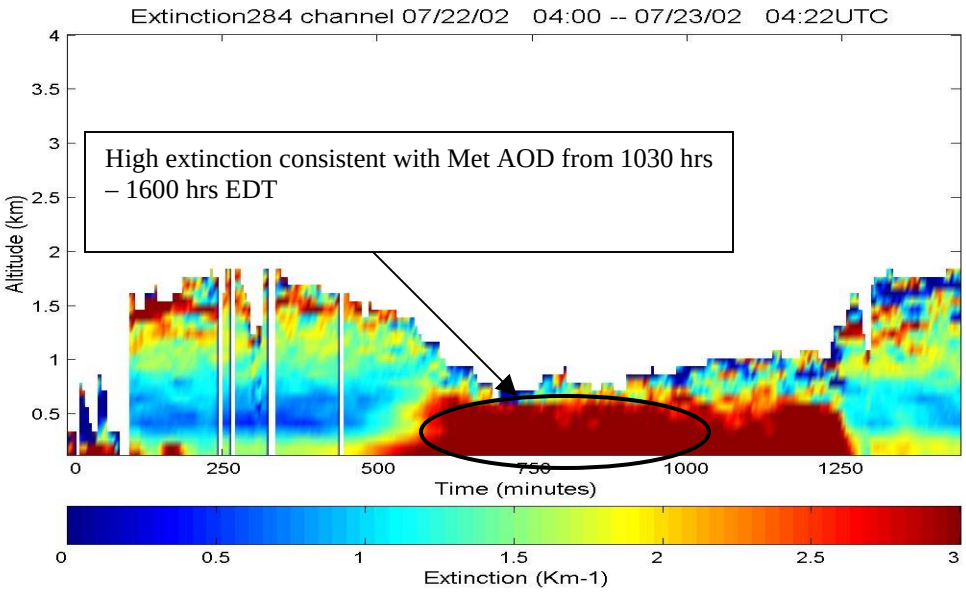

Figure 5.4: Plot of UV extinction on July 22, 2002

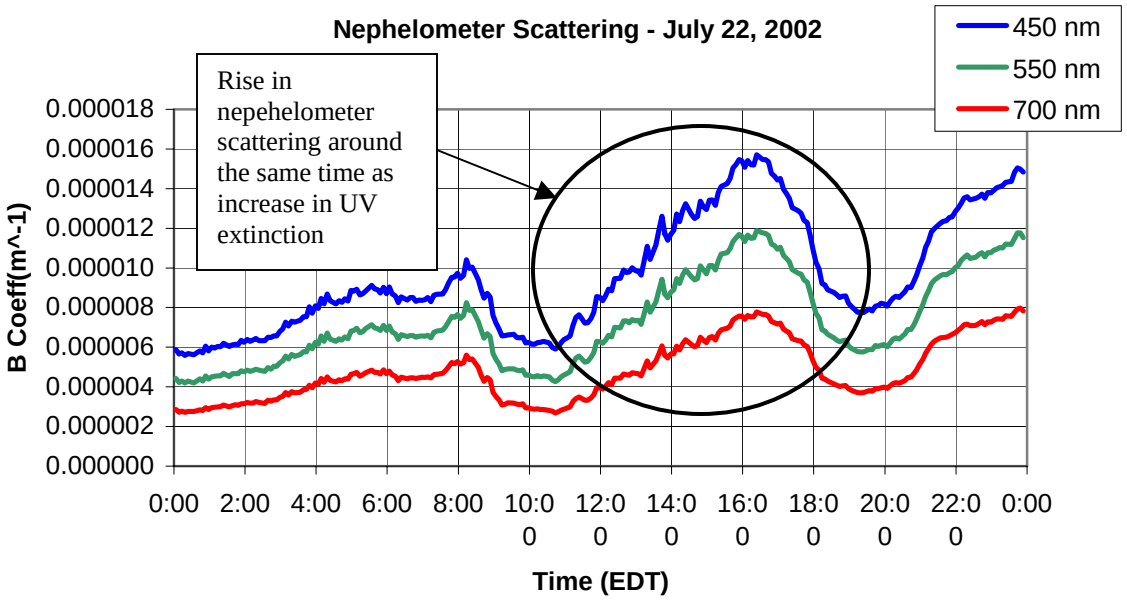

Figure 5.5: Nephelometer Total Scattering Coefficient on July 22, 2002 [Clark, Millersville University]

As a final case study, we analyze July 23, 2002. This was a day of high extinction, although the extinction did not really increase until about 0800 hrs EDT. As a result, the early morning LAPS AOD is only about 0.2, as is corroborated by the relatively low extinction values seen in the visible and UV extinction plots. The visible extinction is in

the range of 0.3 to 0.4 km^{-1} between 1.2 and 2 km, which results in an AOD of ~0.24. This is found to be consistent with the LAPS AOD of 0.2. The Met AOD is found to range from 0.35-0.5, with an average value of approximately 0.4, through the duration of its operation, from around 1030-1600 hrs EDT. As shown in Figure 5.7, the UV extinction between the surface and approximately 500 m at the same time averages about 2.5-3 km^{-1}. However, the ozone concentration during this time period is about 70 to 80 ppb, which gives an ozone absorption value of approximately 55%. Thus, the aerosols contribute to only a little less than half of the observed UV extinction, which amounts to an extinction value of about 1.1 to 1.35 km^{-1}. This corresponds to an AOD of ~0.5 (1.1 $km^{-1} \times 0.5$ km), which is quite consistent with the average Met AOD of 0.4.

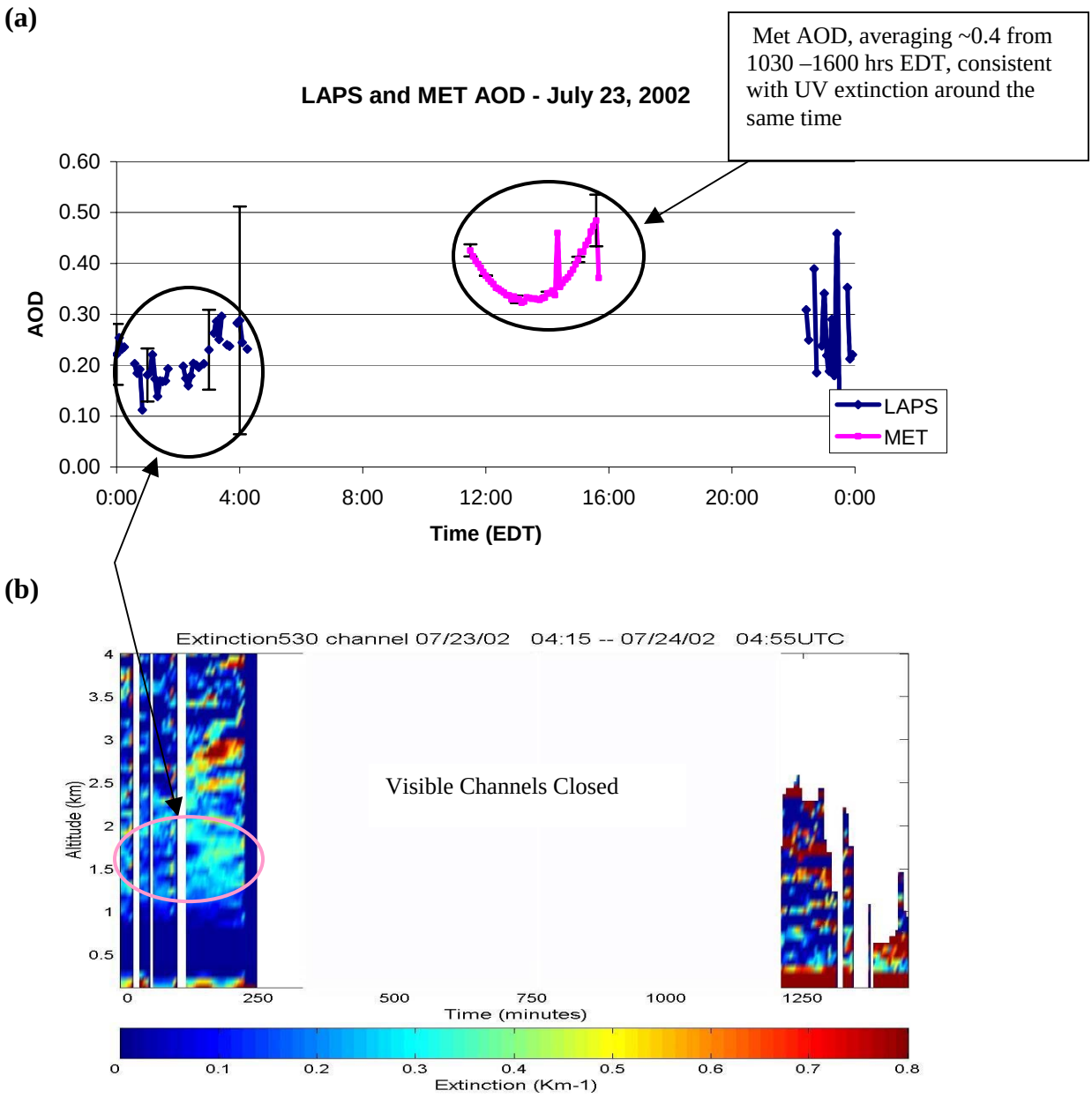

Figure 5.6: Plots of (a) AOD and (b) visible extinction on July 23, 2002.

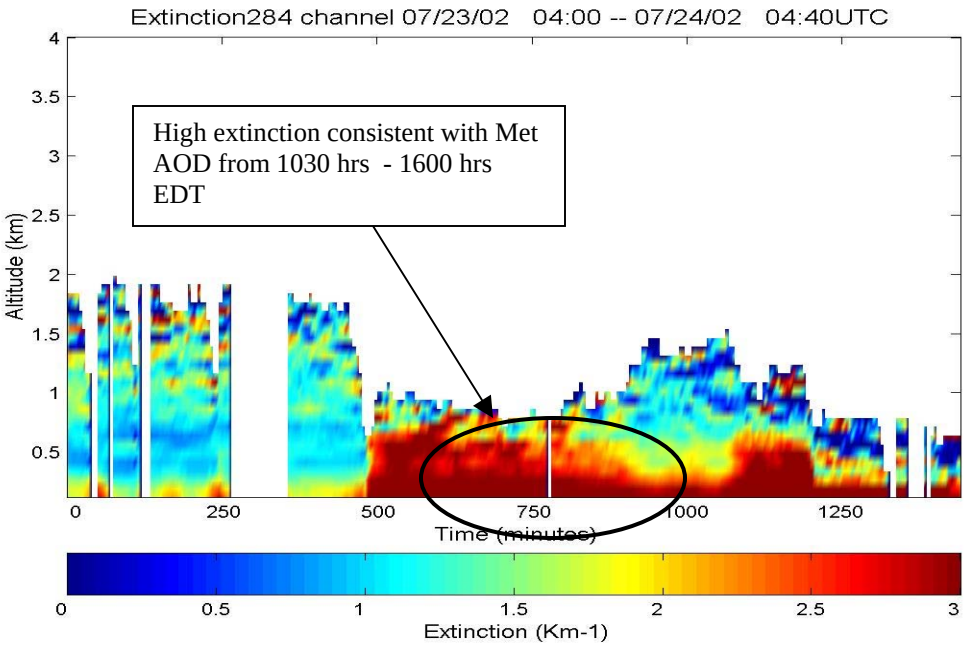

Figure 5.7: Plot of UV extinction on July 23, 2002.

5.3 Summary

Aerosol Optical Depth from LAPS and Met instruments have been compared and analyzed using data obtained during the NEOPS-DEP summer 2002 campaign in Philadelphia. The comparisons have been made on three days in July 2002.

On July 3, 2002, the LAPS AOD shows an increase, from 0.4 to approximately 0.7, at about 0330 hrs EDT, which is at the same time as an increase in the visible and UV extinction. The visible extinction rises to about 0.75 km^{-1} between 1.1 and 1.5 km, which corresponds to an increase in AOD of approximately 0.3 (0.75 km^{-1} $\times$0.4 km). This is consistent with an increase in the AOD from 0.4 to 0.7. The Met AOD is found to have an average value of approximately 0.35 through the duration of its operation, from around 1030-1600 hrs EDT. The UV extinction between the surface and approximately 300m at the same time averages about 1 km^{-1}. At this time, the ozone concentration is

only about 50 ppb, giving an absorption value of approximately 35%. This indicates that 65% of the increased UV extinction observed (0.65 km^{-1}) is due to aerosols, which corresponds to an AOD of ~0.2 compared with a Met AOD of 0.35.

On July 22, 2002, values of LAPS AOD are in the range of 0.6 to 1.4, with a mean of about 0.67, from 0330 to 0400 hrs EDT. The visible extinction values are in the range of 0.9 to 1 km^{-1} between 1.2 and 1.8 km and ~0.5 km^{-1} between 1 and 1.2 km during the same time period, which corresponds to an AOD of about 0.7. This is found to be quite consistent with the mean LAPS AOD of 0.67. The Met AOD is found to range from 0.3-0.5, with an average value of approximately 0.4, through the duration of its operation, from around 1030-1600 hrs EDT. The UV extinction between the surface and approximately 700m at the same time averages about 3 km^{-1}. The ozone concentration during this time period is approximately 70-80 ppb, which gives an ozone absorption value of about 55%. Thus, only a little less than half of the observed UV extinction is due to aerosols, which amounts to an extinction of about 1.35 km^{-1} (45% of the observed extinction). This corresponds to an AOD of ~0.9, which is found to be higher than the average Met AOD of 0.4. An interesting point to be noted here is that the moderately high values of UV extinction (1.35 km^{-1}) purely due to scattering are observed around the same time as a moderate increase in the nephelometer scattering values.

On July 23, 2002, the extinction does not rise until about 0800 hrs EDT. As a result, the early morning LAPS AOD is rather low, averaging only about 0.2, which is consistent with the relatively low values of extinction observed in both the visible and UV time sequences. The visible extinction is in the range of 0.3 to 0.4 km^{-1} between 1.2 and 2 km, which corresponds to an AOD of ~0.24. This is found to be consistent with the

LAPS AOD of 0.2. The Met AOD is found to range from 0.35-0.5, with an average value of approximately 0.4, through the duration of its operation, from around 1030-1600 hrs EDT. The UV extinction between the surface and approximately 500m at the same time averages about 2.5-3 km^{-1}. However, the ozone concentration during this time period is about 70 to 80 ppb, which gives an ozone absorption value of approximately 55%. Thus, the aerosols contribute to only a little less than half of the observed UV extinction, which amounts to an extinction value of about 1.1 to 1.35 km^{-1}. This corresponds to an AOD of ~0.5, which is quite consistent with the average Met AOD of 0.4.

Thus, we find that the LAPS and MET aerosol optical depths compared provide a measure of the amount of solar irradiance reaching the Earth's surface. On days of high early morning extinction, such as July 3 and July 22, the LAPS AOD is in the range of 0.5 to 1.4, whereas on a relatively clear morning, such as the one on July 23, the LAPS AOD averages only about 0.2.

To better understand the effect of atmospheric extinction on particle size distribution, and the percentage of atmospheric extinction due to scattering and that due to absorption, it is necessary to examine the Angstrom exponent and single scattering albedo, which will be presented in the next chapter.

CHAPTER 6

SINGLE SCATTERING ALBEDO AND ANGSTROM EXPONENT

6.1 Introduction

Aerosols have been found to play a key role in the Earth's radiation budget and climate. Aerosols have a direct radiative effect by scattering and absorbing solar radiation and also have an indirect radiative effect by serving as cloud condensation nuclei (CCN), changing cloud microphysics and thereby the cloud albedo. There is, however, a large uncertainty in the evaluation of the aerosol radiative forcing due to a lack of our ability to describe aerosol size distributions and properties.

The aerosol size distribution is considered the most prominent physical property of the aerosol because it determines the optical scattering intensity and distribution

In this chapter, two parameters that are useful in better understanding the variation of aerosol size distribution are presented and analyzed: the single scattering albedo and the Angstrom exponent. The analysis has been made for a few days in the month of July 2002, as part of the NEOPS-DEP summer campaign in Philadelphia. The reason for analyzing these days in particular is to show the effects associated with high extinction on these days, and to compare with data available from other instruments.

We begin with an explanation of how to calculate the single scattering albedo and Angstrom exponent. We then analyze these parameters, beginning with a relatively clear day, and later moving on to episodes of high extinction. The chapter concludes with a summary of the important observations and inferences.

6.2 Single Scattering Albedo and Its Calculation

The single scattering albedo (ω) is defined as the ratio of the scattering coefficient to the extinction coefficient, and measures the ratio of extinction by scattering, Q_{sca}, to total extinction during a single interaction of a photon beam with a particle.

$$\omega = \frac{Q_{sca}}{Q_{sca} + Q_{abs}}$$

The scattering coefficient, Q_{sca}, at 550 nm is obtained from the Millersville University nephelometer, and the absorption coefficient, Q_{abs}, at 550 nm is obtained from the Clarkson University aethalometer. The ratio of the scattering coefficient to the sum of the scattering and absorption coefficients is then calculated to yield the single scattering albedo. The single scattering albedo, then, indicates the percentage of atmospheric extinction due to scattering and that due to absorption. An important point to be noted here is that the single scattering albedo provides a useful quantity as long as the scattering by aerosols is not very high. As the particulate scattering reaches higher values, multiple scattering comes into play. Multiple scattering has been found to be small for visible wavelength lidar scattering from clear air or haze, but a large component in the presence of fog or clouds [Van de Hulst, 1980].

Figure 6.1 shows an example of the single scattering albedo calculation for July 22, 2002. The extinction was relatively low from 0000-0800 hrs EDT, which is consistent with decreasing values of the single scattering albedo. From 0800 hrs to approximately 2000 hrs EDT, the extinction is found to increase, and this is consistent with increasing values of the single scattering albedo, as seen in Figure 6.1

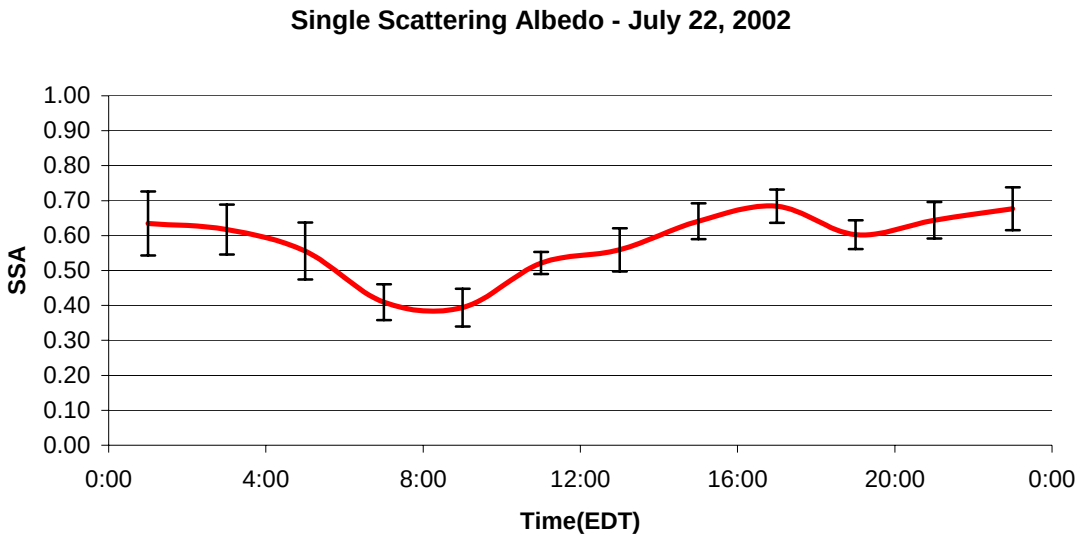

Figure 6.1: Single Scattering Albedo on July 22, 2002.

6.3 Angstrom Exponent and Its Calculation

The Angstrom Exponent is defined as the log-slope exponent of the optical thickness between two wavelengths [Gerber and Hindman, 1982].

$$\alpha_{ij} = -\frac{\log b_i - \log b_j}{\log \lambda_i - \log \lambda_j},$$

where b_i and b_j are the scattering coefficients at wavelengths λ_i and λ_j, respectively. However, in practice, three wavelengths are used to calculate the Angstrom exponent.

Figure 6.2 shows an example of the Angstrom exponent calculation, for July 23, 2002. This day is interesting because the extinction is relatively low during the early morning hours, but then rises as the day progresses. As seen in Figure 6.2, the Angstrom exponent during the early morning hours does not show much variation from one hour to the next, indicating no change in particle size, which is consistent with low values of

extinction during the same time period. This day is discussed in detail later in this chapter.

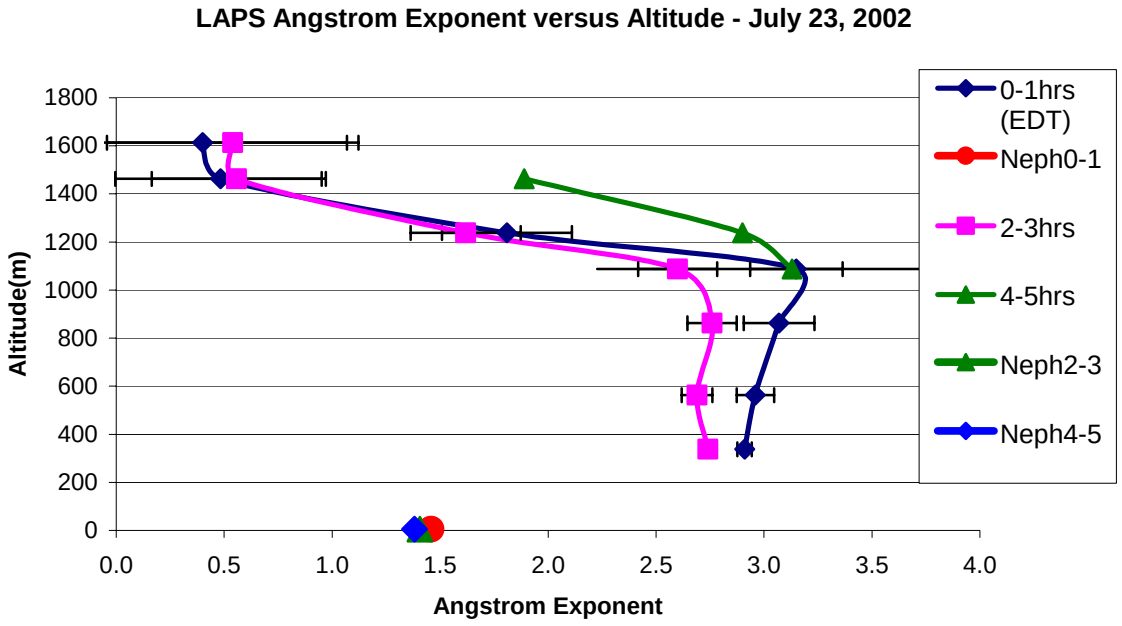

Figure 6.2: Angstrom exponent on July 23, 2002.

The LAPS scattering coefficients at 284 nm, 528 nm, and 607 nm are calculated, with the ozone absorption removed from the 284-nm extinction coefficient. The ozone concentration per cubic meter is first calculated by taking the product of the ozone concentration (parts per billion) and the corresponding atmospheric number density (per cubic meter). The resulting ozone concentration (per cubic meter) is multiplied by the ozone absorption cross-section at 266 nm on the uplag, which is 0.9×10^{-17} cm^2, and by the ozone absorption cross-section at 284 nm on the downlag, which is 0.3×10^{-17} cm^2 (obtained from the Hartley absorption band) to yield the ozone absorption value. This value is finally subtracted from the overall extinction at 284 nm to yield the 284-nm scattering coefficient. An example of the scattering coefficients at the three wavelengths

is shown as a function of wavelength on a log-log scale in Figure 6.3. A curve is fitted through these points using a least squares fit, having the equation:

$$\sigma = a \times \lambda^{-b},$$

where 'a' and 'b' are constants and σ is the extinction coefficient. The negative exponent of the λ term in the equation of this curve gives the Angstrom exponent. This is because scattering is inversely proportional to a certain power of the wavelength, depending on the particle size.

In the example shown in Figure 6.3, the value of the Angstrom exponent resulting from the fitted curve is 1.61, indicating rather large values of particle size, which is found to be consistent with increased values of scattering and extinction, as shown later in this chapter.

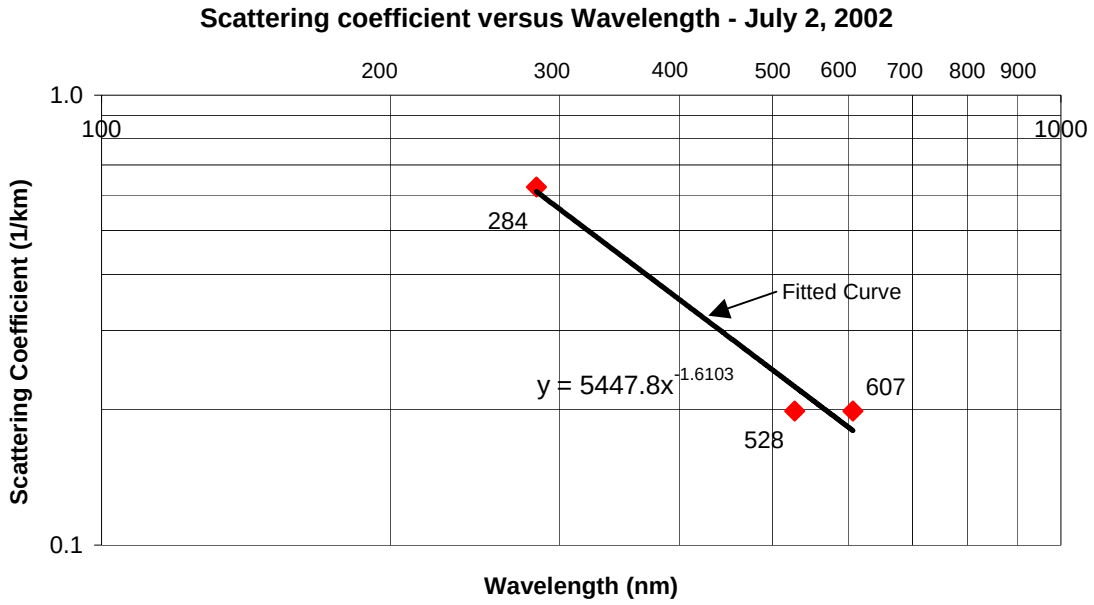

Figure 6.3: Plot showing scattering coefficients at 284 nm, 530 nm, and 607 nm and a curve fitted to obtain the Angstrom exponent.

This process of calculating the Angstrom exponent is repeated for various altitudes and time periods before sunrise and after sunset because the LAPS visible channels remain closed during the day. A similar method is used to calculate the Angstrom exponent from the Millersville University nephelometer using the measured wavelengths of 450 nm, 550 nm and 700 nm.

For $\lambda_j < \lambda_i$, where λ_i and λ_j are the wavelengths at which the scattering coefficients are calculated, the Angstrom exponent is found to decrease as the size of the particle increases [Ansmann et al., 2003]. In a pure molecular atmosphere, extinction varies inversely as the fourth power of the wavelength, giving an Angstrom exponent of 4, whereas in the presence of a cloud, the Angstrom exponent is almost 0. This chapter shows both time-sequence and altitude profiles of the Angstrom exponent.

6.4 Observations/Analysis

The following figures show the variation of the single scattering albedo and the Angstrom exponent with extinction and changes in air mass on a few days in July 2002. We begin with a relatively clear day to better understand the concept of the Angstrom exponent, and we follow this example with a few examples of high extinction.

As seen in Figure 6.4, July 29, 2002 was a relatively clear day with moderate values of extinction and high Angstrom coefficient values that remain fairly uniform. Values of the Angstrom exponent in the range of 3 to 3.5 indicate an atmosphere with very low concentrations of large particles, such as aerosols (since Angstrom exponent is inversely proportional to particle size).

(a)

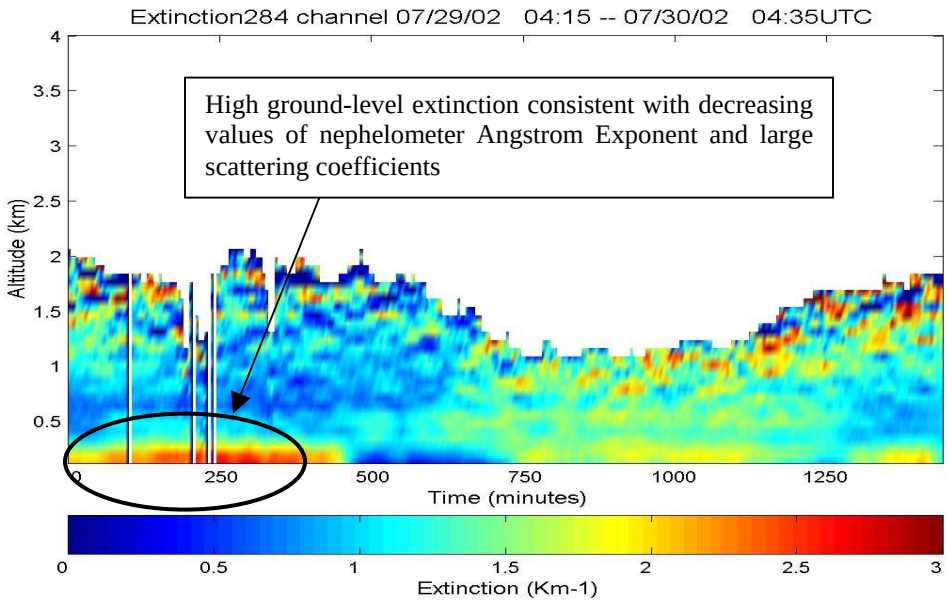

(b)

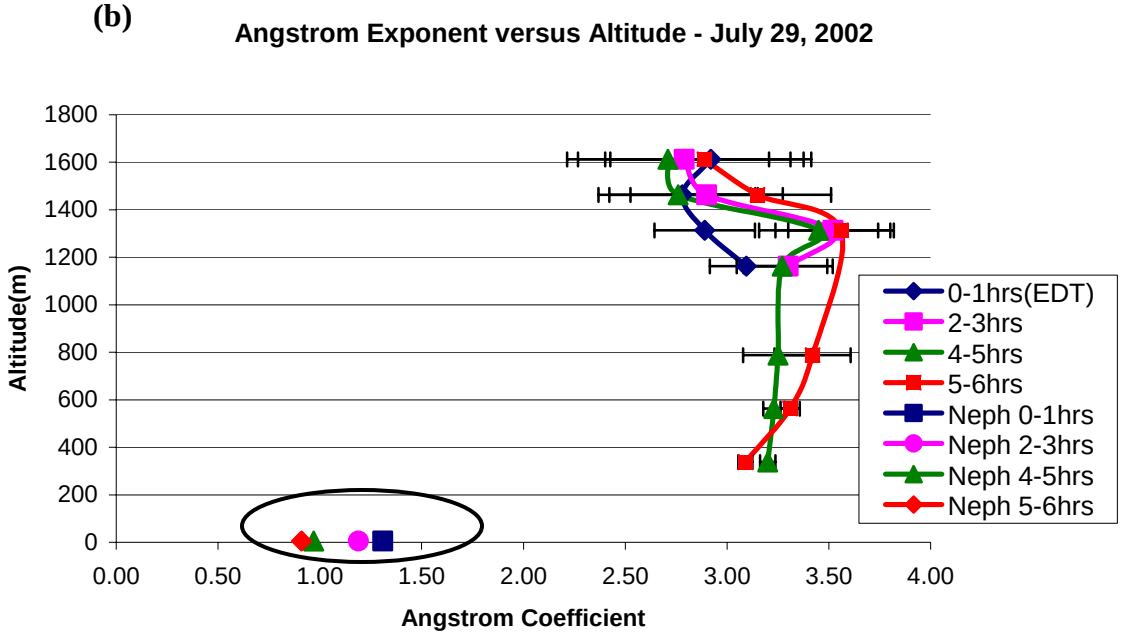

Figure 6.4: Plot showing (a) measured extinction and (b) corresponding Angstrom exponents calculated on July 29, 2002

Also, the uniformity of the Angstrom exponent values indicates no particular change in the particle size as the day progresses, as seen in Figure 6.5.

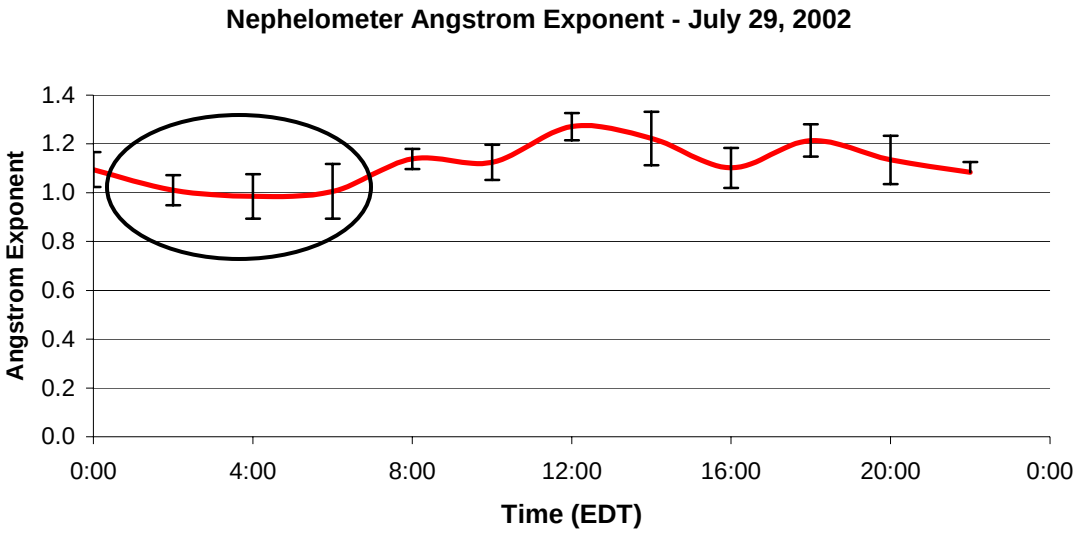

Figure 6.5: Decreasing values of Angstrom exponent from 0000 to 0600 hrs EDT, consistent with high ground-level extinction for the same time period.

This argument is corroborated by the fact that both LAPS and the Millersville University nephelometer show small scattering values, as seen in Figures 6.6 and 6.7.

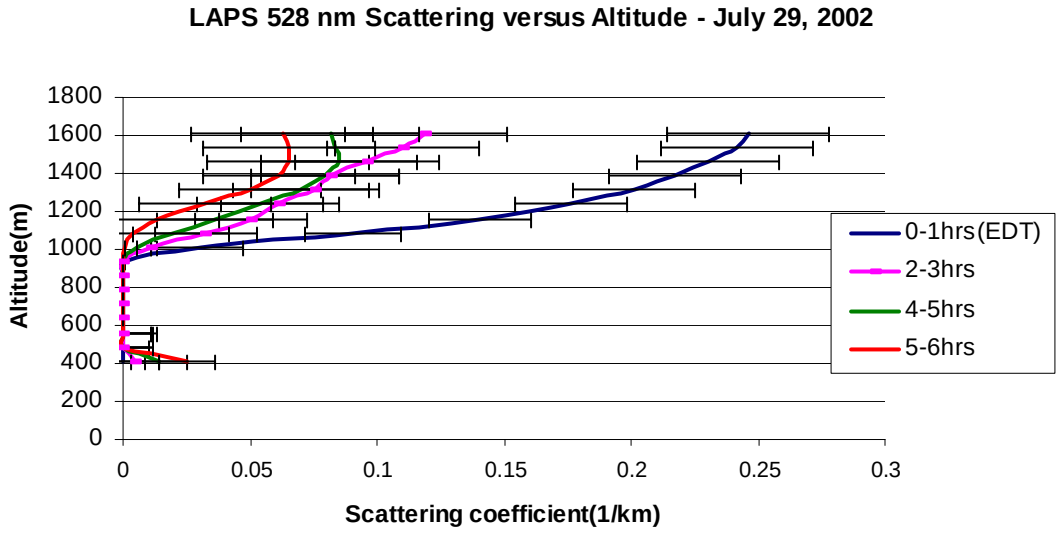

Figure 6.6: Plot showing small values of LAPS scattering coefficients.

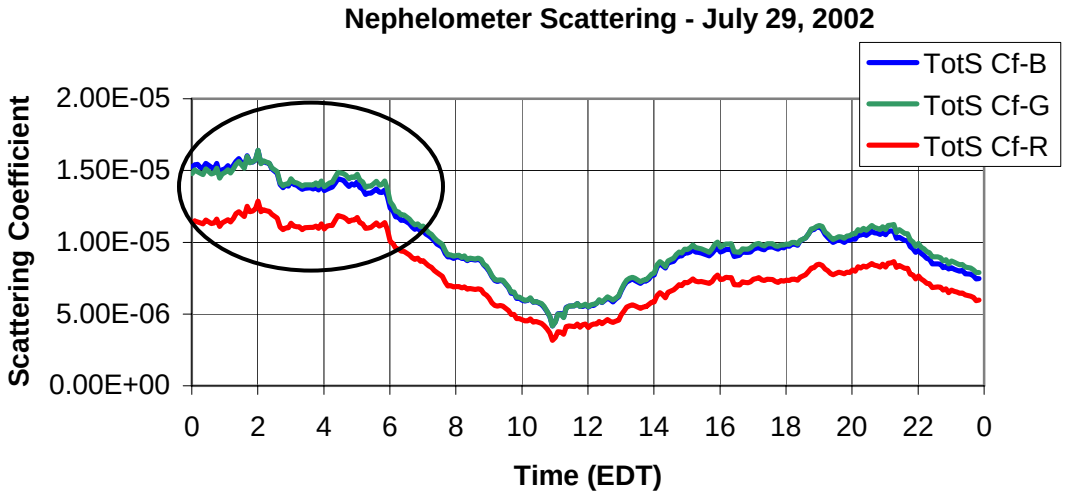

Figure 6.7: Plot showing Millersville University nephelometer scattering on July 29, 2002. Increased nephelometer scattering coefficients from 0000 to 0600 hrs EDT consistent with high ground-level extinction for the same time period.

An important point to note is that the high extinction values at ground level from 0000 hrs to about 0600 hrs EDT are consistent with decreasing values of the nephelometer Angstrom exponent and large scattering values (since decreasing Angstrom exponent values indicate increase in particle size, which corresponds to increased scattering and, thus, increased extinction), as seen circled in Figures 6.4, 6.5 and 6.7. This increase in ground extinction during the early morning hours is due to fog formation, as indicated by the high relative humidity measured by the Met tower (RH~ 80%). Another point worth noting is that the scattering at the green wavelength is greater than the scattering at the blue wavelength for certain periods of time on July 29, as observed in Figure 6.7. This could be due to the fact that there was a greater number concentration of larger particles, thus reducing the wavelength dependence of scattering.

We find that the Angstrom exponent shows relatively high values on a clear day such as July 29, 2002. In addition, it does not exhibit much variation, indicating a slow change in particle size as the day progresses. However, high values of ground extinction,

measured by LAPS, during the early morning hours are consistent with comparatively high scattering coefficients and decreasing values of the Angstrom exponent, both calculated by the nephelometer at ground level. Hence, we find that a comparison of extinction, scattering and Angstrom exponent provide a better understanding of the effect of optical extinction on particle size variation and vice-versa.

Having examined a clear day, we now analyze a few events of relatively high extinction. The most interesting event of the summer 2002 campaign in Philadelphia was probably the Canadian wildfire episode (July 7-9). Air mass entering the region from Canada was highly modified as a result of wildfires in central Quebec, causing the $PM_{2.5}$ concentration to nearly double in value from July 6 to July 7, and remain fairly high through mid-day on July 8, as shown in Figure 6.8. Note that, in Figure 6.8, the Clarkson $PM_{2.5}$ concentration shows peaks at the same time (around noon and 10 p.m. EDT on July 7) as the peaks in the surface aerosol concentration measured by the Millersville University Dustrak Instrument [Hopke, 2002; Clark, 2002]. An important point to be noted here is that the Clarkson University $PM_{2.5}$ was measured under dry conditions, whereas the Millersville University Dustrak Instrument aerosol measurements were made under ambient conditions. It has been found experimentally that the dry aerosol total number concentration is, on the average, about 28% of the ambient aerosol total number concentration [Nessler et al., 2003]. This is found to be consistent with Figure 6.8 (a) and (b), where the Clarkson University $PM_{2.5}$ concentration maximum is about 150 $\mu g/m^3$, which is approximately 25% of the Millersville University surface aerosol concentration maximum (600 $\mu g/m^3$). As shown in Figure 6.9, increased $PM_{2.5}$ concentration is accompanied by large values of the single scattering albedo and a slight decrease in the

Angstrom exponent. Figure 6.9 is quite interesting in that it compares the nephelometer Angstrom exponent with the scattering coefficients for the same time period. The encircled regions of these plots show that the Angstrom exponent decreases in value at the same times as the scattering coefficients rise. This is consistent with the theory that a decreasing Angstrom exponent indicates an increase in particle size, which is reflected in increased scattering coefficients. The rise in the single scattering albedo over the entire duration of this episode and the corresponding decrease in the Angstrom Exponent are not significant because although the scattering coefficients rise, the absorption rises almost to the same extent due to increase in the carbon concentration in the region. This is expected because, as shown in Figure 6.10, a smoke pall covers a fairly large region, causing an increase in carbon concentration. Another point worth noting here is that although the single scattering albedo is reasonable under clear sky or light haze conditions, multiple scattering becomes an important consideration in the presence of clouds, smoke or heavy haze [Measures, 1984]. In fact, at visible wavelengths, multiple scattering becomes a major component for extinction values of 0.5 km^{-1} or higher. Thus, in the Canadian wildfire episode and the haze episode of July 1-3 (discussed later in this chapter), the single scattering albedo should not be considered as the only measure of the percentage of extinction due to scattering, because multiple scattering also plays a role in these meteorological events.

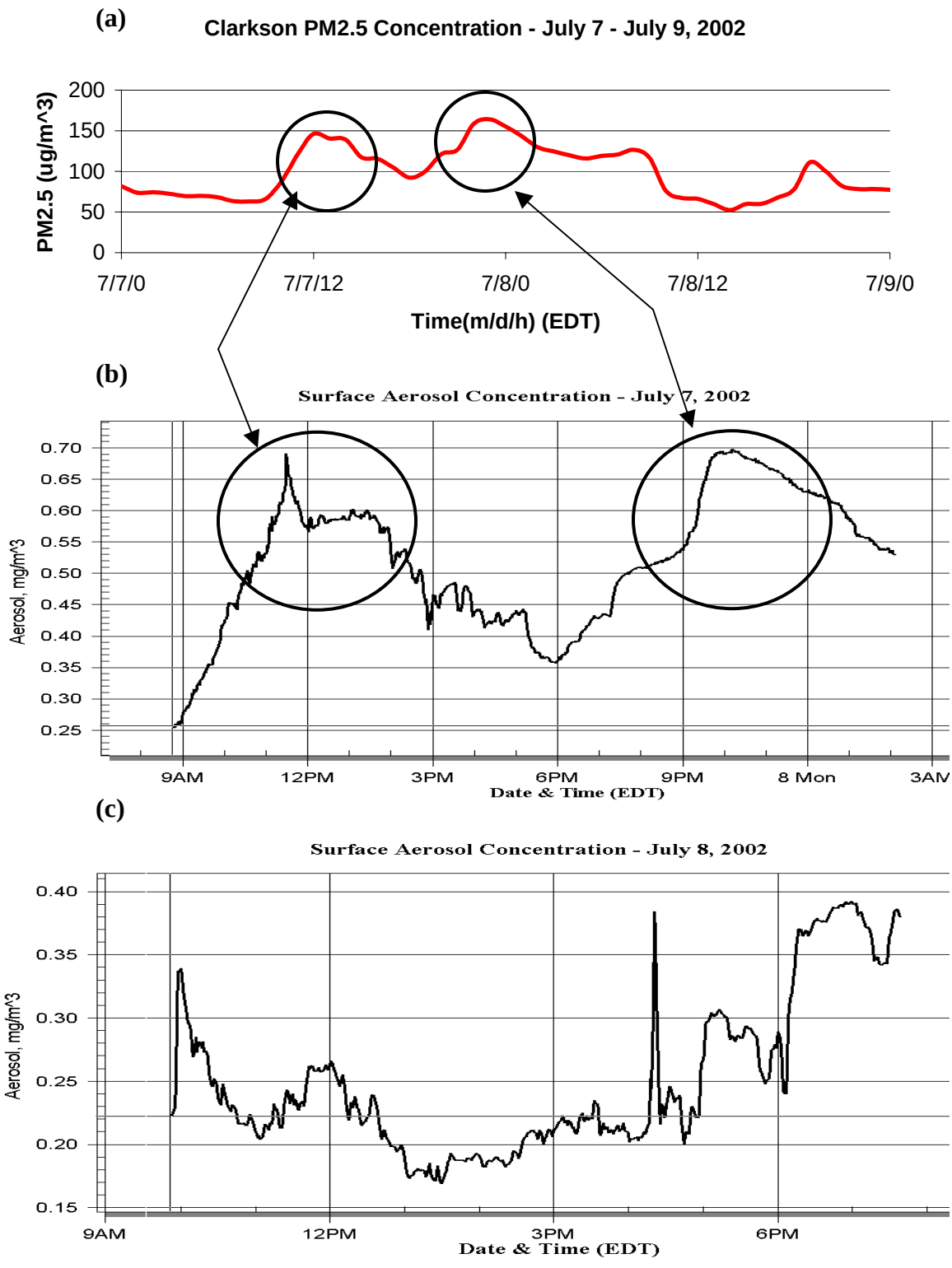

Figure 6.8: Measurements from July 7-9, 2002 (a) $PM_{2.5}$ concentration measured by TEOM [Hopke, Clarkson University], (b) spikes in surface aerosol concentration, measured by Dustrak Instrument [Clark, Millersville University], and (c) decrease in aerosol concentration by July 8.

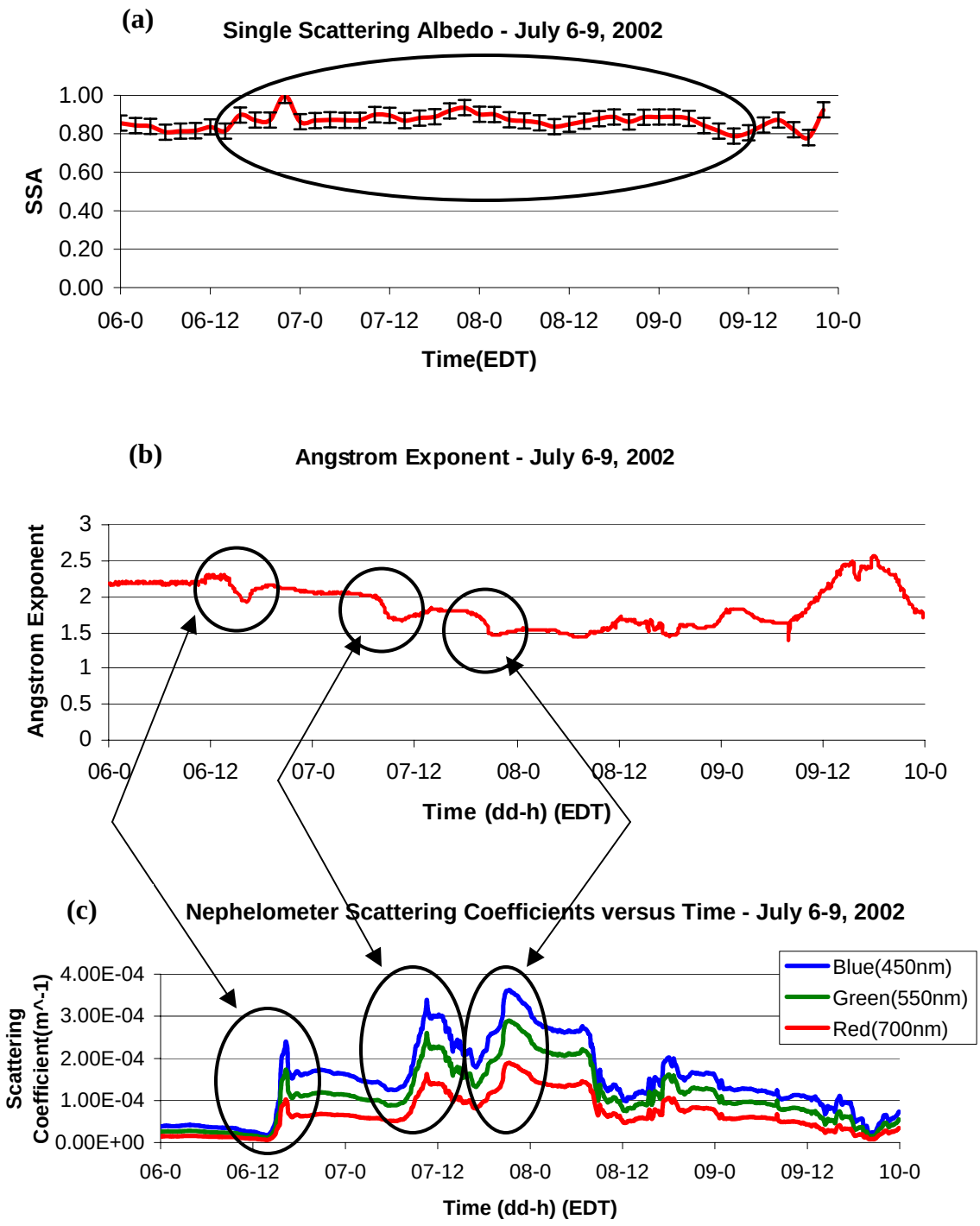

Figure 6.9: Measurements from July 6-9, 2002 are used to calculate (a) High single scattering albedo, (b) Dips in the Angstrom exponent from the three-wavelength nephelometer, and (c) spikes in the scattering coefficient [Clark, Millersville University].

(a)

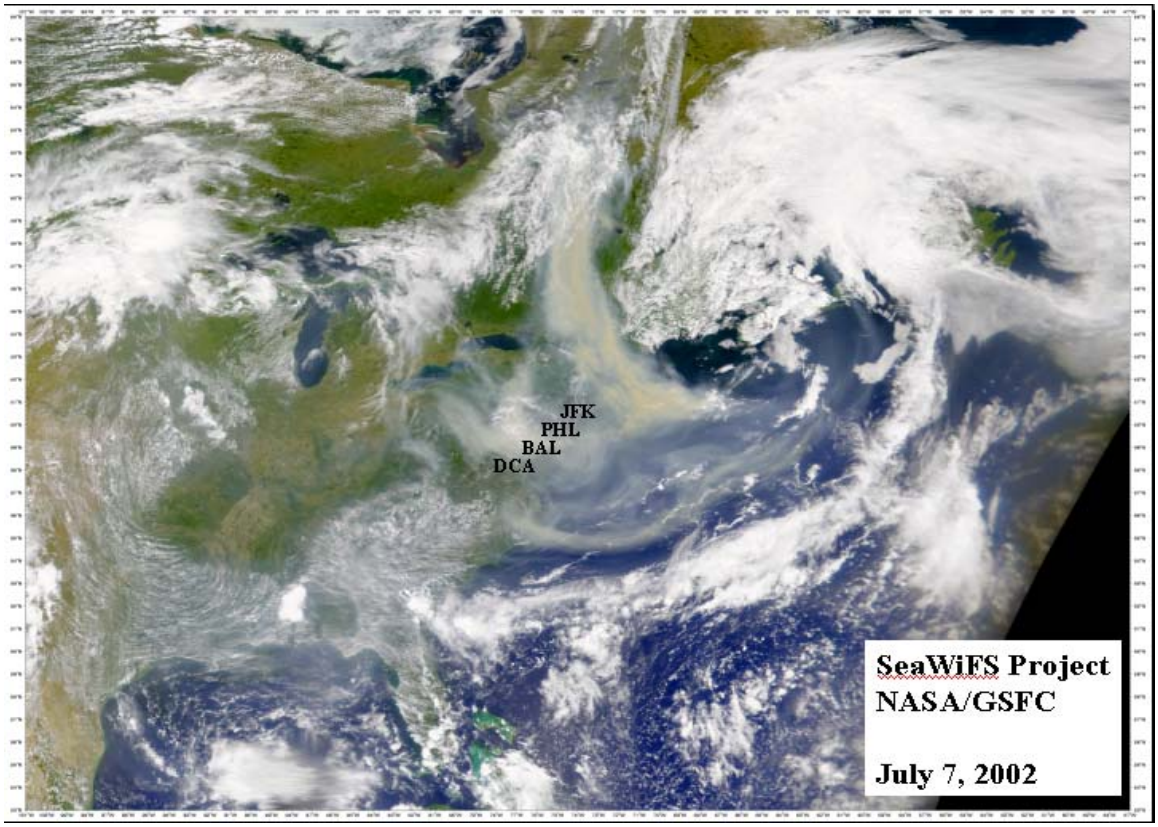

(b)

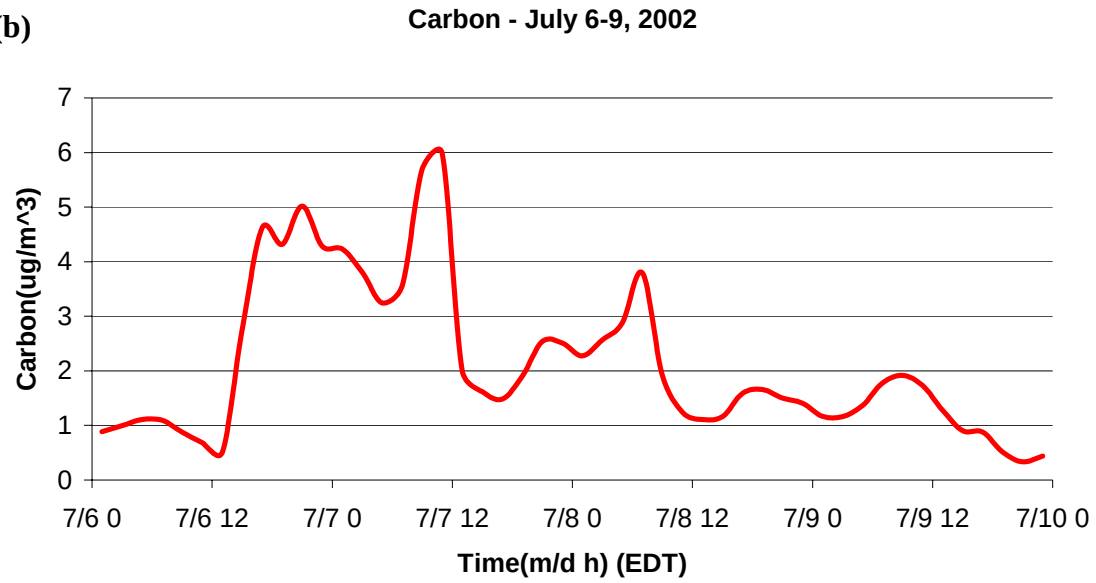

Figure 6.10: (a) Satellite image showing smoke plume from Quebec forest fire at noon [Courtesy of NASA/GSFC] (b) increase in carbon concentration, on July 7, 2002 [Clarkson University].

By July 8 and 9, $PM_{2.5}$ concentrations fall, as shown in Figure 6.11. This could be due to deeper mixing and better boundary-layer photochemistry, as the smoke pall thins.

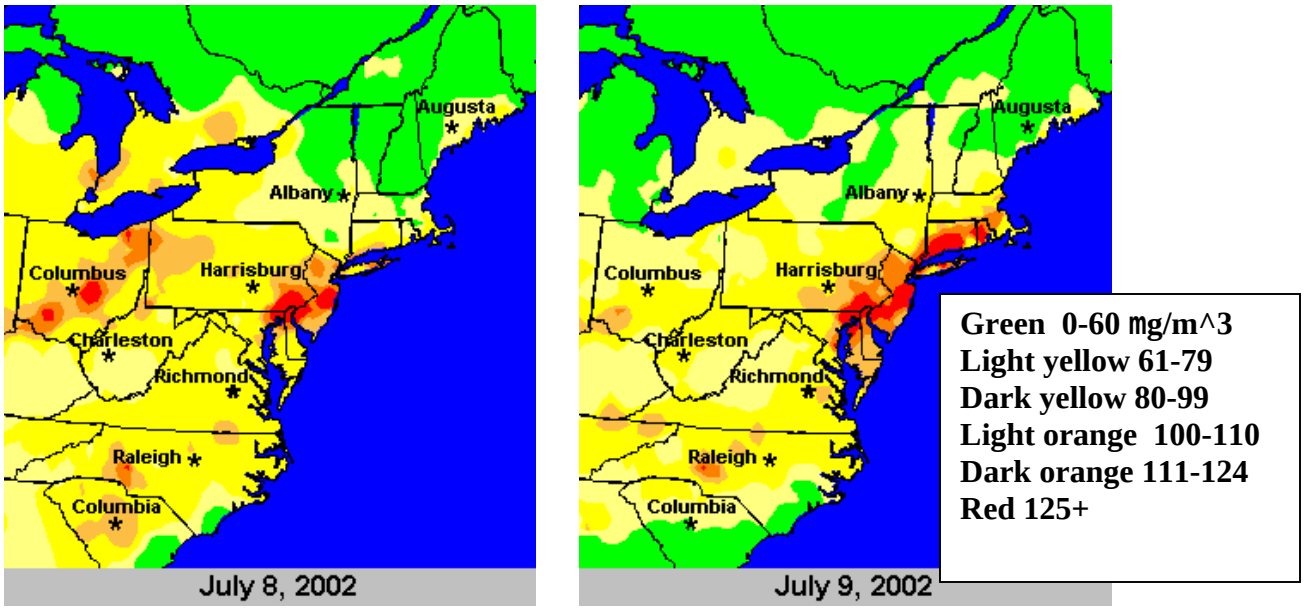

Figure 6.11: $PM_{2.5}$ concentrations on July 8 and 9, 2002 fall at noon as the smoke pall thins [Ryan, 2002].

Another event worthy of investigation is the haze event from July 1-3, 2002. The onset of this episode followed the general circulation pattern of the summer of 2002. There was a low-pressure region over the Canadian Maritimes and a ridge centered over the upper Midwest. By July 1, weather conditions are conducive to ozone and $PM_{2.5}$ formation. Haze remains banked west of the I-95 corridor on July 1 and then moves rapidly eastward on July 2. Enhanced $PM_{2.5}$ concentrations are observed in the region, but the highest concentrations are found in a brief period between July 2 and July 3, as shown in Figure 6.12.

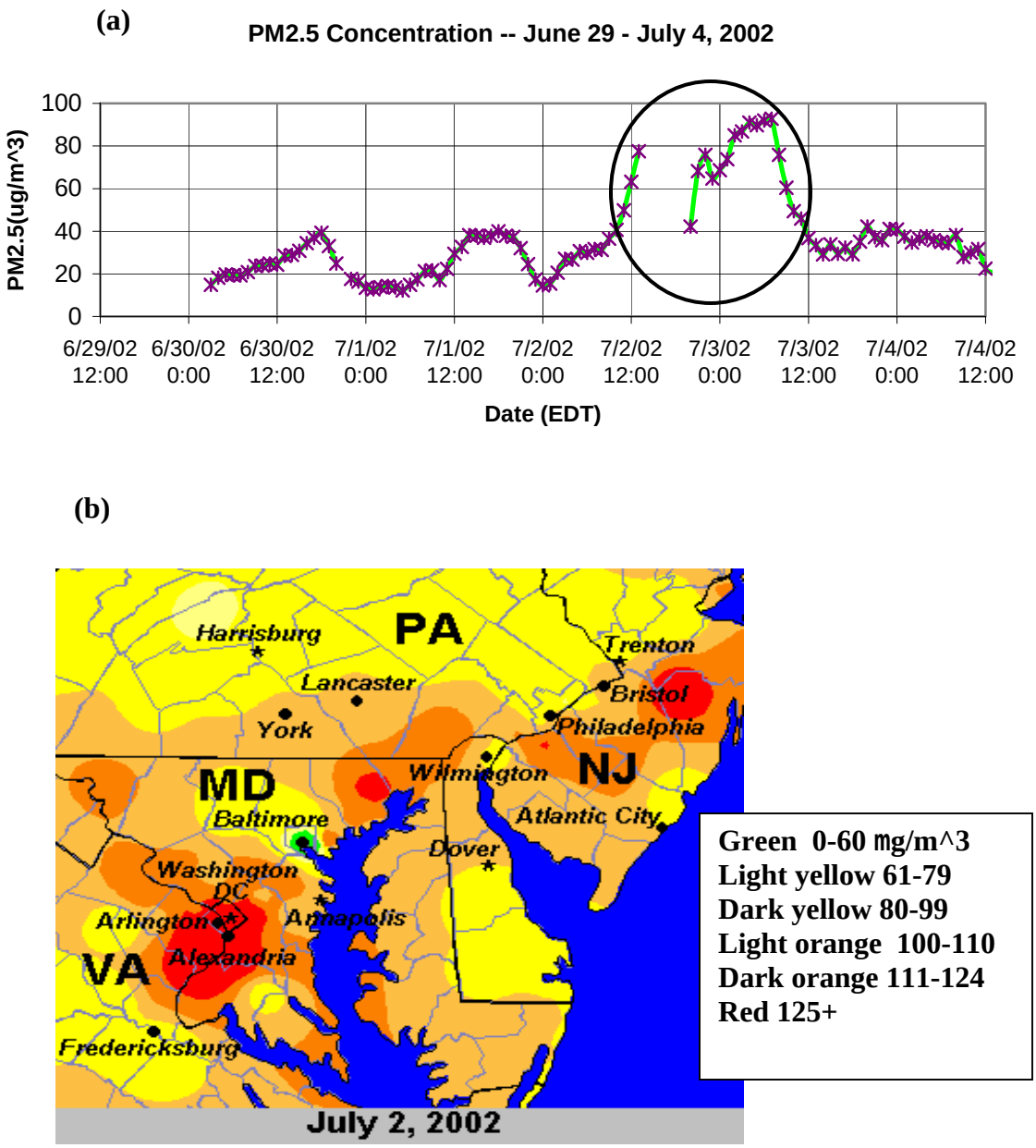

Figure 6.12: Increased $PM_{2.5}$ concentrations(Figures (a) and (b)) around noon on July 2, 2002 as a result of haze being transported into the region [Clarkson University, Ryan, 2002].

This increase in $PM_{2.5}$ is attributed to a layer of haze being transported into the region from the upper Ohio valley and Michigan, as shown in Figure 6.13. The back trajectories show that at higher altitudes (5000 m), at this time, clean air is brought into the region from Canada, whereas at the lower altitudes, within the boundary layer, haze, carrying

pollutants, is brought into the region from the Ohio valley and Michigan. These pollutants serve as precursors to $PM_{2.5}$ formation, thus causing an increase in the observed extinction. Relatively high values of extinction are observed sporadically through the course of July 2, accompanied by a corresponding increase in the single scattering albedo and a decrease in the Angstrom exponent during the early morning hours, as shown in Figures 6.14 and 6.15. An important point to note is that as the day progresses and the convective boundary layer develops, the pollutants are mixed all the way to the ground by convective heating and mixing, thus causing an increase in the observed extinction to the ground, as seen around noon and again around 1600 hrs EDT.

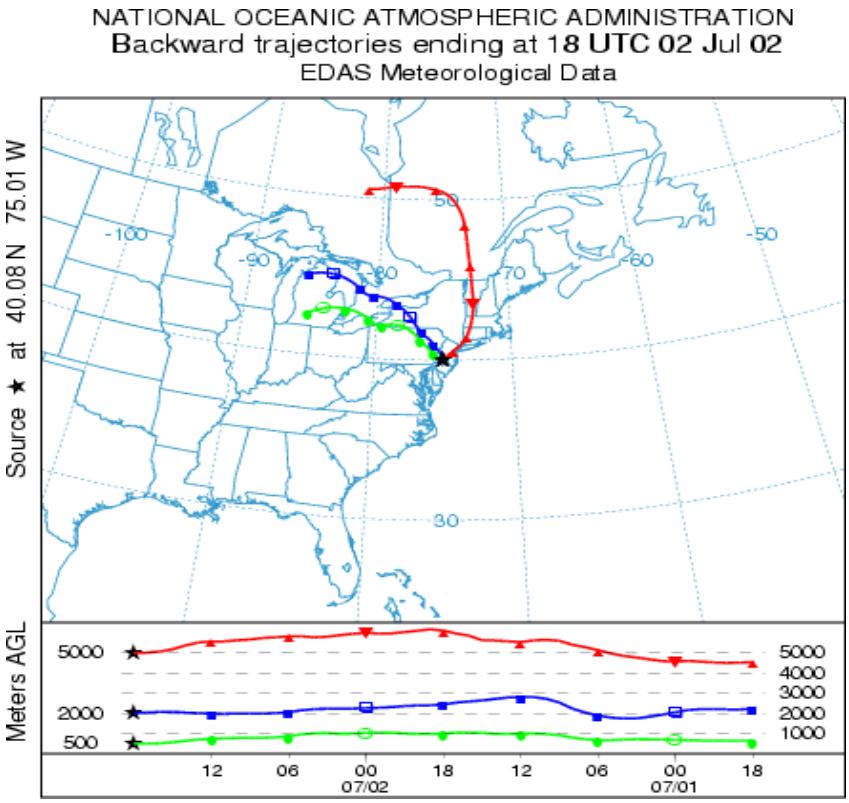

Figure 6.13: Back trajectories showing transport of air parcel to Philadelphia on July 2, 2002.

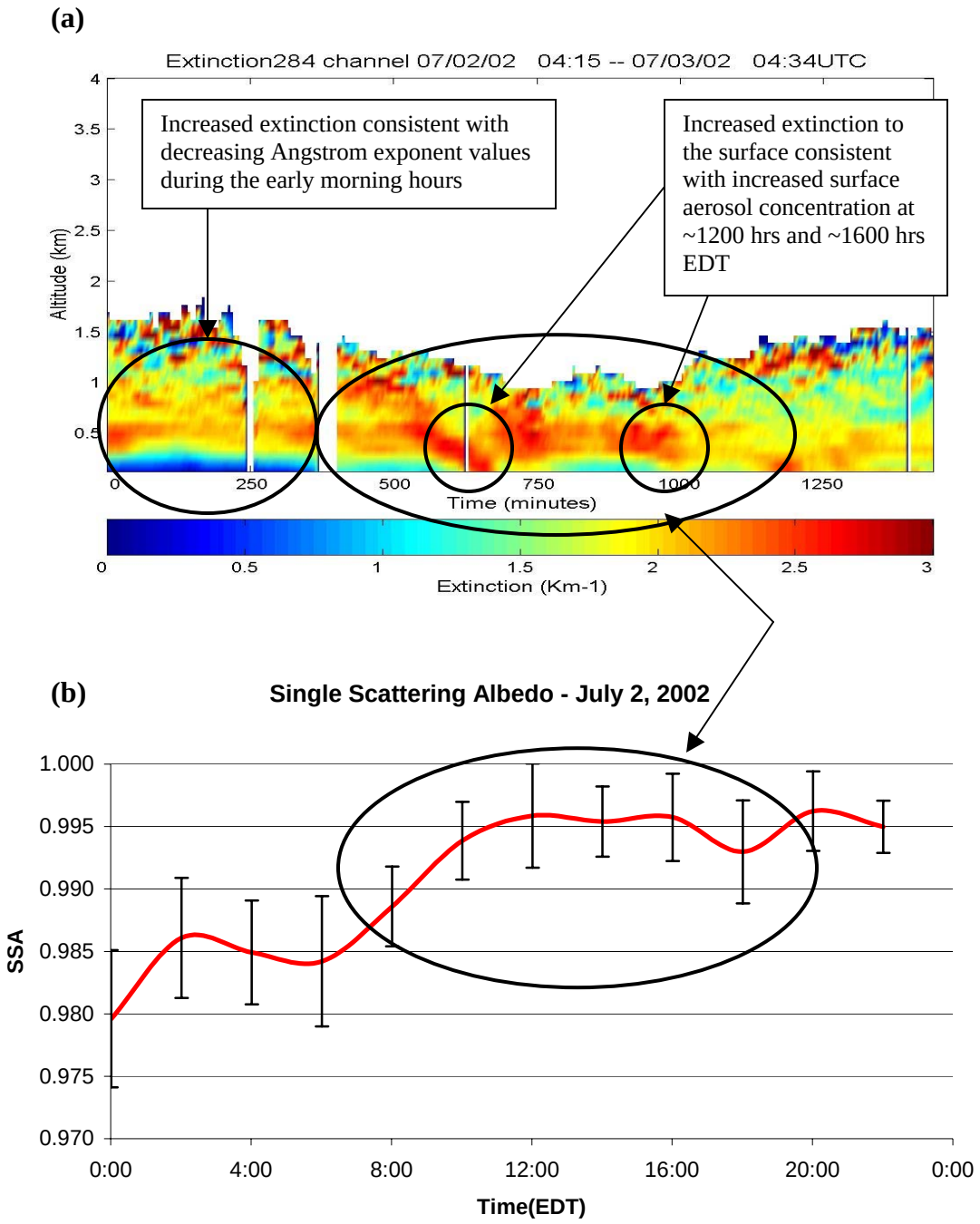

Figure 6.14: (a) Increased extinction and (b) single scattering albedo on July 2, 2002.

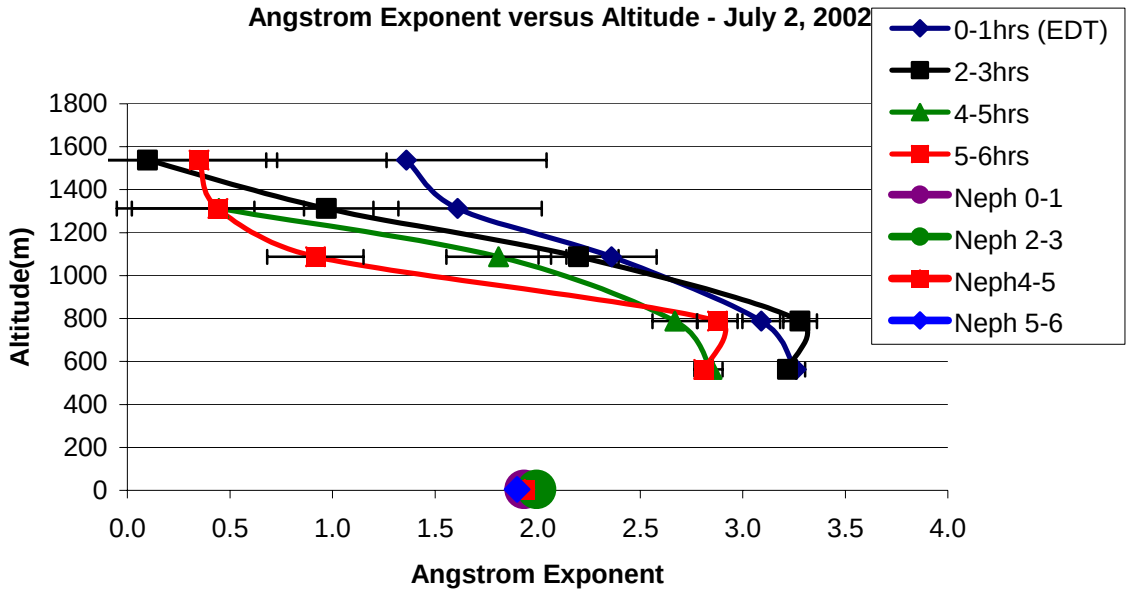

Figure 6.15: Decreasing Angstrom exponent values during the early morning hours of July 2, 2002.

The single scattering albedo is found to be around 99%, indicating scattering contributes most of the measured extinction. The surface aerosol concentrations in the region, measured by the Millersville University Dustrak Instrument, are also found to be relatively high during the same time period, as shown in Figure 6.16.

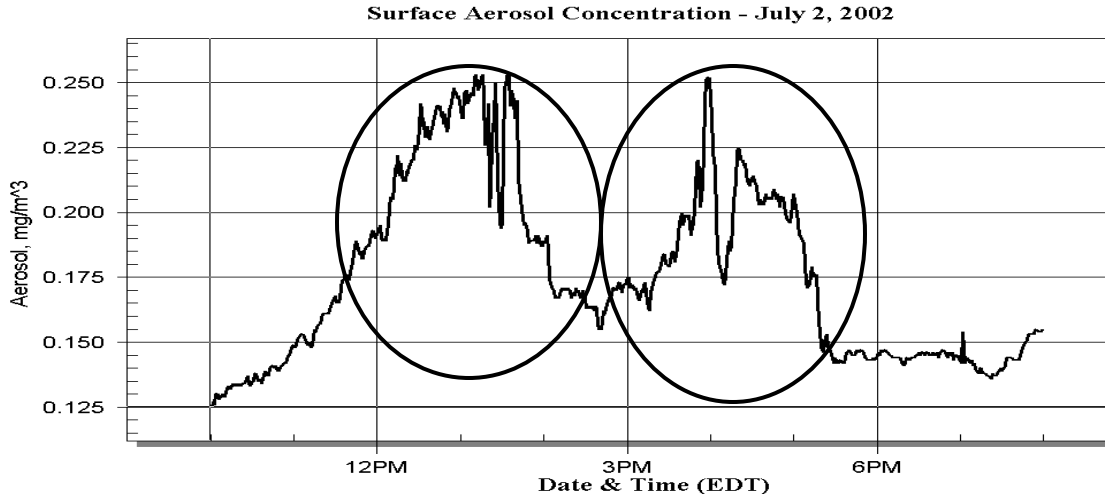

Figure 6.16: Surface aerosol concentration [Clark, Millersville University] on July 2.

As observed in Figure 6.16, spikes in the surface aerosol concentration at approximately 1200 hrs and again at 1600 hrs EDT are consistent with high values of extinction all the way to the ground, shown in Figure 6.14 (a).

The progressive flattening of the Angstrom exponent curve in Figure 6.15, as the day progresses, suggests an increase in particle size, which is found to be consistent with increased $PM_{2.5}$ and aerosol concentrations in Figures 6.12 (a) and 6.16, respectively. This is corroborated by the fact that the LAPS scattering and extinction coefficients are found to increase significantly as the day progresses, as shown in Figures 6.18 and 6.19, respectively. However, an interesting observation here is that Figures 6.17 and 6.18 are very close to one another. Figure 6.17 is obtained by removing absorption from the total extinction (Figure 6.18). Thus, the fact that the scattering and extinction coefficients are almost identical indicates that the absorption in this case is negligible, and this is consistent with very low values of ozone (10-20 ppb) during the early morning hours of July 2, 2002.

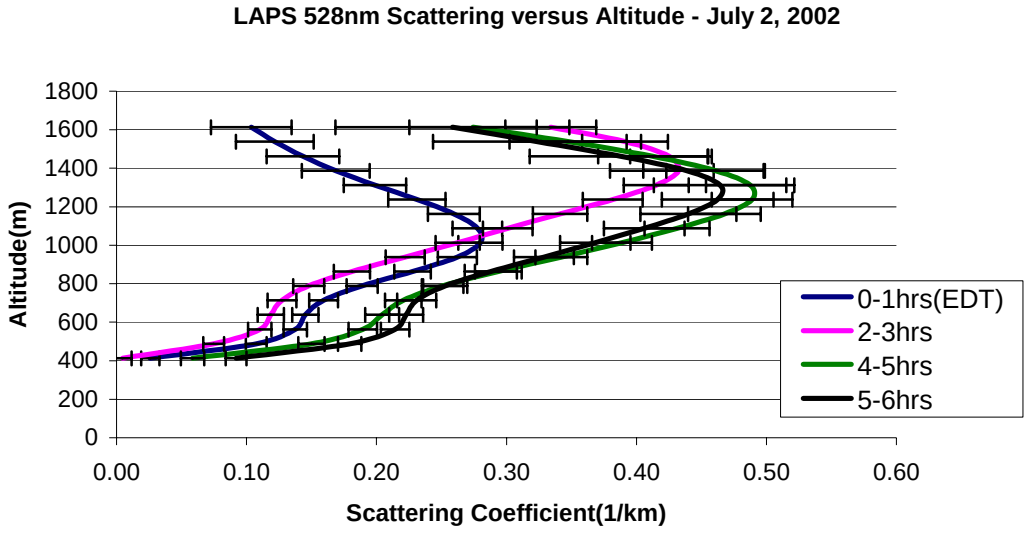

Figure 6.17: Plot showing increase in LAPS scattering values as the day progresses, on July 2, 2002.

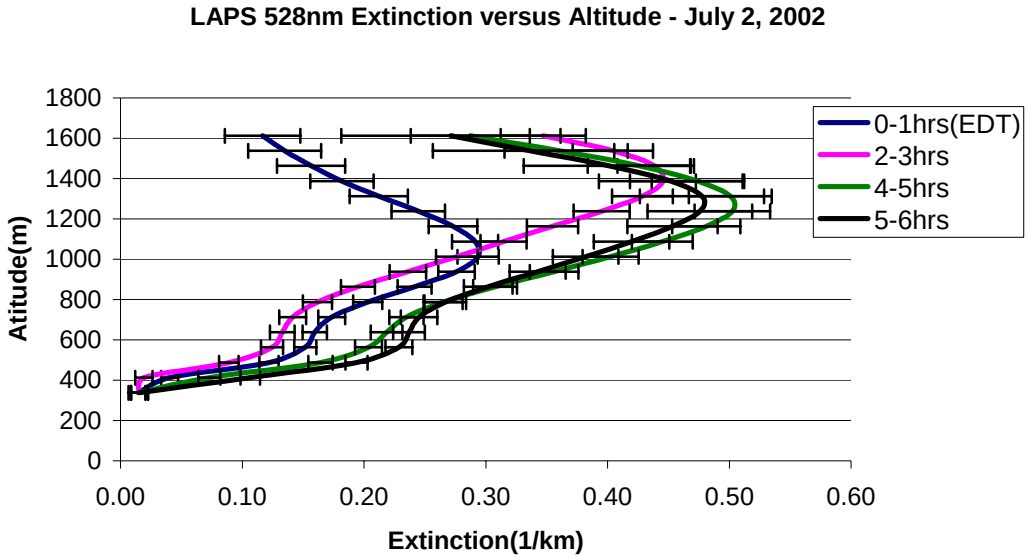

Figure 6.18: Plot showing increasing extinction values on July 2, 2002.

Finally, around mid-day on July 3, the $PM_{2.5}$ concentration is found to decrease from approximately 100 mg/m^3, as seen in Figure 6.12, to about 80-90 mg/m^3, as seen in Figure 6.19. This suggests the passage of the haze cloud over Philadelphia

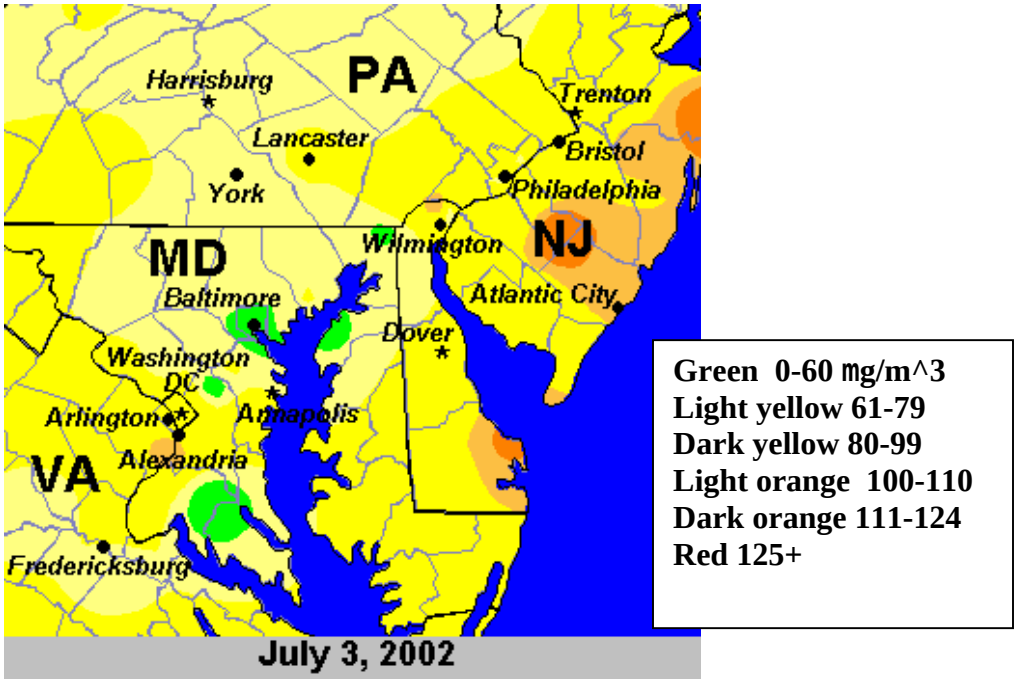

Figure 6.19: Decreased $PM_{2.5}$ concentrations around noon on July 3, 2002 [Ryan, 2002].

As a final case study, we analyze July 23, 2002. Once again, high values of extinction are observed between 0800 hrs and 2000 hrs local, as seen in Figure 6.20. During the same time period, the single scattering albedo is found to vary between 35-55%, averaging at about 40%, as shown in Figure 6.21, indicating that the observed extinction is probably more due to ozone absorption than scattering. The Angstrom component during the early morning hours does not show the same progressive decrease (Figure 6.15) as in the July 2 haze case, but remains fairly uniform, indicating only small changes in particle size as the day progresses, as shown in Figures 6.21 and 6.22. However, the decrease in Angstrom exponent values above 1100 m is due to possible cloud formation at that altitude. This point is corroborated by the fact that the vertical profiles of LAPS scattering and extinction show a significant increase at altitudes above 1100 m, as seen in Figures 6.23 and 6.24, respectively. In addition, the Met tower shows a relative humidity of approximately 80% during the same time period.

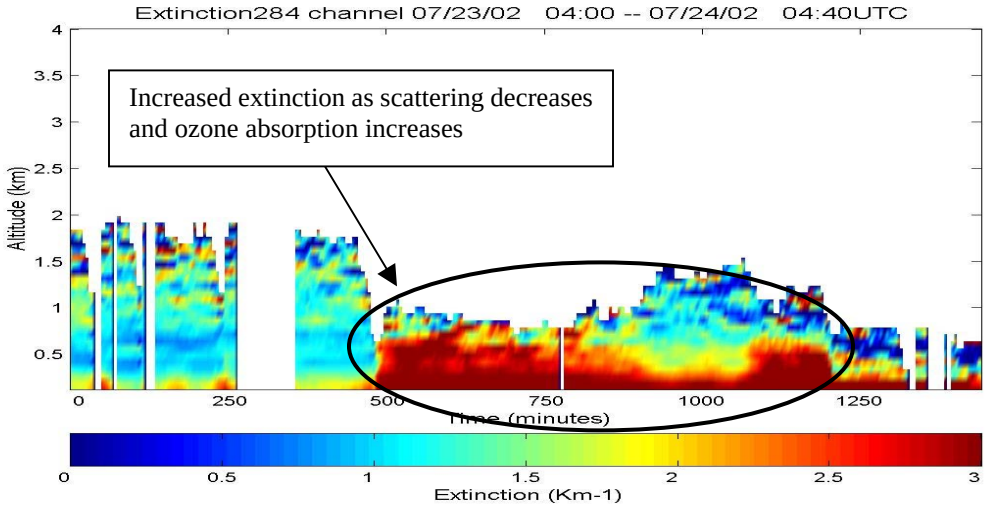

Figure 6.20: Plot of extinction on July 23, 2002, showing an increase from 0800-2000 hrs EDT.

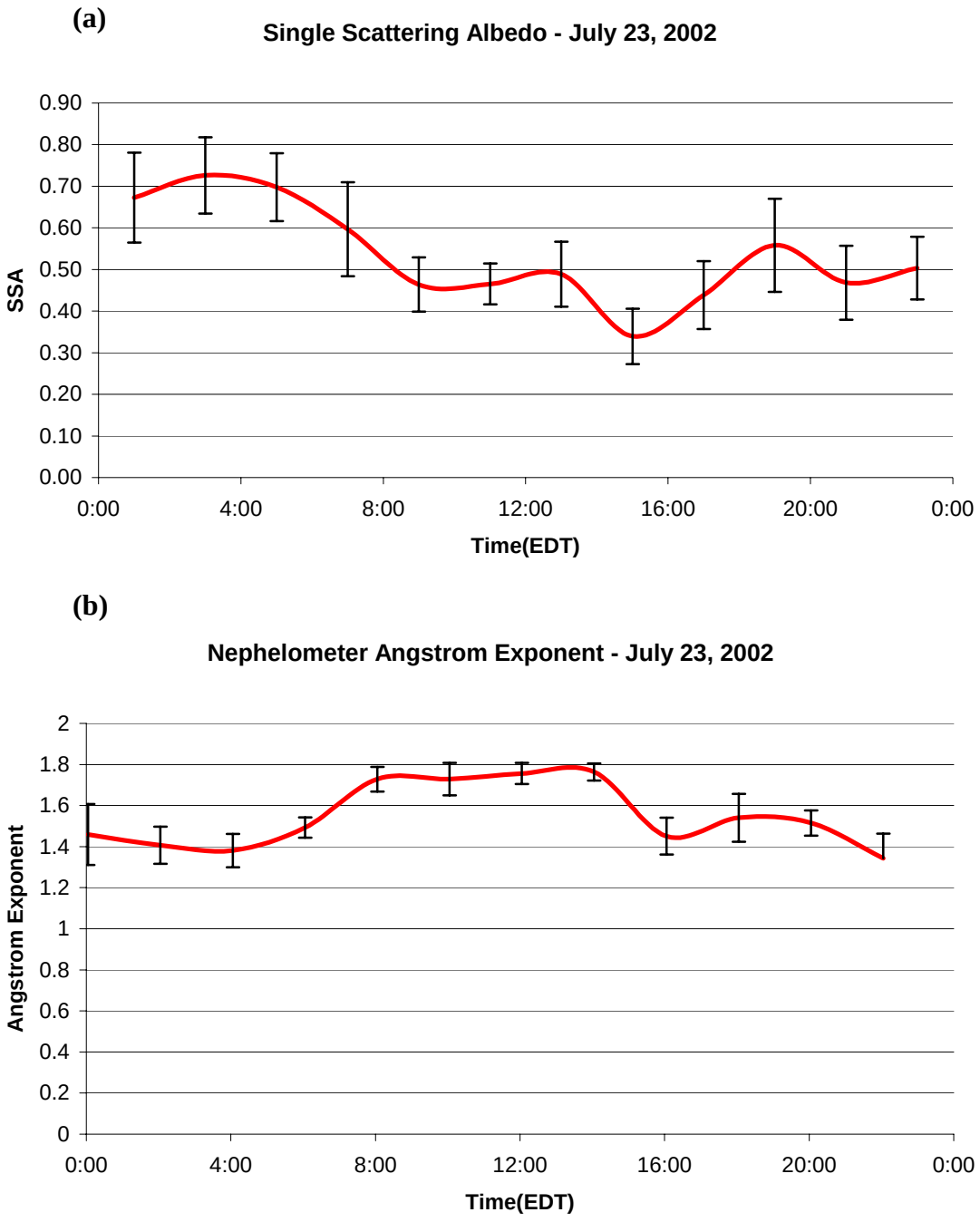

Figure 6.21: Plots of (a) single scattering albedo and (b) nephelometer Angstrom exponent, showing no significant change, on July 23, 2002.

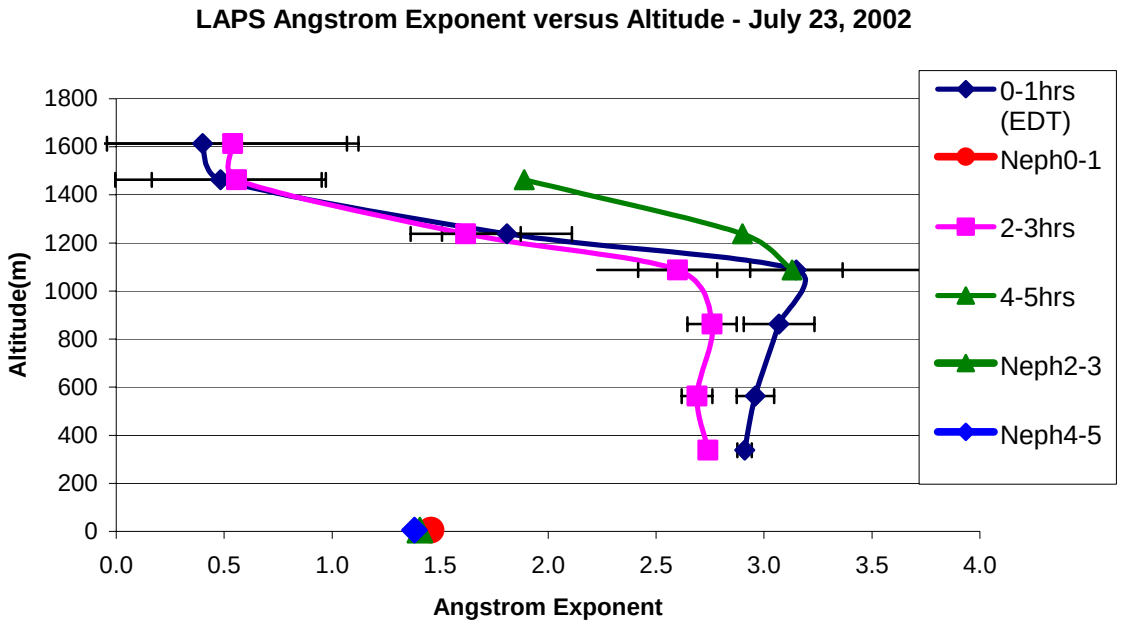

Figure 6.22: Nephelometer and LAPS Angstrom exponents on July 23, 2002.

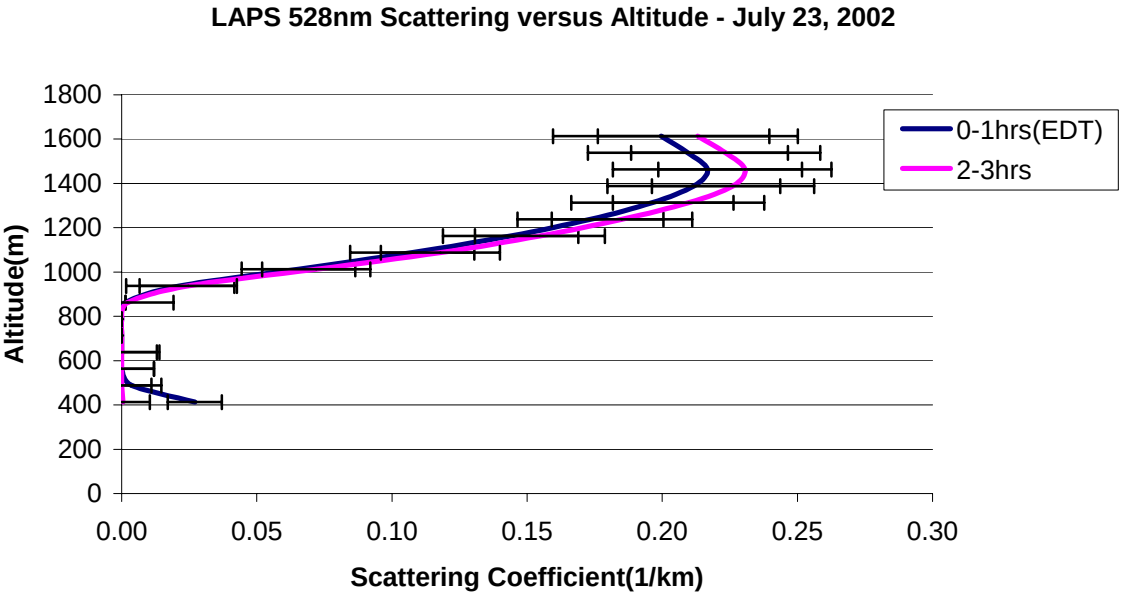

Figure 6.23: Plot showing increase scattering values at altitudes above 1100 m, on July 23, 2002.

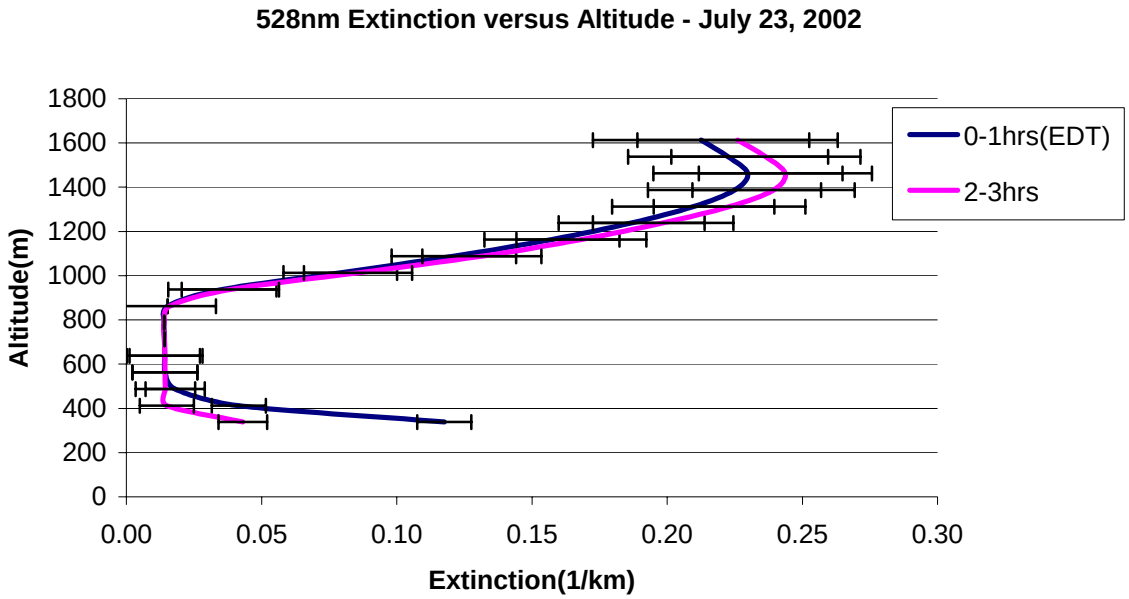

Figure 6.24: Plot showing increased extinction values at altitudes above 1100 m, on July 23, 2002.

The ozone absorption coefficient during the early hours of the day is relatively moderate, in the range of 0.3 to 0.5. However, as the day progresses, the ozone absorption contributes to approximately 55% of the observed extinction, indicating that a large part of the observed extinction is due to ozone absorption, rather than scattering.

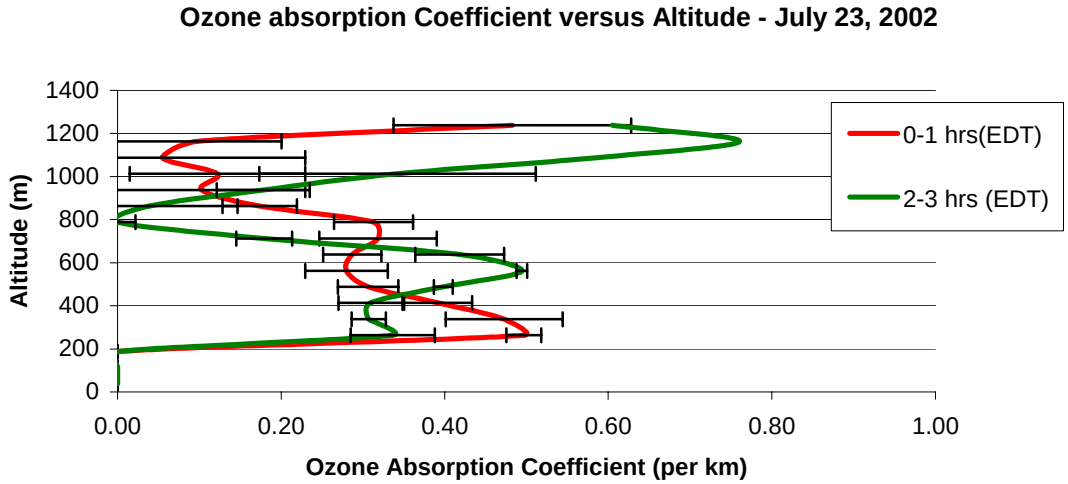

Figure 6.25: Moderate values of ozone absorption coefficient during the early hours of July 23, 2002.

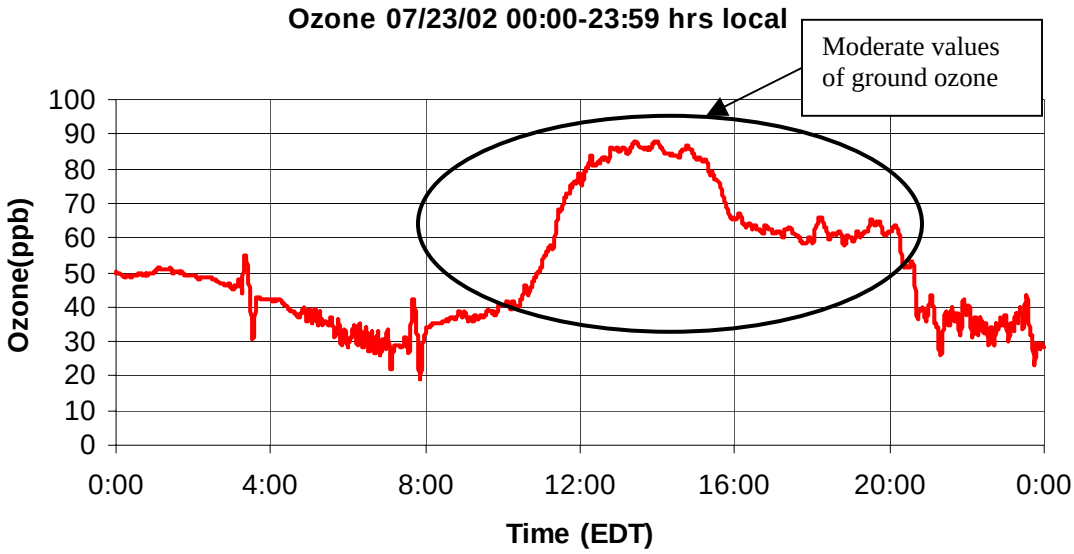

Figure 6.26: Ground ozone on July 23, 2002.

Further evidence to support this argument is provided by the fact that the ground ozone during the course of the day rises to about 85 ppb, as shown in Figure 6.26. This increase in ground ozone around 1000 hrs EDT is around the same time the extinction increases, indicating that ozone is the major contributor to the observed extinction.

The small percentage of scattering seen during the day is probably due to the presence of particulate matter (PM) in the region around the same time period, as shown in Figure 6.27. This PM could be the result of pollutants transported northward from the Midwest and Virginia on July 23, as shown by the back trajectories in Figure 6.28. The back trajectories show that at higher altitudes (5000 m), the pollutants are transported northward from the state of Virginia, whereas at the lower altitudes, within the boundary layer, these pollutants are brought into the region from the Midwest and the Atlantic.

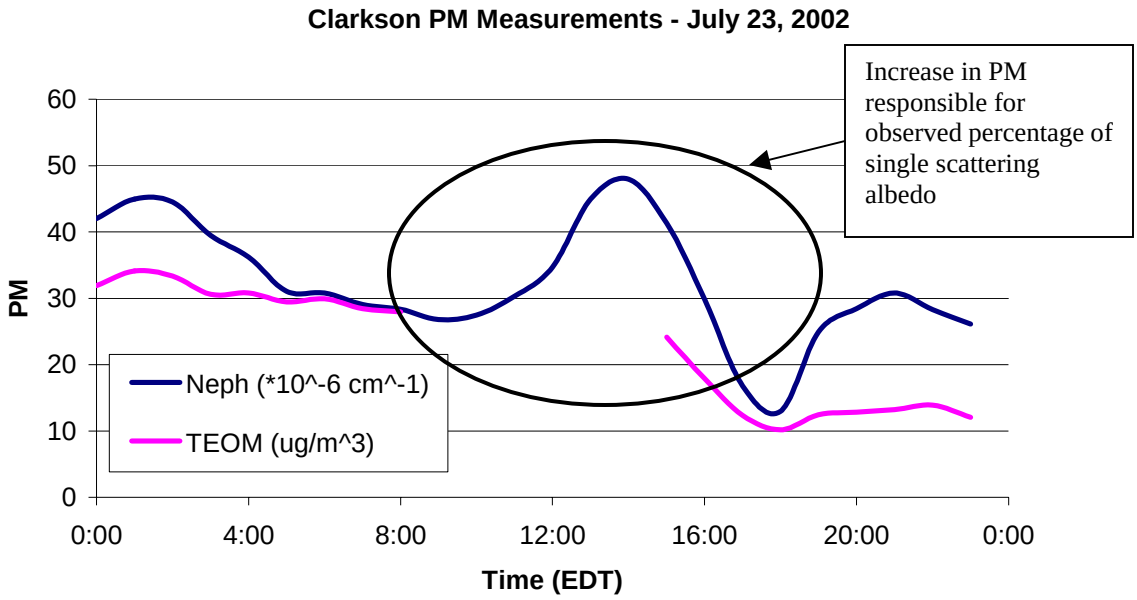

Figure 6.27: Particulate Matter (PM) measurements on July 23, 2002 [Hopke, Clarkson University].

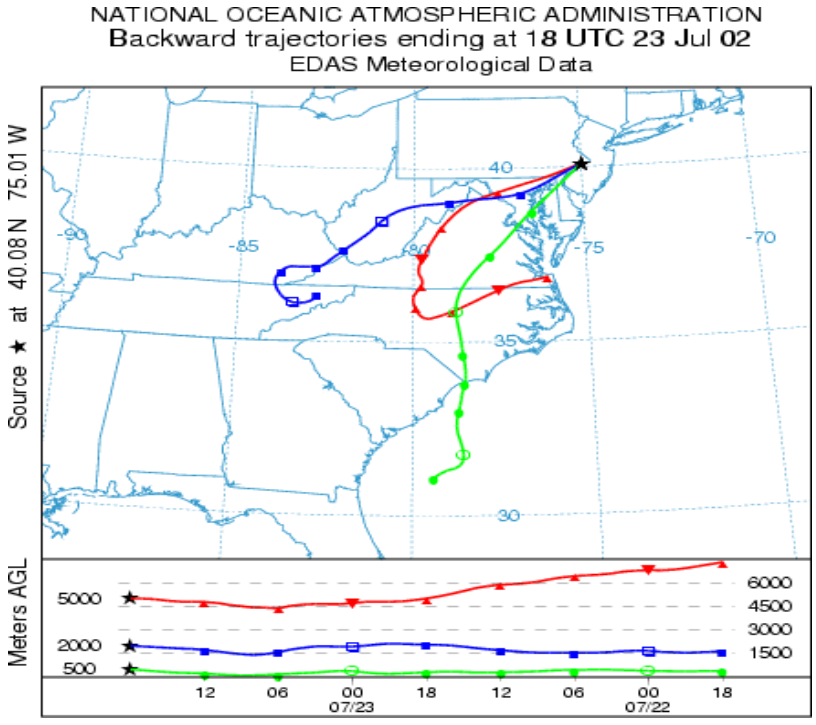

Figure 6.28: Back trajectories showing transport of pollutants on July 23, 2002.

As the day progresses and the convective boundary layer develops, the pollutants are mixed down to the ground, causing an increase in the observed PM concentration. This is because these pollutants serve as precursors to PM formation. With the approach of sunset, reduced activity is observed within the convective boundary layer as it is cooled, which causes a corresponding decrease in the PM concentration.

6.5 Summary

In this chapter, we have analyzed four episodes of varying effects on the single scattering albedo and Angstrom exponent.

We begin by analyzing July 29, 2002, which is a relatively clear day, as indicated by moderate values of extinction and low scattering coefficients, measured by both LAPS and the Millersville University nephelometer. The Angstrom exponent is found to be in the range of 3 to 3.5, and is not found to vary much as the day progresses. This indicates low concentration of large particles. In addition, the uniformity of the Angstrom exponent with time and altitude indicates no particular change in particle size as the day progresses, which, in turn, means a relatively clear day with no clouds or haze, and this is consistent with the extinction and scattering profiles. However, there is a brief period early in the morning when the extinction at ground level is relatively high, and this is consistent with comparatively large scattering coefficients and decreasing values of the Angstrom exponent, as measured by the nephelometer at ground level. Also, during this time period, the Met tower shows a relative humidity of approximately 80%, which could be the cause of fog formation at ground level, causing the increase in extinction.

The Canadian wildfire episode on July 7-9, 2002 resulted in smoke from wildfires in Quebec modifying the air mass entering the Philadelphia region and causing an increase in $PM_{2.5}$ concentration. The single scattering albedo is found to be close to 90%, indicating large amounts of scattering. However, there is no sharp rise in the single scattering albedo because, although the scattering increases, the absorption rises almost to the same extent due to increase in the carbon concentration in the region. The gradually decreasing values of the Angstrom exponent, accompanied by the presence of large amounts of aerosols in the region, justify the high values of the single scattering albedo. In addition, small dips in the nephelometer Angstrom exponent over the three-day period are consistent with spikes in the scattering coefficients observed at the same times. However, appoint worth noting here is that the single scattering albedo should not be considered as the only measure of the percentage of extinction due to scattering because multiple scattering also plays a role in the presence of smoke, clouds or heavy haze.

The haze event from July 1-3, 2002 is a good example of high extinction due to scattering from aerosols. A haze plume over the region causes a sharp rise in the $PM_{2.5}$ concentration from noon on July 2 to mid-day on July 3. A sharp rise in the single scattering albedo values to almost 99%, accompanied by a gradual flattening of the Angstrom exponent curve, indicates large amounts of scattering, which is reflected in the relatively high values of extinction during this period. In addition, large values of extinction all the way to the ground at 1200 hrs and again at 1600 hrs EDT are consistent with spikes in the surface aerosol concentration at the same times.

On July 23, 2002, we find that the single scattering albedo varies between 35-55%, accompanied by uniform values of Angstrom exponent. This indicates that the

extinction, which is found to be rather high, is primarily due to ozone absorption rather than scattering due to aerosols. Further evidence to support this argument is provided by the fact that the ground ozone during the course of the day rises to about 85 ppb. This increase in ground ozone around 1000 hrs EDT is around the same time the extinction increases, indicating that ozone is the major contributor to the observed extinction. The relatively moderate percentage of scattering observed is due to PM formation in the region as a result of pollutants carried northward from the Baltimore area. Also, the decrease in Angstrom exponent values above 1100 m is consistent with high values of relative humidity (approximately 80%) and a sharp increase in both the scattering and extinction vertical profiles above 1100 m, as measured by LAPS. This indicates the presence of a cloud at that altitude.

Thus, we find that the single scattering albedo and the Angstrom exponent provide a better understanding of how particle size distribution is related to optical extinction, and indicate the percentage of extinction due to scattering and that due to absorption.

CHAPTER 7

CONCLUSIONS

Data obtained during the NEOPS-DEP summer 2002 campaign in Philadelphia have been analyzed, and they provide a better understanding of optical extinction properties. The data presented is primarily from the month of July, when relatively high extinction was observed on several days. Some of the interesting points to note are summarized below:

- The single scattering albedo, which is the ratio of the scattering coefficient to the extinction coefficient, indicates the percentage of extinction due to scattering and that due to absorption.
- The Angstrom exponent, defined as the log-slope exponent of the spectral optical thickness between two wavelengths, is found to decrease as particle size increases, and thus serves as a good indicator of the change in particle size.
- The aerosol optical depth (AOD) provides a measure of how much light is prevented from passing through a column of the atmosphere by airborne particles. On cloud-free days, when compared with extinction, it provides a different view of atmospheric transmission characteristics.

The Penn State Raman lidar (LAPS) was used to measure optical extinction at ultraviolet (284 nm) and visible (530 nm) wavelengths. It was also used to measure vertical profiles of the Angstrom coefficient. The MET tower solar radiation sensor was used to measure solar irradiance, while the Millersville University nephelometer and the

Clarkson University aethalometer and OC/EC instruments were used to measure the single scattering albedo and Angstrom coefficient.

Analysis of data reveals general consistency between the LAPS and Met tower transmittances for three days selected in July 2002, and provides a more complete picture of the variations in optical extinction. On July 2, the LAPS visible transmittance was observed to fall by about 0.2 compared to the other days and was found to be due to a haze layer over the region.

Comparison of aerosol optical depth (AOD) from the Met tower on three days, indicate that increases in AOD are consistent with high values of extinction and the calculated AOD using the LAPS extinction time sequence profiles. High AOD values are also consistent with increased scattering coefficients, as observed in the nephelometer data. The high extinction values observed on a majority of these days are found to result from scattering by aerosols. This conclusion is supported by several cases when the single scattering albedo is found to increase (indicating increased amounts of scattering), and the Angstrom exponent is found to decrease (indicating increase in particle size). The Clarkson University and Millersville University measurements from TEOM and optical scatter instruments show increased aerosol and PM concentrations on these days, which cause the increase in extinction. This PM is believed to be the result of pollutants brought into the region from the Ohio River valley (July 2, 2002) or northwards from the Baltimore area (July 23, 2002), as indicated by the back trajectories on these days.

Thus, LAPS serves as an effective tool for analyzing and understanding the processes associated with optical extinction. In conjunction with other instruments, the LAPS profiles provide a complete picture of the variations in properties related to

extinction, and thus helps develop a link between meteorological events and the atmospheric constituents governing them.

REFERENCES

Albritton, Daniel L., and Daniel S. Greenbaum, "Atmospheric Observations: Helping Build the Scientific Basis for Decisions Related to Airborne Particle Matter," Proceedings of the PM Measurements Research Workshop, Chapel Hill, North Carolina, July 22-23, 1998.

Ansmann, Albert, Dietrich Althausen, Ulla Wandinger, Kathleen Franke, Detlef Iler, Frank Wagner, and Jost Heintzenberg, "Vertical profiling of the Indian aerosol plume with six-wavelength lidar during INDOEX: A first case study," *Geophys. Res. Lett.*, Vol. 27(7), pp. 963-966, 2000.

Ansmann, Albert, Detlef Müller, Ina Mattis, Ulla Wandinger, and Dietrich Althausen, "Saharan Dust over a central European EARLINET-AERONET site: Combined observations with Raman lidar and Sun photometer," *J. Geophys. Res*., Vol. 108 (D12), pp. 4345, 2003

Bevington, Philip R. and D. Keith Robinson, Data Reduction and Analysis for the Physical Sciences, WCB/McGraw-Hill, Boston, 1969. pp. 38-52.

Birmili W., H. Berresheim, "The Hohenpeissenberg Aerosol Formation Experiment (HAFEX): a long-term study including size-resolved aerosol, H_2SO_4, OH, and monoterpenes measurements," *Atmos. Chem. Phys.*, Vol. 3, pp. 361-376, 2003.

Charlson, R.J., S.E. Schwartz, J. M. Hales, R. D. Cess, J. A. Coakley, J. R. Hansen, D. J. Hoffman, "Climate Forcing by Anthropogenic Aerosols," *Science*, 255, pp. 423-430, 1992.

Durbin, William, "*Lidar Measurements of Ozone in the Lower Atmosphere*," Master of Science Thesis for Penn State University, Department of Electrical Engineering, December, 1997.

Esposito, Steven T., "*Applications and Analysis of Raman Lidar Techniques for Measurements of Ozone and Water Vapor in the Troposphere*," Master of Science Thesis for Penn State University, Department of Electrical Engineering, May, 1999.

Gerber, H. E., Hindman, E. E., Light Absorption by Aerosol particles, Spectrum Press, Hampton, 1982.

Hansen, J., and L. Travis, "Light Scattering in Planetary Atmospheres," *Space Sci. Rev.*, Vol.16, pp. 527-610, 1980.

Haris, P.A.T., "*Pure Rotational Raman Lidar for Temperature Measurements in the*

Lower Troposphere," Ph.D. Dissertation, The Pennsylvania State University, 1995.

IGAP, The International Global Aerosol Program Plan, Joint Working Group on the International Aerosol Climatology Project (IACP), Science Issues, GAW-76, August 1991.

Iler Detlef, Ulla Wandinger, Dietrich Althausen, and Markus Fiebig, "Comprehensive Particle Characterization from Three-Wavelength Raman Lidar Observations: Case Study," *App. Optics-LP*, Vol. 40(27), pp. 4863-4869, 2001.

Jenness, J.R., D.B. Lysak, Jr., and C.R. Philbrick, "Design of a Lidar Receiver with Fiber-Optic Output," *Applied Optics*, Vol. 36, No. 18, 4278 – 4284, 1997.

Junge, C.E., Air Chemistry and Radioactivity, Academic Press, New York City, 1963.

Kasten and Young, Revised optical air mass tables and approximation formula, *App. Optics*, Vol. 28, pp. 4735-4738, 1989.

Kiehl, J. T., B. P. Briegleb, "Comparison of the observed and calculated clear sky greenhouse effect: Implications for climate studies," *J. Geophys. Res.*, 97, pp. 10037-10049, 1992.

Li, G., "*Study of Atmospheric Aerosol and Particle Properties using lidar,"* PhD. Dissertation for Penn State University, Department of Electrical Engineering, December 2003.

Li, G., G.S. Chadha, K.R. Mulik, and C.R. Philbrick, "Characterization of Properties of Airborne Particulate Matter from Optical Scattering Using Lidar," Proceedings of the A&WMA Specialty Conference and Exhibition, PM2000: Particulate Matter and Health, Charleston, South Carolina, , pp. 4ASP1: 8-10, January 24-28, 2000.

Li, G., and C.R. Philbrick, "Lidar Measurement of Airborne Particulate Matter," Proceedings of SPIE Reprint, Vol. 4893, pp. 94-104, October 24-25, 2002.

Mathias, V., D. Balis, F. deTomasi, R. Eixmann, L. Komguem, I. Mattis, A. Papayannis, G. Pappalardo, X. Wang, "Comparative Statistics of Aerosol Extinction in EARLINET," Poster session 2, Poster Contributions to the EARLINET Symposium at Hamburg, Germany, February 2003.

Measures, Raymond M., Laser Remote Sensing.Wiley-Interscience, New York: 1984.

Mulik, Karoline R., "*Evolution of Ozone and Particulate Matter During Pollution Events Using Raman Lidar*," Master of Science Thesis for Penn State University, Department of Electrical Engineering, May, 2000.

Nessler, R., N. Bukowiecki, S. Henning, E. Weingartner, B. Calpini, and U. Baltensperger, "Simultaneous dry and ambient measurements of aerosol size distributions at the Jungfraujoch," *Tellus B.*, Vol. 55 (3), pp. 808-819.

Novitsky, E. J., "*Multistatic Lidar Profile Measurements of Lower Tropospheric Aerosol and Particulate Matter*," Master of Science Thesis for Penn State University, Department of Electrical Engineering, May, 2002.

O'Brien, M.D., T.D. Stevens, and C.R. Philbrick, "Optical Extinction from Raman Lidar Measurements," Optical Instruments for Weather Forecasting, SPIE, Vol. 2832, pp. 45-52, 1996.

Particulate Matter Science for Policy Makers: A NARSTO Assessment, pp. S-3 to S-5, S-6, S-30, S-31, February 2003.

Phil Hopke (private communication), Clarkson University, 2002.

Philbrick, C.R., "Raman Lidar Measurements of Atmospheric Properties," Atmospheric Propagation and Remote Sensing III, SPIE, Vol. 2222, 922-931, 1994.

Philbrick, C. Russell, "Investigations of Factors Determining the Occurrence of Ozone and Fine Particles in Northeastern USA," Measurement of Toxic and Related Air Pollutants - Proceedings of a Specialty Conference Cosponsored by the Air and Waste Management Association and the U.S. EPA's National Exposure Research Lab, Volume 1, pp. 248-260, 1998.

Philbrick, C. Russell, "Raman Lidar Capability to Measure Tropospheric Properties," Proceedings of the Nineteenth International Laser Radar Conference, NASA Langley Research Center, Hampton, VA, NASA Conf. Publ. 207671, pp. 289-292, July 1998.

"Pinning down the sun-climate connection", Science News Online, Jan 20, 2001.

Ryan, William, Ozone Forecast and Technical Discussion, Department of Meteorology, University of Maryland, http://www.meto.umd.edu/~ryan/aug2125.htm, 1999-2002.

Richard D. Clark (private communication), Millerville University, 2002.

Sakai T., Shibata T., "Raman lidar and aircraft measurements of tropospheric aerosol particles during the Asian dust event over central Japan: Case study on 23 April 1996," *J. Geophys. Res*, Vol.108, No.D12, 4349, June 2003.

Schneider, J. and R. Eixmann, " Three years of routine Raman lidar measurements of tropospheric aerosols: Backscattering, extinction, and residual layer height," *Atmos. Chem. Phys.*, Vol. 2, pp. 313-323, November 2002.

Schwartz, S. E., " The whitehouse effect-shortwave radiative forcing of climate by anthropogenic aerosols: An overview," *J. Aerosol Sci.*, Vol. 3, pp. 359-382, 1996.

Seinfeld, J. H. and S.N. Pandis, Atmospheric Chemistry and Physics, From Air Pollution to Climate Change, John Wiley & Sons, Inc., New York: 1998.

Stevens, Timothy D., "*Bistatic Lidar Measurements of Lower Tropospheric Aerosols*," Doctor of Philosophy Thesis for Penn State University, Department of Electrical Engineering, May, 1996.

Turner D.D., R.A Ferrare, Brasseur Heilman L.A., W.F. Feltz, T.P. Tooman, "Automated Retrievals of Water Vapor and Aerosol Profiles from an Operational Raman Lidar," *Journal of Atmospheric and Oceanic Technology*, Vol. 19, pp. 37-50, January 2002.

Van de Hulst, H.C., Multiple Light Scattering Tables, Formulas, and Applications, Vol.1&2, Academic Press: New York, 1980.

Watson, J. G., and J. C. Chow, Reconciling Urban Fugitive Dust Emissions Inventory and Ambient Source Contribution Estimates: Summary of Current Knowledge and Needed Research, Desert Research Institute, Energy and Environmental Engineering Center, DRI Document No. 6110.4D2, 1999.

Whitby, K. T., "The Physical Characteristics of Sulfur Aerosols," *Atmospheric Environment*, Vol. 12, pp. 135-159, 1978.

Whitby, K. T., R. B. Husar, B. Y. H. Liu, "The Aerosol Distribution of Los Angeles Smog," *Journal of Celluloid and Interface Science*, Vol. 39, No.1, pp. 177-204, 1973.

http://www.climatronics.com

"NASA study finds increasing solar trend that can change climate," http://www.scienceblog.com/community/article1272.html